ΕΘΝΙΚΟ ΜΕΤΣΟΒΙΟ ΠΟΛΥΤΕΧΝΕΙΟ

ΣΧΟΛΗ ΝΑΥΠΗΓΩΝ ΜΗΧΑΝΟΛΟΓΩΝ ΜΗΧΑΝΙΚΩΝ

ΤΟΜΕΑΣ ΘΑΛΑΣΣΙΩΝ ΚΑΤΑΣΚΕΥΩΝ

«Δυναμική συμπεριφορά και μέσες δευτεροτάξιες δυνάμεις σε μεταβαλλόμενη βαθυμετρία»

ΔΙΠΛΩΜΑΤΙΚΗ ΕΡΓΑΣΙΑ

ΟΙΚΟΝΟΜΙΔΟΥ Χ. ΧΑΡΙΣ

Επιβλέποντες : Καθ. Μαυράκος Α. Σπ.
Εθνικό Μετσόβιο Πολυτεχνείο (Ε.Μ.Π.)

Prof. Molin B.
Ecole Centrale Marseille (E.C.M.)

Αθήνα, Ιούλιος 2012

NATIONAL TECHNICAL UNIVERSITY OF ATHENS
SCHOOL OF NAVAL ARCHITECTURE AND MARINE ENGINEERING
LABORATORY FOR FLOATING STRUCTURES AND MOORING SYSTEMS

"Sea-keeping and wave drift forces in varying bathymetry"

DIPLOMA THESIS

OIKONOMIDOU C. HARIS

Supervisors :

Prof. Mavrakos S. A.
National Technical University of Athens (N.T.U.A), Greece

Prof. Molin B.
Ecole Centrale Marseille (E.C.M.), France

Centrale Marseille

Athens, July 2012

Η σελίδα αυτή είναι σκόπιμα λευκή.

ΕΘΝΙΚΟ ΜΕΤΣΟΒΙΟ ΠΟΛΥΤΕΧΝΕΙΟ

ΣΧΟΛΗ ΝΑΥΠΗΓΩΝ ΜΗΧΑΝΟΛΟΓΩΝ ΜΗΧΑΝΙΚΩΝ

ΤΟΜΕΑΣ ΘΑΛΑΣΣΙΩΝ ΚΑΤΑΣΚΕΥΩΝ

«Δυναμική συμπεριφορά και μέσες δευτεροτάξιες δυνάμεις σε μεταβαλλόμενη βαθυμετρία»

ΔΙΠΛΩΜΑΤΙΚΗ ΕΡΓΑΣΙΑ

ΟΙΚΟΝΟΜΙΔΟΥ Χ. ΧΑΡΙΣ

Επιβλέποντες : Καθ. Μαυράκος Α. Σπ.
Εθνικό Μετσόβιο Πολυτεχνείο (Ε.Μ.Π.)

Prof. Molin B.
Ecole Centrale Marseille (E.C.M.)

Εγκρίθηκε από την τριμελή εξεταστική επιτροπή την .....

(Υπογραφή)	*(Υπογραφή)*	*(Υπογραφή)*
.....	.....	.....
Μαυράκος Α. Σπ.	Γρηγορόπουλος Ι. Γρ.	Χατζηγεωργίου Κ. Ι.
Καθηγητής Ε.Μ.Π.	Καθηγητής Ε.Μ.Π.	Αναπλ. Καθηγητής Ε.Μ.Π.

Αθήνα, Ιούλιος 2012

Περίληψη

Στην παρούσα διπλωματική εργασία, οι δευτεροτάξιες δυνάμεις (Drift forces) διερευνώνται θεωρητικά, πειραματικά και αριθμητικά. Οι συγκεκριμένες δευτεροτάξιες δυνάμεις είναι δυνάμεις διεγειρόμενες από τους θαλάσσιους κυματισμούς και μπορούν να προκαλέσουν την παρέκκλιση ενός πλοίου από την πορεία του. Υπάρχουν μέσες δευτεροτάξιες δυνάμεις (Mean Drift forces) που εμφανίζονται σε μονοχρωματικούς κυματισμούς και δευτεροτάξιες δυνάμεις χαμηλής συχνότητας (Low frequency Drift forces) που οφείλονται σε πολυχρωματικούς κυματισμούς. Οι δυνάμεις δεύτερης τάξης αν και μικρότερες σε μέτρο από τις πρωτοτάξιες δυνάμεις, δύνανται να προκαλέσουν έντονες αποκρίσεις. Ένα πρακτικό πρόβλημα που συνδέεται με τις δευτεροτάξιες δυνάμεις είναι ότι με την άνοδο της ζήτησης του φυσικού αερίου καθίσταται αναγκαία η εγκατάσταση νέων μονάδων παραγωγής και αποθήκευσης φυσικού αερίου στα ανοιχτά της θάλασσας. Η αλληλεπίδραση μεταξύ ενός πλοίου μεταφοράς υγροποιημένου φυσικού αερίου (LNG) και ενός σταθμού αποθήκευσης και επεξεργασίας στα ανοιχτά, δημιουργεί πληθώρα υδροδυναμικών προβλημάτων, στα οποία υπεισέρχονται οι δευτεροτάξιες δυνάμεις.

Οι δευτεροτάξιες δυνάμεις επηρεάζονται από ποικίλες πηγές και παράγοντες σε μέτρο και σε πρόσημο. Όσον αφορά στην ιστορική εξέλιξη των θεωριών που αφορούν στην εκτίμησή τους, υπάρχουν δυναμικές θεωρίες για τον υπολογισμό των μέσων και των χαμηλόσυχνων δευτεροτάξιων δυνάμεων και μη δυναμικές θεωρίες για την εκτίμηση της σημασίας των συνεκτικών φαινομένων στις μέσες δευτεροτάξιες δυνάμεις. Στην παρούσα διπλωματική εργασία, από τις δυναμικές θεωρίες αναλύονται η μέθοδος άμεσης ολοκλήρωσης της πίεσης (Near-field or Direct integration method) και η μέθοδος της ορμής (Far-field or Momentum method). Επιπλέον, γίνεται μια μικρή αναφορά στις μη δυναμικές θεωρίες.

Το πειραματικό και θεωρητικό κομμάτι της διπλωματικής εργασίας διεκπεραιώθηκε υπό το πλαίσιο του προγράμματος ERASMUS σε συνεργασία με το Πανεπιστήμιο Ecole Centrale Marseille (ECM). Αφορά στο δισδιάστατο πρόβλημα μίας ορθογώνιας φορτηγίδας. Ιδιαίτερη προσοχή δόθηκε στο φαινόμενο των αρνητικών (με κατεύθυνση αντίθετη της κατεύθυνσης διάδοσης του κύματος) μέσων δευτεροτάξιων δυνάμεων. Εξετάστηκαν οι συνθήκες υπό τις οποίες η μέση δευτεροτάξια δύναμη γίνεται αρνητική καθώς και το αν η πηγή αυτού του φαινομένου είναι δυναμική ή οφείλεται σε φαινόμενα συνεκτικότητας.

Η μέση δευτεροτάξια δύναμη μετρήθηκε και υπολογίστηκε για διάφορες διατάξεις. Με στόχο τη μελέτη της επίδρασης του φαινομένου της μεταβαλλόμενης βαθυμετρίας στο πρόσημο της δευτεροτάξιας δύναμης, μια απότομη μετάβαση του βάθους του πυθμένα και ένας τοίχος μπροστά από το μοντέλο εισήχθησαν στη γεωμετρία του προβλήματος. Η μέτρηση της κίνησης του μοντέλου επιτυγχάνεται από ένα σύστημα αποτελούμενο από δύο ηλεκτροφωταυγείς διόδους (τοποθετημένες πάνω στο μοντέλο) και μία αριθμητική βιντεοκάμερα. Στη συνέχεια, η διαδικασία μέτρησης διεκπεραιώνεται μέσω διαδοχικών προγραμμάτων matlab. Το γραμμικό θεωρητικό μοντέλο στηρίζεται στη διακριτοποίηση του πεδίου ροής με κατάλληλη διακριτοποίησή του σε περιοχές ορθογωνικής γεωμετρίας. Το γραμμικό πρόβλημα ακτινοβολίας-περίθλασης λύνεται με αναπτύγματα ιδιοσυναρτήσεων Fourier και οι δευτεροτάξιες δυνάμεις υπολογίζονται με την μέθοδο της ορμής χρησιμοποιώντας δύο κατακόρυφες τομές ανάντι και κατάντι της ροής. Επιπλέον όροι απόσβεσης προσμετρούνται στην κατακόρυφη ταλάντωση (heave) και στον διατοιχισμό (roll), για την μοντελοποίηση των συνυπαρχόντων συνεκτικών φαινομένων και για την αποφυγή φαινομένου έντονου συντονισμού.

Στα συνολικά αποτελέσματα, παρατηρείται καλή συμφωνία μεταξύ πειραμάτων και θεωρίας. Οι αποκλίσεις στη δευτεροτάξια δύναμη αποδίδονται στην αδυναμία της δευτεροτάξιας απόκρισης να φθάσει σε κατάσταση ισορροπίας. Αρνητική δευτεροτάξια δύναμη παρατηρείται στην περίπτωση του τοίχου και συμπεραίνεται ότι είναι αποτέλεσμα

δυναμικών φαινομένων. Επιπλέον, η εμφάνιση της αρνητικής δευτεροτάξιας δύναμης επηρεάζεται από την έντονη ταλάντωση του μοντέλου και της ελεύθερης επιφάνειας στην κατακόρυφη κατεύθυνση. Ωστόσο, δεν πρέπει να αμεληθούν συνυπάρχοντα μη- γραμμικά φαινόμενα, όπως είναι ο διαχωρισμός της ροής, τα οποία μπορούν να προκαλέσουν απόσβεση των αρνητικών δευτεροτάξιων δυνάμεων.

Λέξεις κλειδιά: << δευτεροτάξιες δυνάμεις, δισδιάστατο πρόβλημα, διακριτοποίηση του πεδίου ροής, μέθοδος της ορμής, δυναμική προέλευση των αρνητικών δευτεροτάξιων δυνάμεων, καθ' ύψος συντονισμός τύπου παλινδρομούντος εμβόλου (piston mode resonance), συνυπάρχοντα μη- γραμμικά φαινόμενα >>

Abstract

In the present thesis the drift forces are theoretically, experimentally and numerically investigated. Drift forces are second-order wave exciting forces which may cause a vessel to loose its course, i.e. to drift away. There are mean drift forces acting in regular waves and low-frequency drift forces occurring in an irregular sea-state. Drift forces although being smaller in magnitude than their first-order counterparts, may excite large amplitude motions, especially in the modes of motions where hydrostatic restoring forces are lacking or they are small. A practical problem linked with the drift forces is connected with the rising demand for natural gas and the incentive for new import facilities placed offshore. The interaction between a LNG carrier and an offshore LNG receiving terminal gives rise to many hydrodynamic issues where the drift forces are involved.

Drift forces are influenced by diverse sources and factors in magnitude and in sign. Concerning the historical development of theories for their evaluation, there are potential theories used to calculate the mean and low frequency drift forces and non-potential theories used to evaluate the viscous effects in mean drift forces. As far as the potential methods of evaluation are concerned, the Near-field or Direct integration method and the Far-field or Momentum method are analysed in the present thesis. A small reference to the non-potential theories is also made.

The experimental and numerical investigation has been carried out in the framework of the ERASMUS Programme in collaboration with the Ecole Centrale Marseille (ECM). It concerns the 2-D problem of a rectangular barge with square bilges. Special attention has been paid to the occurrence of negative (opposite to the wave direction) mean drift force phenomenon. The circumstances under which this force becomes negative as well as whether the source of this phenomenon is potential or viscous are examined.

Wave drift force is measured and calculated for different configurations. Under the scope of studying the effect of the variable bathymetry on the sign of the drift force, an abrupt depth transition and a wall in front of the barge were implemented in the geometry of the problem. In order to measure the movement of the barge, a system consisted of two electroluminescent diodes located on the barge and a numerical video-camera was used. The procedure of measurement is fulfilled through a sequence of matlab programs. The linear theoretical model is based on the discretization of the flow-field using rectangular sub-domains. The linear radiation-diffraction problem is solved by eigen-function expansions and the calculation of the drift force is obtained from momentum considerations (Far-field method) with two vertical cuts at upstream and downstream infinity. Extra dissipation terms at heave and roll responses are added in order to model the dependency on viscous phenomena and to avoid excessive resonance.

In the global results, good agreement between experiments and theory is observed. Discrepancies at drift are attributed to the difficulty of drift to attain a stable state. Negative drift force is observed in the case of the wall and is deduced to be of potential origin. The excessive oscillation of the barge and the free surface in the heave direction influences the occurrence of negative drift forces. However, there are co-existing non-linear effects as it is the flow separation which may cause the damping of the negative drift force.

Key words: << drift forces, 2-D problem, discretization of the flow-field using rectangular sub-domains, momentum considerations, dissipation terms, potential origin of negative drift forces, piston mode resonance, co-existing non-linear effects >>

Aknowledgments

Following a chronologic order, I would like to express my deepest gratitude to Prof. S. A. Mavrakos and Assc. Prof. I. K. Chatjigeorgiou for responding positively to my willing to fulfill part of my Diploma thesis in Ecole Centrale Marseille (ECM), in the framework of the ERASMUS Programme.

Special thanks to Prof. B. Molin and Mr. O. Kimmoun for taking the responsibility and giving me the opportunity to undertake the experimental part of my Diploma thesis at the wave flume of Ecole Centrale Marseille. I am grateful to Prof. B. Molin for his availability and help during the first days of my arrival in Marseille. Also thanks to Prof. B. Molin for his scientific knowledge and support and thanks to Mr. O. Kimmoun for his crucial help at the conduct of the experiments. Furthermore, I also express my gratitude to Mr. O. Kimmoun for helping me solve computer problems and validate the experiments. Thanks to Prof. B. Molin and Mr. O. Kimmoun I had the opportunity to attend the 26^{th} International Workshop on Water Waves and Floating Bodies (IWWWFB26), which was held in Athens. This was a great experience for me and aroused my interest in hydrodynamics.

Furthermore, I am thankful to Prof. S. A. Mavrakos for the pleasant co-operation and fruitful discussions. I would like to thank him for his useful comments until the completion of the present thesis.

At this point, I would like to acknowledge my parents for their moral and financial support during my studies and during the ERASMUS period. Especially, I would like to thank my father who dedicated great part of his time discussing with me about the present thesis.

Last but not least, I would like to thank my friend Aggelos Gkiokas for his useful help at matlab, as well as for his support and his help in correcting this thesis.

TABLE OF CONTENTS

1. INTRODUCTION

In recent years, there is rising demand for natural gas and this fact creates the incentive for new import facilities. The natural gas is cooled down at a temperature of -160°C and liquefied in order to be transported. In the liquefied form, at atmospheric pressure, LNG occupies only 1/600th of its volume at gaseous state and is therefore more economical to be stored and transported over long distances. In addition to the condensation of the natural gas, the liquefaction procedure removes the impurities such as carbon dioxide, water and sulfur. The end result is an odorless, colorless product consisting mostly of methane (approximate range 85% to 99%). The clean LNG (liquid natural gas) is therefore not menacing for the environment and not damaging for the equipment of its transportation.

The LNG Supply Chain contains five different steps as it is illustrated in Figure 1-1. The liquefaction plant is similar to a large refrigerator with compressors, condensers, pressure expansion valves and evaporators. Then the LNG is piped in storage tanks. The following step of the transportation can occur either via pipelines or by LNG carriers. Moreover the LNG arrives at the receiving terminal, to be stored, regasified and piped to the end-user such as a power plan when needed.

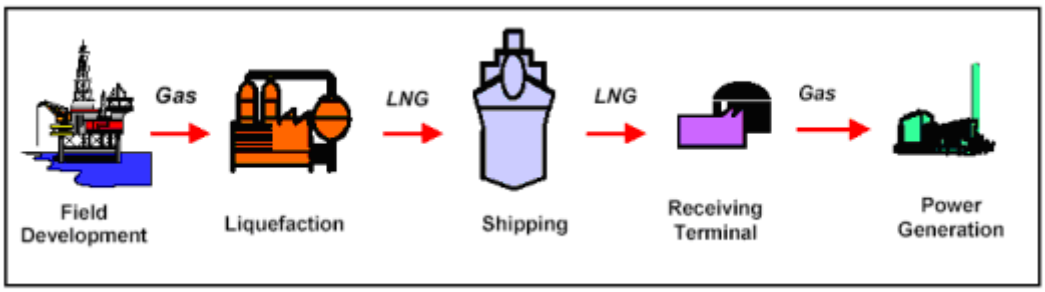

Figure 1-1: The LNG Supply Chain.

The receiving terminal must mainly include marine jetty facilities for discharging LNG, special tanks for LNG storage, process equipment for the regasification of the liquefied natural gas. The selection of the length of the unloading jetty is very important and is a function of different parameters: waterdepth, overall length of the LNG carrier, other specific site conditions that have been selected to offer the maximum flexibility for the transportation requirements. In addition to the jetty, a turning circle will also be demanded to permit the turning of the LNG carrier either on arrival or on departure.

As mentioned in Foss (2006), LNG receiving terminals have been built mostly on-shore despite the long history of offshore crude oil receiving facilities around the world. Nowadays, there are a lot of different projects of developing receiving and regasification offshore terminals, which can be floating or fixed. There are both opportunities and challenges linked with offshore development. In some locations, an offshore receiving terminal may provide a better alternative due to the use of existing offshore facilities and pipelines and easier access for LNG tankers. Possible drawbacks could be the limited or distant access to natural gas distribution pipelines, the lack of onshore services and in most instances, higher initial investments.

There are many hydrodynamic issues as well arising from the concurrence of hard environmental conditions and the complex bathymetry. A lot of calculation problems are mainly present in near-shore activities. The practical problem comes out

from the existence of the floating oil or gas production annex storage facility, to which the export tanker is moored during loading operations. For example, reference is made to a LNG carrier moored to a FSRU (Floating Storage Regasification Unit) (see Fig. 1-2).

A common hydrodynamic issue is the prediction of the wave induced mooring loads. The mooring system must be designed in a way that prevents an intense wave induced response so that it permits the LNG transfer. Moreover, it is important to define the critical loads for the structure and the environment. A critical parameter to this problem is the period of the sea in comparison with the natural periods of the movements under consideration. Furthermore, the turning circle is also responsible for a varying bathymetry region and its impact on the total loads must be taken into consideration.

Last but not least, it arises the problem of numerical simulation of the motions of a LNG carrier moored to a storage unit. In such a problem, accurate prediction of the wave drift force and moment on **each vessel** is important and must be taken into account in the design of the mooring system. The narrow spacing between the adjacent vessels introduces an added complexity.

Figure 1-2: LNG-carrier during its procedure of unloading along a FSRU.

2. BACKGROUND AND THEORY

2.1 General

Problems of **time-dependent interactions** between waves and marine structures concern both naval architects and civil engineers. There do exist methods to solve this hydrodynamic body-wave interaction problem but in both aspects there are limitations one has to take into account. Naval architects are occupied in defining the motions and the structural loads imposed on a ship by the sea waves. **Linearized water-wave theory** based on the ideal-fluid, irrotational-flow model is a very good tool. However, the excitation and damping of roll motion as well as the **viscosity effects** cannot be treated adequately by this approach.

Civil engineers from their part focus on wave loads on fixed structures which can be analyzed approximately by the use of **Morison's formula**. Morison's formula includes the loads associated with both viscosity and inertia of the water but it does not take into account any **diffraction effects**. It is widely used in offshore truss constructions for structural elements which can be considered as hydrodynamic slender bodies. This formula is simple in its application but there are still some doubts concerning the validity of the superposition of an inertia force and a viscous force. Actually, the Morison's formula is the most generally used method which includes viscosity phenomena but it is very primitive.

As offshore platforms become a dominant subject, both of these approaches are required to predict forces and motions and both diffraction and viscosity have to be accounted for. *Thus, what is missing by both methods is a combined consideration of diffraction of incident waves and of viscosity effects* [Ogilvie (1983)].

The periods where the sea waves give rise to an important amount of energy cover a range of 3 to 20 sec. At these periods, the waves generate oscillations to the floating structures and from their part, the floating structures respond by a movement of the same period whose amplitude is related almost linearly to the waves' amplitude. In case of resonance, we must be alert to catastrophic responses.

Aiming to avoid the resonance, a practical technique usually used is to transpose the natural periods of the structures before or after the period of the sea. This is why it is generally preferable to have smooth anchorage, so as the natural periods of the horizontal movements are in the order of the minute or more. To whatever extent, it is naïve to believe that by directing to a technique like this the phenomenon of resonance will be annulated. Practically, it is always observed a response at the natural periods even if they are far away from the waves' periods. Non-linear mechanisms are held responsible for the appearance of these phenomena [Molin (2002)].

For classical ship-motions problems, the linearized water-wave theory gives accurate results. As far as platform problems are concerned there are some non-linear phenomena which play a very important role. At this point, we introduce the second-order wave forces, called wave drifting forces. These forces cause the vessel to loose its course, i.e. to **drift away**. At first, it is clarified that second-order implies forces that are quadratic functions of the height of the incident waves. Right after, we do mention that there are mean second-order drift forces acting in regular waves and low frequency drift forces occurring in irregular waves. The drift-force problem is a time-dependent problem because the waves and thus the motion of the vessel are a function

of time. As it is suggested by their name, the second-order forces are well smaller in magnitude than their first-order counterparts that are predicted by the linear theory. By working out the results of Zhao et al. (1988), Faltinsen (1990) shows that the linear wave excitation forces of a wave amplitude of 1m are 100 times larger than the mean wave drifting forces and that for a wave amplitude of 10 m the first-order force is about 10 times larger. This fact depicts the need for accuracy both in the calculations and the experiments. However, the reason we are high interested to these forces is that, as pointed out by Hsu and Blenkarn (1970) and Remery and Hermans (1972), slowly varying wave drifting forces may give rise to large amplitude low-frequency horizontal motions of **moored** vessels in irregular waves despite their small magnitude. These scientists laid great stress also on the importance of defining the mean second-order forces in regular waves in the same problem. It is very important to predict the magnitude of these forces acting on a platform within the scope of ensuring that their responses are kept in acceptable limits.

Furthermore, we will make an attempt to elucidate the importance of the word moored. An unrestrained ship or platform has no natural frequencies in its horizontal-plane motions (surge, sway, yaw) and this is attributed to the absence of hydrostatic restoring coefficients for these motions. A floating platform in offshore technology must be restrained with respect to its horizontal position, most usually thanks to mooring lines fixed to anchors and in this case natural frequencies of oscillations come into play. What is remarkable is that these frequencies take a much lower value than the frequencies of the incident waves which give rise to the familiar responses of heave, pitch and roll. This fact results in another phenomenon which is not predicted by the linear theory: **resonance of the system with low-frequency second-order excitations**.

In order to refer to the effect of resonance, it has to be confirmed that there are found low-frequency waves in the wave spectrum as well. An accurate explanation is the following: because of the non-linearity of the free-surface conditions, usually we cannot make reference to one single wave frequency. For example, the existence of two waves of different frequencies always implies the existence of waves at the sum and at the difference (beat) frequencies. The beat frequencies may occur near the resonance frequency of the moored platform in surge, sway or yaw. The only way to restrict this resonant response can be provided by the relevant hydrodynamic damping mechanisms. To sum up, if the incident wave system acts in a continuous spectrum of wave frequencies, as it is the sea surface which is a continuous mean with infinite number of degrees of freedom, a low-frequency disturbance must be expected, and if the damping is small (as it is usually the case in such motions) a highly amplified resonant motion comes out.

To this end it is also important to neglect the interaction between waves and body and consider merely the fluid motions in the environment called “free waves”. Ogilvie (1983) shows that drift force may be inherent in the formulation of the second-order incident wave velocity potential. Reference will be made to the case of sinusoidal unidirectional waves in deep water. It is well-known that to first-order a fluid particle with equilibrium co-ordinates X_0 and Z_0 moves in a clockwise circle about the equilibrium position (on the free surface). To second-order, however, the fluid particles have a steady horizontal transport velocity component. This may be small, but it can be by no means negligible. What is remarkable is the fact that this steady horizontal velocity component is always in the incident wave propagation direction.

2.2 Common problems

There are a lot of common problems arising from the existence of the mean and slowly-varying wave loads (difference frequency loads). Referring to a moored ship, its equilibrium attitude with respect to the direction of incident waves is affected by the second-order forces and moments. It is important to mention however that drifting is affected by the direction of the waves. Concerning moored vessels, the drifting impact may seem to be limited when the system encounters head waves. Furthermore, the slowly varying components and the phenomenon of resonance may cause severe damage to the mooring system. This is practical in the framework of the analysis of offshore loading systems.

Drifting effects arise also in the case of a freely floating ship. As mentioned in Prins (1995), an important contribution to the drifting phenomenon is introduced by the incoming waves. Moreover, from measurements, a significant increase of the drift forces is observed due to the forward speed of the ship. These ships face an added resistance above their resistance in calm water, which has to be overcome by their engines. This fact implies that in the drift force problem, the combined effect of both current and forward speed has to be considered. But also in harbor circumstances the drifting forces may become critical owing to the impact of shallow water. Hence bottom effects have to be also considered.

Besides, sum frequency forces can cause problems. These forces can result resonant oscillations of tension-leg platforms (TLPs) in vertical plane motions (heave, pitch, roll). In literature this is the so called phenomenon of “springing” or “ringing” and can contribute to fatigue problems in the tension legs. Due to the springing, we can also find a ship resonating as a vibrating beam in response to periodic wave excitation. Low-frequency motions in the vertical plane may be significant as well. For example, large-volume structures are sometimes designed with small waterplane areas in order to decrease their natural frequency of heave. It is common to find natural periods of 30 to 60 sec. Consequently, this kind of structures can undergo second-order vertical-plane resonances similar to the horizontal-plane resonances.

The vertical components of the second-order forces are sometimes known as suction forces. This term is generally used for submarine vessels when hovering or travelling near the free surface and is in connection with the mean wave induced vertical force and pitching moment of the vehicle [Ogilvie (1963)]. The suction force can impose a problem concerning the control of the vehicle in the vertical plane.

2.3 Historical development of theories

To start with, the physical similarity between the drift force problem and the added resistance problem is accentuated. Actually, the added resistance is simply the longitudinal component of the mean second-order wave force for the case of non-zero forward speed. Noteworthy is the fact that initially attention was paid to the added resistance problem. In recent years, owing to the development in offshore technology and to the increase in the number of vessels being moored at sea, the zero forward speed problem is also considered. In addition to the initial interest in the mean wave forces, the consideration of the low frequency wave forces has also begun.

Suyehiro (1924) is considered to be the first one to report the existence of wave drifting forces. He observed a steady side force on a model rolling in beam seas. He attributed this force to the **wave reflection** of the incoming waves by the model.

Watanable (1938) applied to a different mechanism; namely, interaction between the incident waves and the motions of the ship for explaining the second-order drifting phenomenon. His calculations partly agreed with Suyehiro's experimental results. Havelock (1942) developed a more mathematical analysis but concerning the mean longitudinal drifting force on a vessel heaving and pitching in regular head waves. The disadvantage of these theories is that they are not completely accurate, as a lot of very important phenomena are not taken into account. For instance, **diffraction effects** and **hydrodynamic effects** are only partly taken into consideration.

Maruo (1960) presented expressions for the calculation of the mean horizontal second-order drift forces exerted on bodies exposed to regular sea waves and floating in infinite waterdepth. Briefly, his theory is based on the conservation of energy and momentum of the fluid restricted by three bounders: the hull, the free surface, and a control surface far from the body. Newman (1967) extended Maruo's formula to include also yaw drift moments. In both works the control surface has been set to infinity and the second-order terms were expressed in terms of Kochin functions grace to the far-field asymptotic behavior of the velocity potential. Faltinsen and Michelsen (1974) have developed similar theories to Maruo's approach by accounting for the finite water depth case. Moreover, a development by Molin (1979a) introduced the mean wetted surface boundary of the body as control surface. The theories of Maruo, Newman, Faltinsen and Michelsen, and Molin are three-dimensional and exact to second-order within potential theory. Their basic assumptions do not introduce restrictions on the hull form.

Nevertheless, the application of the momentum method in studying the heave force and the mean pitch and roll moments is generally not preferable due to the integrations to be carried out over the free-surface and the sea-bottom. Mavrakos (1988) has proved that in case of truncated or compound vertical cylinders, where analytic representations of the required first-order velocity potential are disposable, these integrations can be evaluated analytically. Mavrakos derived some new expressions for the mean vertical force and pitching moment on an arbitrarily shaped floating body for both finite and infinite water depth. However, there still remains a great difficulty in the solution of a problem including an interacting group of bodies attributed once again to the free-surface and the sea-bottom integrations involved.

Gerritsma and Beukelman (1971) estimated the increase in wave resistance of vessels travelling in head seas. They assumed that the mean resistance increase (longitudinal drift force) can be found by equating the damping energy radiated by the heaving and pitching vessel with the work done by the incoming waves.

In a series of papers Pinkster (1976, 1977, 1979a, 1979b, 1980) has provided us with one of the most thorough analyses. Pinkster suggested a method based on direct integration of all pressure contributions to the second-order wave forces on the wetted hull of the body. He gives insight in the mechanism of interaction between waves and body. His method is also in accordance with the potential theory. Later, Pinkster and Hooft (1978), Pinkster (1979b) expanded this theory to three-dimensional cases by making use of the second-order non-linear incident wave potential in order to calculate the mean and low-frequency part of the wave drifting forces (see also *Chapter 3.13*).

Last but not least, Wahab (1974), Pijfers and Brink (1977) introduced methods of calculating the drift forces which take into account viscous effects. Viscous effects may become significant as far as slender constructions, i.e. semi-submersibles, are concerned. Huse (1976) has reported a qualitative indication of the viscous effect on the mean wave drift forces acting on semi-submersibles.

In total, the theories elaborated in the past can be grouped in four main categories:

1. Potential theories which derive the mean second-order forces relying on the application of the momentum conservation principle to a control volume surrounding the body. These theories take advantage of the far-field behaviour of the potentials describing the motions. Some of the scientists who have dealt with this category are the following:
   -Maruo (1960)
   -Newman (1967)
   -Faltinsen and Michelsen (1974)
   -Molin (1979a)
   -Mavrakos (1988, 1995)
   -Lee and Newman (1971)

   The momentum conservation principle has been implemented in finite control volumes as well; as opposed to those of infinity extent (far-field). These methods have been developed in relation with multi-body configurations, where the application of the classical form of the momentum method in the far-field would have resulted in evaluating the total force on the entire multi-body system and not on the drift-force calculation of each member of the configuration. In that context, Lee and Newman (1994) and Mavrakos (1995) presented formulations of the momentum conservation principle in finite control volumes that surround each body of the configuration, while Chen (2007) introduced an alternative formulation, the so-called "middle-field" method, also based on finite control volumes surrounding each participating body in the multi-body configuration.

2. An alternative formulation of calculating the mean drift forces as well as the low frequency second-order forces, which is also exact to potential theory is based on the direct integration of the fluid pressure over the instantaneous wetted surface of the body, keeping all relevant terms up to second-order. In some of these cases the final expressions ensue from using Gauss theorem, modified to equivalent expressions which have to be evaluated on a fictitious boundary at great distance from the vessel. Hence, in this case it must be made once again use of the asymptotic or far-field behaviour of the potential characterizing the flow. Theories in this category are thanks to:
   -Watanable (1938)
   -Havelock (1942)
   -Ogilvie (1963)
   -Pinkster (1976), (1979a), (1979b)
   -Faltinsen and Loken (1978)

3. The third category refers to potential theories which calculate the mean second-order forces by equating the damping energy radiated by the oscillating vessel to work done by the incoming waves. These theories are approximative and assume a slender body. Examples of these theories are owing to:
   -Gerritsma and Beukelman (1971)
   -Kaplan and Sargent (1976)

4. The fourth category includes theories which exploit Morison's equation and the relative motion concept in order to evaluate viscous effects in the mean drift force. These methods are applicable to semi-submersible structures which are assumed to consist of slender elements. Representatives of this theory are:
   -Wahab (1974)
   -Pijfers and Brink (1977)
   -Huse (1976)

In our study, we are going to analyze the first two methods which are according to potential theory. In addition, a small reference to the theory linked with the fourth category will be made.

2.4 The second-order potential and Newman's argument

The majority of all existing papers contain a kind of assumption that eliminates the need to solve for the second-order potential at the difference frequency ω_i-ω_j. It is the simplifying assumption of Newman (1974) which allows us to act in this way. His approach is going to be described in greater extent at a later time. At this point, only considerations and comparisons with Newman's results by other researchers are mentioned.

It is proved that the mean drift force does not depend on the second-order potential, whereas in principle the low-frequency force does depend on the second-order potential. Briefly, what Newman suggests is to express the low-frequency force in terms of the mean drift force. A lot of scientists made an attempt to solve the second-order problem in order to prove the validity of Newman's argument. Molin (1979b) managed to avoid the exact evaluation of the second-order potential by introducing an assisting radiation potential and using Green's second identity. This formulation was followed further by several investigators who calculated the second-order force's components on vertical axisymmetric bodies [Eatock Taylor and Hung (1987)], [Abul-Azm and Williams (1988)], [Mavrakos and Peponis (1992)]. The first attempt to consistently predict the complete sum- and difference second-order force's components has been made by Loken (1986) who solved for the second-order velocity potential in the case of an arbitrarily shaped body. Later, Kim and Yue (1989, 1990) calculated the double-, sum- and difference second-order potential in case of vertical axisymmetric bodies using a boundary integral formulation involving general order free-surface ring-source Green functions. The general second-order hydrodynamic problem in three dimensions has also been treated by Zaraphonitis and Papanicolaou (1991) who evaluated the second-order potentials and associated forces on arbitrarily shaped large floating bodies using improved integration techniques for the free-surface integration.

However, Newman's argument is well-founded only in the case of **deep water** and requires that the two frequencies forming the difference ω_i-ω_j are **within a short distance**. In order to clarify the two preconditions, reference is made once again to a case of free waves (no body present) in the presence of at least two frequencies. There are two components for the difference-frequency problem; the first one being found directly from $\Phi^{(1)}{}_w$ and the second one depending on $\Phi^{(2)}{}_w$. Actually, it is shown that the amplitude of the fluid velocity associated with the second-order potential goes to zero as the beat frequency approaches zero, in a case of deep water. This result (which can be proved only for free waves) confirms that $\Phi^{(2)}$ can be omitted. Sometimes, the

wavelength associated with these beat-frequency waves may be very, very long and in this case one must treat them as shallow-water waves. In such a problem, the fluid velocities arising from the second-order beat-frequency potential do not disappear as the beat frequency approaches zero. It must be noted that this happens only for second-order waves because of their **very low frequency**. First-order waves can well continue being treated as deep water waves.

Bowers (1976) studied the longitudinal drift force on a moored ship in head waves. In his analysis, he had to consider the second-order difference-frequency waves as shallow-water waves. The typical wave period in the spectrum of incident waves, in his problem, was about 5 sec. This is linked to a wavelength of about 40 m which can be taken as a deep-water wave. The natural frequency of the mooring system was 0.1 rad/sec or less, corresponding to wavelengths of 250 m or even more. This is why the difference-frequency motion associated with the natural frequency of the mooring system is undoubtedly a shallow-water motion. Therefore, Newman's argument is invalid and Bower's had to include both first-order and second-order potential's effects in his calculations. According to Bowers' computed results and comparisons between the cases with and without the effects of $\Phi^{(2)}$, the importance of the second-order potential was more evident for surge movement.

Pinkster and Huijsmans (1982) found that their computed forces, concerning low-frequency forces on a semi-submersible in waves, were 30% to 40% lower than their measured forces. In their analysis second-order potential is neglected and as stated by Bowers the discrepancies can be justified by the non-existence of $\Phi^{(2)}$. Nevertheless, while comparing different theories the dissimilarities between them must not be left behind. Pinkster and Huijsmans solved a problem of a semi-submersible, and they did include diffraction effects at least within the scope of the first-order potential. Bowers was concerned with a ship in head waves only, without calculating diffraction effects. As a result, the comparison between them is not obvious.

Newman's argument in not valid for the vertical-plane motions mentioned already, because the corresponding resonance frequencies are considerably higher than in the horizontal-plane motions. The vertical-plane problems encompass this great difficulty.

2.5 Different types of wave forces

A summary of all the different types of wave forces is going to be presented so that the classification of the wave drift forces is possible. A structure exposed to the action of sea waves is subjected to forces that arise from the presence of different mechanisms. The following types of forces are marked out:

a. Froude-Kryloff forces are the forces exerted to the fictitious contour of the structure from the sea waves. The basic assumption used in defining these forces is that the presence of the body does not deform the fluid field, therefore the body is considered to be invisible. These forces are easily calculated through the direct integration of the pressure's flow field of the simple harmonic wave on the wetted surface of the body.

b. Diffraction forces are the forces generated if the presence of the body and the following deformation of the wave field are taken into consideration. The body is assumed to be present but immovable. Hence, a new potential due to the diffraction effect is introduced. In the framework of linear theory, the superposition principle is

valid and we can sum the undisturbed incident wave potential and the diffraction potential. The forces that come out from this summation constitute the hydrodynamic exciting loads.

c. Radiation forces emanate from the movement of the structure, when a moving structure is considered. This movement of the structure gives rise to waves which are characterized by the radiation potential. The radiation potential in its turn leads to radiation forces exerted on the moving structure. In a linear theory consideration, in a similar way the characteristic potential can be also added to the other potentials.

d. Resistance forces are due to the viscosity of the flow field and are proportional to the velocity square. They are present if the fluid is real. The drag forces obtained by the Morison's formula belong to this category.

e. Other forces: The sea wave exciting forces have a non-linear nature. Therefore, they can be divided in forces of different orders. The forces described in a, b and c constitute the first-order forces, which are calculated by the solution of the linear problem. Moreover, there are the forces of second-order and of superior order. Drift-forces correspond to second-order forces. It is also important to mention that the radiation forces and the Froude-Kryloff forces are usually reported in bibliography as fluid inertia forces.

In areas of the fluid flow where the drag forces exerted on the body can be neglected (when they have a value inferior to the 10% of the total force) it can be made use of the potential theory. The flow is assumed to be incompressible, inviscid and irrotational. Such a consideration is realistic in the majority of calculation problems of the loads of massive offshore constructions as long as the significant phenomena of diffraction of the flow are taken into consideration.

3. NEAR-FIELD METHOD

The Pinkster's potential method for calculating the drift forces, termed also the "Direct Pressure Integration" or the "Near-Field" method, is going to be presented. This is a method applicable to all six degrees of freedom and yields results for both **mean** and **low-frequency** wave drifting forces. The procedure is based on direct integration of all contributions to the second-order forces over the **instantaneous** wetted surface of the hull of the structure. The body is considered to move with zero or very low forward speed.

3.1 Perturbation Theory

The theory is developed in accordance with perturbation theory methods which however include some limitations. The perturbation theory is a very useful tool predicting non-linear effects at the cost of restriction in fairly small wave amplitudes and wave slopes. In this theoretical context, it is also assumed that the side walls of the structure meet the undisturbed free surface at right angles in order to avoid singularities not predicted by linear theory.

By referring to a perturbation analysis, it is assumed that there is a small parameter $\varepsilon<<1$, called steepness which can act as a basis for series expansions representations of all quantities that come up. For example, the steepness may depict the relation between the amplitude of the waves and the wavelength. We can therefore imagine this parameter equal to $\varepsilon=\frac{H}{2\lambda}$.

Practically, the velocity potential Φ of the flow and all quantities derivable from the flow such as waveheight, pressures, potentials, motions etc., are considered to vary only very slightly relative to some initial, static value. They can all take the following written form:

$$X=X^{(0)}+\varepsilon X^{(1)}+\varepsilon^2 X^{(2)}+\dots,$$

where the affixes $^{(0)}$, $^{(1)}$, $^{(2)}$ denote respectively the static value, the first-order oscillatory variation and the second-order variation.

Ogilvie (1983) in his analysis refers to the existing problem of invalidation of the basic assumptions of the perturbation theory, when the horizontal excursions of a platform are found larger compared with the platform's dimensions. Triantafyllou (1982) solved this problem by observing that the platform's velocity may remain quite small (if we associate it with the small amplitude of fluid particle velocities), even while allowing large excursions of the platform in the horizontal plane. According to him, the entire hydrodynamic problem can be analyzed to a series of linear hydrodynamic problems.

3.2 Co-ordinate Systems

Three different co-ordinate systems are applied. The linearization process is present in the formulation of these systems and therefore they are developed with respect to the mean position of the body and to the mean free surface. The first $G\text{-}x_1\text{-}x_2\text{-}x_3$ is a Cartesian ship-fixed co-ordinate system which follows the movement of the ship. The system's point of origin is the centre of gravity G and the positive direction of the $G\text{-}x_3$ axis is vertically upwards in the mean position of the oscillating vessel. It is chosen in a way so that its planes of symmetry coincide with the body's planes of symmetry. The hull geometry of a ship is unambiguously defined relative to this system and the position of a point on this surface is described by the vector $\vec{x}$. The orientation of a surface element in this system is defined by the outward pointing normal vector $\vec{n}$ (a vector pointing to the fluid and not to the surface of the body). This system can be also named as the system of "body axes".

The second co-ordinate system $0\text{-}x_1\text{-}x_2\text{-}x_3$ is a fixed inertia system with axes parallel to the $G\text{-}x_1\text{-}x_2\text{-}x_3$ system, when the body lies in a calm state. The system's origin is on the mean free surface of the fluid in calm state.

Finally, the third system $G\text{-}x_1'\text{-}x_2'\text{-}x_3'$ has origin in the centre of gravity G of the body and its axes remain at all times parallel to the axes of the fixed system $0\text{-}x_1\text{-}x_2\text{-}x_3$. The system is subjected only to translation motions with respect to the fixed inertia system $0\text{-}x_1\text{-}x_2\text{-}x_3$ and coincides with $G\text{-}x_1\text{-}x_2\text{-}x_3$ when the latter is in its mean position.

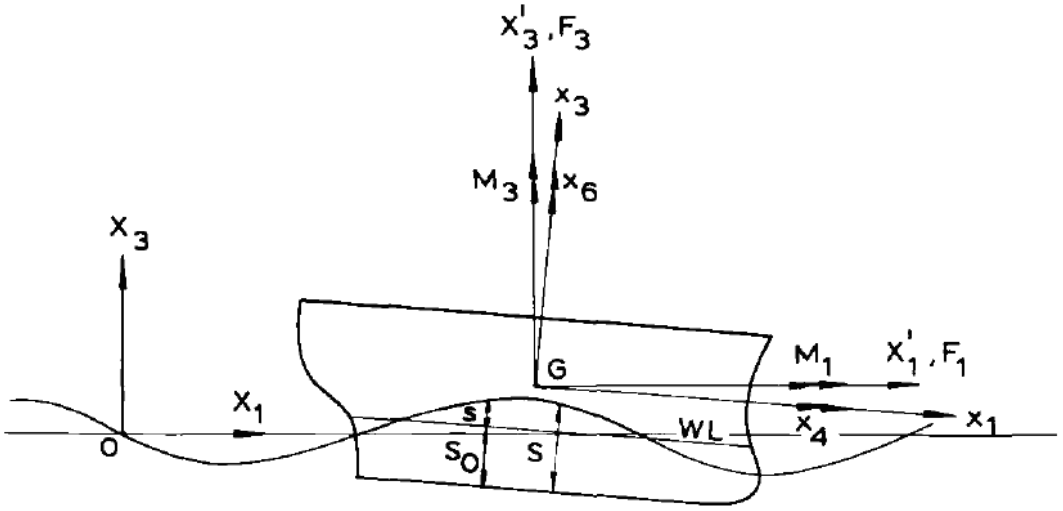

Figure 3-1: Co-ordinate systems [Fig. from Pinkster (1979)].

From the preceding schema we observe that the Eulerian angles x_4, x_5 and x_6 represent the angular motions of the body about the body axes.

3.3 Motions of a point on the body

Assuming that the body is floating in small amplitude waves subjected to the first-order hydrodynamic forces, the arising displacement of a point P (on the surface) of the body has to be a small **first-order quantity** as well. It is convenient to express the displacement vector $\overrightarrow{X}$ relative to the fixed system of axes $0\text{-}x_1\text{-}x_2\text{-}x_3$ because this is going to be our system of reference through which we are going to depict all our variables:

$$\overrightarrow{X} = \varepsilon \overrightarrow{X}^{(1)} \qquad \varepsilon << 1 \tag{3.1}$$

In kinematics, the displacement of a rigid body can be represented by its translation, namely the position of one of the particles of the body specifically chosen as a reference point (typically coinciding with the center of mass or centroid of the body), together with its angular position (also known as orientation or attitude of the body). Thus, the position $\vec{X}^{(1)}$ is consisted of two components: linear and angular respectively:

$$\overrightarrow{X}^{(1)} = \overrightarrow{X}_g{}^{(1)} + R^{(1)} \cdot \vec{x} \tag{3.2}$$

where $\vec{X}_g{}^{(1)}$ is the first-order displacement vector of the point G relative to the fixed system of axes $0\text{-}x_1\text{-}x_2\text{-}x_3$, $\vec{x}$ is the time invariable vector of the position of a point P on the body relative to the system $G\text{-}x_1\text{-}x_2\text{-}x_3$ and $\vec{R}^{(1)}$ the matrix which contains the rotation angles about the system $G\text{-}x_1\text{-}x_2\text{-}x_3$, in our case the first-order oscillatory angular motions.

$$R^{(1)} = \begin{bmatrix} 0 & -x_6^{(1)} & x_5^{(1)} \\ x_6^{(1)} & 0 & -x_4^{(1)} \\ -x_5^{(1)} & x_4^{(1)} & 0 \end{bmatrix} \text{ and } \vec{x} = \begin{bmatrix} x_1 \\ x_2 \\ x_3 \end{bmatrix} \tag{3.3}$$

The prefixes $x_4^{(1)}, x_5^{(1)}, x_6^{(1)}$ are respectively the first-order roll, pitch and yaw motions.

In a similar way, we may analyze the velocity $\vec{v}$ of the point P relative to the fixed system of axes. This is also a first-order quantity. Thus, for the first-order problem the perturbation series provides us with the following equation:

$$\vec{v} = \dot{\vec{X}} = \varepsilon \dot{\vec{X}}^{(1)} \tag{3.4}$$

where

$$\dot{\vec{X}}^{(1)} = \dot{\vec{X}}_g{}^{(1)} + \dot{R}^{(1)} \cdot \vec{x} \tag{3.5}$$

and

$$\dot{R}^{(1)} = \begin{bmatrix} 0 & -\dot{x}_6^{(1)} & \dot{x}_5^{(1)} \\ \dot{x}_6^{(1)} & 0 & -\dot{x}_4^{(1)} \\ -\dot{x}_5^{(1)} & \dot{x}_4^{(1)} & 0 \end{bmatrix} \tag{3.6}$$

.

The existence of the outward pointing normal vector $\vec{n}$ in the system of axes G-x_1-x_2-x_3 has been already denoted. Moreover, the surface orientation vector $\vec{n}$ will be transformed to a vector $\vec{N}$ in the fixed system of axes. This transformation will be also accurate for the third system of axes G-x_1'-x_2'-x_3', with axes always parallel to the 0-x_1-x_2-x_3 system. The vector $\vec{N}$ is time variable; the orientation of the surface elements is affected by the rotation of the body.

$$\vec{N} = \vec{N}^{(0)} + \varepsilon \vec{N}^{(1)} = \vec{n} + \varepsilon \vec{N}^{(1)} \tag{3.7}$$

where

$$\vec{N}^{(1)} = R^{(1)} \cdot \vec{n} \tag{3.8}$$

$R^{(1)}$ is once again given by equation (3.3).

Even if it is not our case, it is reported that equations (3.2), (3.5) and (3.8) are valid for all orders. The general form of (3.2) is the following and in a similar manner the general forms of (3.5) and (3.8) are formed.

$$\overrightarrow{X}^{(i)} = \overrightarrow{X}_g^{(i)} + R^{(i)} \cdot \vec{x} \quad \text{i} = 0, 1, 2,.. \tag{3.9}$$

where,

$$R = \begin{bmatrix} a_{11} & a_{12} & a_{13} \\ a_{21} & a_{22} & a_{23} \\ a_{31} & a_{32} & a_{33} \end{bmatrix}$$

with,

$$\begin{aligned}
a_{11} &= \cos x_5 \cdot \cos x_6 \\
a_{12} &= \sin x_4 \cdot \sin x_5 \cdot \cos x_6 - \cos x_4 \cdot \sin x_6 \\
a_{13} &= \cos x_4 \cdot \sin x_5 \cdot \cos x_6 + \sin x_4 \cdot \sin x_6 \\
a_{21} &= \cos x_5 \cdot \sin x_6 \\
a_{22} &= \sin x_4 \cdot \sin x_5 \cdot \sin x_6 + \cos x_4 \cdot \cos x_6 \\
a_{23} &= \cos x_4 \cdot \sin x_5 \cdot \sin x_6 - \sin x_4 \cdot \cos x_6 \\
a_{31} &= -\sin x_5 \\
a_{32} &= \sin x_4 \cdot \cos x_5 \\
a_{33} &= \cos x_4 \cdot \cos x_5
\end{aligned}$$

Furthermore, the rotation matrix is developed to a Taylor series in order to provide us with $R^{(0)}$, $R^{(1)}$, $R^{(2)}$. Equation (3.3) is the result of this procedure for the first-order. The fact that in equation (3.7) $\vec{N}^{(0)} = \vec{n}$, comes also from this procedure. The way we have defined the system of axes justifies this result as well.

3.4 Fluid Motions and Boundary Conditions

The fluid domain is bounded by the free surface, the wetted surface of the floating object and the sea bottom. The fluid under consideration is water; therefore it is assumed to be incompressible at all times. Furthermore, supposing that the fluid is inviscid, irrotational and homogeneous the fluid motions can be described by a velocity potential Φ and hence the velocity in the fluid is $\vec{V} = \vec{\nabla}\Phi$. As already mentioned, the velocity potential can be expressed through a perturbation series:

$$\Phi = \varepsilon\Phi^{(1)} + \varepsilon^2\Phi^{(2)} + \ldots \tag{3.10}$$

The potentials are considered relative to the fixed system of $0\text{-}x_1\text{-}x_2\text{-}x_3$ axes.

In this problem, there exist **two unknown** quantities: the potential $\Phi(\vec{x},t)$ and the free surface elevation $\eta(x_1,x_2,t)$, which must satisfy the following boundary conditions. Basically, these boundary conditions are non-linear. The axes are the same as for the potentials, i.e. fixed in space:

1. Everywhere **within the fluid field** $D = D(\eta)$ the Laplace equation, which expresses the continuity of the flow and the irrotationality of the flow field, is satisfied. This equation represents the physical principle of conservation of mass. This is a linear equation itself:

$$\Delta\Phi = \vec{\nabla}^2\Phi = 0\,,\ \vec{x} \in D \tag{3.11}$$

Since Φ satisfies the linear Laplace equation, each $\Phi^{(i)}$ in the perturbation series also satisfies the Laplace equation. For our case, it must be satisfied to first and to second-order.

2. At the **water surface** ∂D_F we have two boundary conditions. The two boundary conditions which follow are written in a linearized form. This fact restricts our results to small amplitudes of both the motions and the incoming wave field. Naturally, the boundary conditions are applied to the actual moving free surface $x_3 = \eta$. Implementing a linearization procedure by means of Taylor series expansions, they are transformed into boundary conditions at the fixed mean free surface $x_3 = 0$. Because there are no exterior restrictions to the water surface, these boundary conditions will be referred to as the free surface:

- The pressure should be constant on the free surface and equal to the atmospheric pressure p_0 (dynamic condition).

$$\dot{\Phi} + g\eta = 0 \quad \vec{x} \in \partial D_F : x_3 = 0 \tag{3.12}$$

- The fluid normal to the free surface is equal to the velocity of the surface in the same direction. This fact states that a fluid particle cannot leave the surface, or in other words that no fluid particles pass through the free surface (kinematic condition).

$$\frac{\partial \Phi}{\partial x_3} = \dot{\eta} \quad \vec{x} \in \partial D_F : x_3=0 \tag{3.13}$$

By removing the dependence on the free surface elevation $\eta(x_1,x_2,t)$, the two equations are combined and to first-order the following homogeneous condition is obtained:

$$g\Phi^{(1)}{}_{X_3} + \ddot{\Phi}^{(1)} = 0 \quad \vec{x} \in \partial D_F : x_3=0 \tag{3.14}$$

The second-order boundary condition is non-homogeneous and is satisfied if:

$$g\Phi^{(2)}{}_{X_3} + \ddot{\Phi}^{(2)} = -2 \cdot \vec{\nabla}\Phi^{(1)} \cdot \vec{\nabla}\dot{\Phi}^{(1)} + \dot{\Phi}^{(1)}(\Phi^{(1)}{}_{X_3X_3} + \frac{1}{g} \cdot \ddot{\Phi}^{(1)}_{X_3}) \quad \vec{x} \in \partial D_F : x_3=0 \tag{3.15}$$

3. The boundary condition at the **sea floor** ∂D_Π states that to first and to second-order no fluid particles may cross this boundary. Therefore, both the normal component of the fluid velocity and the normal component of the surface velocity must be equal to zero:

$$\frac{\partial \Phi^{(i)}}{\partial \vec{n}} = U_n = 0 \quad (i = 1,2) \ , \ x_3=-h \tag{3.16}$$

where $\vec{n}$ is the normal vector of a point on the surface of the sea bottom and U_n is the bottom surface velocity.

4. The **floating body wetted** surface ∂D_B is assumed to be impermeable, so no fluid particles can pass through this boundary. This fact is expressed by the condition of continuity of the normal velocities between the fluid and the floating object:

$$\vec{\nabla}\Phi \cdot \vec{N} = \vec{U} \cdot \vec{N} \quad , \ \vec{x} \in \partial D_B \tag{3.17}$$

where $\vec{U}$ is the velocity of the body surface itself.

An equivalent form of equation (3.17) is the following:

$$V_n = U_n \quad , \ \vec{x} \in \partial D_B$$

At first, the condition must be satisfied to first and to second-order at the instantaneous position of the hull surface. Right after, we will write down the linear expansion.
To first-order the boundary condition is as follows:

$$\vec{\nabla}\Phi^{(1)} \cdot \vec{n} = \vec{U}^{(1)} \cdot \vec{n} \tag{3.18}$$

And its linear expansion has the same form:

$$\vec{\nabla}\Phi^{(1)} \cdot \vec{n} = \vec{U}^{(1)} \cdot \vec{n} \tag{3.19}$$

To second-order:

$$\vec{\nabla}\Phi^{(2)} \cdot \vec{n} = (\vec{U}^{(1)} - \vec{\nabla}\Phi^{(1)}) \cdot \vec{\mathrm{N}}^{(1)} \tag{3.20}$$

Linear expansion:

$$\vec{\nabla}\Phi^{(2)} \cdot \vec{n} = -(\vec{\mathrm{X}}^{(1)} \cdot \vec{\nabla})\vec{\nabla}\Phi^{(1)} \cdot \vec{n} + (\vec{U}^{(1)} - \vec{\nabla}\Phi^{(1)}) \cdot \vec{\mathrm{N}}^{(1)} \tag{3.21}$$

To second-order, there is an additional term which is due to the procedure of linearization, when applying the Taylor expansion to the velocity $\vec{\nabla}\Phi^{(1)}$. In the linearized equations, the potentials and their derivatives must be considered at the mean position of the body.

5. To make the solution of our mathematical model unique, an extra condition has to be imposed, which is called **radiation condition**. This condition describes how the potential $\Phi(\vec{\mathrm{x}},t)$ acts in very large distances away from the body. It suggests that $\Phi(\vec{\mathrm{x}},t)$ must describe only waves which travel away from the body. Otherwise there would be solutions for waves having been created at infinity, fact that has no physical meaning. When studying the equations analytically, this condition can be imposed to infinity. However, in numerical studies limited computer time and memory may impede this. In this case, this condition has to be given on an artificial boundary.

3.5 Potentials

The first order potential $\Phi^{(1)}$ can be decomposed to a sum of three potentials: the potential due to the undisturbed incoming waves, the diffraction potential, and the radiation potential:

$$\Phi^{(1)} = \Phi^{(1)}{}_{\mathrm{w}} + \Phi^{(1)}{}_{\mathrm{d}} + \Phi^{(1)}{}_{\mathrm{R}} \tag{3.22}$$

The diffraction potential and the radiation potential express respectively the disturbance of the free surface field due to the presence of the body (when it is considered to be motionless) and the movements of the body. These two potentials substitute the unknown potentials which have to be defined in a way that the total potential $\Phi^{(1)}$ satisfies all the boundary conditions. The first-order potential of the undisturbed **incoming** waves does not have to comply with the radiation condition as it refers to incoming waves, whereas the radiation condition has to be applied to the potentials $\Phi^{(1)}{}_{\mathrm{d}}$ and $\Phi^{(1)}{}_{\mathrm{R}}$. The physical meaning of the diffraction and radiation potential will be clarified after their substitution in the floating object's boundary condition.

Therefore, we substitute equation (3.22) in boundary condition (3.19) and our problem takes the following form:

$$\{\vec{\nabla}\Phi^{(1)}{}_{\mathrm{w}} + \vec{\nabla}\Phi^{(1)}{}_{\mathrm{d}} + \vec{\nabla}\Phi^{(1)}{}_{\mathrm{R}}\}\ \vec{\mathrm{n}} = \vec{U}^{(1)} \cdot \vec{n} \tag{3.23}$$

Afterwards, since the main problem is linear it can be decomposed to two problems:

$$\text{Diffraction Problem:} \qquad \vec{\nabla}\Phi^{(1)}{}_{d} \cdot \vec{n} = -\vec{\nabla}\Phi^{(1)}{}_{w} \cdot \vec{n} \tag{3.24}$$

$$\text{Radiation Problem:} \qquad \vec{\nabla}\Phi^{(1)}{}_{R} \cdot \vec{n} = \vec{U}^{(1)} \cdot \vec{n} \tag{3.25}$$

From equation (3.24) it is obvious that in order to determine the diffraction potential, the body is assumed to be motionless and there exist only the undisturbed incoming waves. The Radiation Problem suggests that the radiation potential depends exclusively on the real motions of the body but in calm water. According to the solution of the first-order problem, the combination of $\Phi^{(1)}{}_{d}$ with $\Phi^{(1)}{}_{w}$ provides us with the first-order wave exciting forces. Moreover, through $\Phi^{(1)}{}_{R}$ the hydrodynamic reaction forces are defined, which can be expressed in terms of added mass and damping coefficients. More details on this procedure are written down in the description of the proposed theoretical model. Complete first-order solutions are discussed at length in literature. In the following, it is assumed that the first-order solution is known.

In the second-order problem, it is firstly found a potential satisfying the **free-surface** condition, without regard to the body condition. By combining equations (3.22) and (3.15), a general form for the second-order potential is obtained:

$$\Phi^{(2)} = \Phi^{(2)}{}_{ww} + \Phi^{(2)}{}_{dd} + \Phi^{(2)}{}_{bb} + \Phi^{(2)}{}_{wd} + \Phi^{(2)}{}_{wb} + \Phi^{(2)}{}_{db} + \Phi^{(2)}{}_{dw} + \Phi^{(2)}{}_{bw} + \Phi^{(2)}{}_{bd} + \Phi^{(2)}{}_{d} \tag{3.26}$$

where the first nine components of the right side are particular solutions to the following type of boundary condition:

$$g\Phi^{(2)}{}_{ww_{X3}} + \Phi^{(2)}{}_{ww_{tt}} = -2\vec{\nabla}\Phi^{(1)}{}_{w} \cdot \vec{\nabla}\Phi^{(1)}{}_{w_t} + \Phi^{(1)}{}_{w_t} \left\{ \Phi^{(1)}{}_{ww_{X3X3}} + \frac{1}{g}\Phi^{(1)}{}_{ww_{ttX3}} \right\} \tag{3.27}$$

The last potential $\Phi^{(2)}{}_{d}$ is a kind of "ordinary" potential which is in agreement with the linearized homogeneous free surface condition:

$$g\Phi^{(2)}{}_{d_{X3}} + \Phi^{(2)}{}_{d_{tt}} = 0 \tag{3.28}$$

Equation (3.26) will be simplified by assuming only two components for the second-order potential. The first component, representing the sum of the first nine components on the right-hand side of equation (3.26), may be considered as the second-order equivalent of the first-order undisturbed wave. In general, this potential presents a problem due to the complexity of the second-order surface boundary condition. The second component is without any change the potential $\Phi_{d}^{(2)}$.

$$\Phi^{(2)} = \Phi^{(2)}{}_{w} + \Phi^{(2)}{}_{d} \tag{3.29}$$

Concerning the radiation condition in the second-order problem, it must be imposed exclusively in the calculation of $\Phi^{(2)}{}_{d}$. Likewise to the first-order problem where there was no radiation condition for $\Phi^{(1)}{}_{w}$, in this problem a radiation condition

for $\Phi^{(2)}{}_w$ needs not to be imposed. The components of $\Phi^{(2)}{}_w$ are particular solutions to the free surface boundary condition (3.27) which is valid over the complete free surface.

Since the expression for the second-order potential has been simplified, an approach to the second-order **body boundary** condition can be made. Through the combination of equations (3.29) and (3.21) it is obtained:

$$\left(\vec{\nabla}\Phi^{(2)}{}_w + \vec{\nabla}\Phi^{(2)}{}_d\right)\cdot\vec{n} = -(\vec{X}^{(1)}\cdot\vec{\nabla})\vec{\nabla}\Phi^{(1)}\cdot\vec{n} + (\vec{U}^{(1)} - \vec{\nabla}\Phi^{(1)})\cdot\vec{N}^{(1)} \tag{3.30}$$

Or

$$\vec{\nabla}\Phi^{(2)}{}_d\cdot\vec{n} = \left\{-\vec{\nabla}\Phi^{(2)}{}_w - (\vec{X}^{(1)}\cdot\vec{\nabla})\vec{\nabla}\Phi^{(1)}\right\}\cdot\vec{n} + (\vec{U}^{(1)} - \vec{\nabla}\Phi^{(1)})\cdot\vec{N}^{(1)} \tag{3.31}$$

Equation (3.31) illustrates directly how the second-order diffraction potential $\Phi^{(2)}{}_d$ is formed. It is deduced that $\Phi^{(2)}{}_d$ firstly acts in a way similar to $\Phi^{(1)}{}_d$ as it compensates the second-order velocity components of $\Phi^{(2)}{}_w$. Moreover, it compensates the second-order correction to the first-order velocity $\vec{\nabla}\Phi^{(1)}$, which is the additional term due to the Taylor expansion, mentioned in (3.21). It is also evident that the second-order diffraction potential depends on the difference between the first-order velocity $\vec{U}^{(1)}$ of the body surface and the first-order fluid velocity $\vec{\nabla}\Phi^{(1)}$ in a direction along the first-order normal $\vec{N}^{(1)}$. Pinkster (1980) during the procedure of decomposition of the second-order potential includes the additional component of $\Phi^{(2)}{}_R$. The potential $\Phi^{(2)}{}_R$ is equivalent to $\Phi^{(1)}{}_R$ but it satisfies the boundary condition on the body carrying out **low frequency second-order motions** in still water. As it is the case for $\Phi^{(1)}{}_R$, $\Phi^{(2)}{}_R$ may be also expressed in terms of hydrodynamic reaction forces. In our problem, this potential is not studied as it has been assumed that the body is strictly allowed to act in response to the first-order oscillatory hydrodynamic forces.

If the right-hand side of equation (3.31) is known, $\Phi^{(2)}{}_d$ can be solved using numerical methods. From the solution of $\Phi^{(2)}{}_d$ and $\Phi^{(2)}{}_w$, the low frequency second-order wave exciting forces are defined. However, the major problem is the verification of the non-homogeneous second-order free surface condition and thus, the definition of the second-order potential becomes a tremendous undertaking. A general formula for this can be found in Wehausen and Laitone (1960), but the numerical work prevents anyone from fulfilling this task. Nevertheless, the formulation of the entire problem is not pointless since essential information can be still obtained from the formulation of the problem itself.

Furthermore, reference will be made to Pinkster's approximative method, offering at least an indication of the magnitude of the $\Phi^{(2)}$ contribution to the low frequency wave drifting forces.

3.6 Pressure in a point within the fluid

After the determination of the velocity potential Φ and the potential's boundary conditions, the fluid pressure can be defined. Considering the fluid to be

ideal or inviscid, which means that the fluid has no resistance to shear stress, the pressure distribution can be obtained using the Bernoulli equation:

$$p = p_0 - \rho g X_3 - \rho \Phi_t - \frac{1}{2}\rho\left|\vec{\nabla}\Phi\right|^2 + C(t) \tag{3.32}$$

where p_0 stands for the atmospheric pressure and $C(t)$ is a function independent of co-ordinates. Both of these parameters may be taken equal to zero without loss of generality.

In the same time, it can be formulated a definition of the pressure based on the existence of different order pressure components. Assuming that the point is performing small, first-order oscillations $\vec{X}^{(1)}$ in the wave frequency, about a mean position $\vec{X}^{(0)}$, applying a Taylor expansion to the pressure in the mean position and combining these results with equation (3.32) the following expression is derived:

$$p = p^{(0)} + \varepsilon p^{(1)} + \varepsilon^2 p^{(2)} \tag{3.33}$$

where:

Hydrostatic pressure : $$p^{(0)} = -\rho g X_3^{(0)} \tag{3.34}$$

First-order pressure : $$p^{(1)} = -\rho g X_3^{(1)} - \rho \Phi^{(1)}_t \tag{3.35}$$

Second-order pressure: $$p^{(2)} = -\frac{1}{2}\rho\left|\vec{\nabla}\Phi^{(1)}\right|^2 - \rho\Phi^{(2)}_t - \rho(\vec{X}^{(1)} \cdot \vec{\nabla}\Phi^{(1)}_t) \tag{3.36}$$

Theoretically, the hydrostatic component $-\rho g X_3^{(2)}$ owing to the second-order vertical motion should have been also included in the calculation of $p^{(2)}$. This component is neglected since it is part of the second-order reaction forces due to second-order motions of the body.

Based on the Taylor expansion, the derivatives of the potentials also have to be considered in the mean position of the point.

This expression has been formed for a point within the fluid but it is also valid for a point on the hull of the body. This may not seem logical as it is well-known that a point on the hull can be part of the time within and rest of the time outside the actual fluid domain. Nevertheless, according to Joseph (1973) this is permissible if the potential functions are adequately “smooth” at the boundaries.

3.7 Second-order wave force

In the case of harmonic waves, the motion of the ship may be also expected harmonic and thus drifting would be unexpected. Nevertheless, there has been observed drifting even in harmonic waves and there comes up a mean drifting force which is not equal to zero. This is due to the existence of second-order effects since the mean value of the first-order quantities is zero. An attempt will be made to explain

why there is a mean second-order drifting force on a structure exposed to regular incident harmonically oscillating waves. A major contribution to the horizontal mean drifting force, as it will be proved, is the relative vertical motion between a surface piercing body and the waves. Any point in the free-surface zone of the structure is alternately within and outside the actual fluid domain and consequently a non-zero mean pressure is observed even in regular harmonically oscillating waves. Thus, if the relative vertical motion changes around the waterline, we do refer to **non-zero mean wave forces**. This is the case for large-volume structures which modify the incident waves' field.

Before proceeding to the calculation of the drift forces, the applied system of axes has to be selected. The force acting on the body is studied, thus it would be practical to have the object within the frame of the default co-ordinate system. The axes of $G\text{-}x_1'\text{-}x_2'\text{-}x_3'$ system of co-ordinates, which is always parallel to the fixed system $0\text{-}x_1\text{-}x_2\text{-}x_3$, seems to be the most appropriate one.

The body is subjected to the following fluid force:

$$\vec{F} = -\iint_S p \cdot \vec{N} dS \tag{3.37}$$

with S the instantaneous wetted surface and $\vec{N}$ the instantaneous normal vector to the surface element dS, relative to the default system of axes.
This computation is not as easy as it seems to be. The actual position of the body is not known and according to the linearization process all quantities have been calculated on the average position. To this end, it would be practical the separation of the instantaneous wetted surface S into a perturbed and an unperturbed term which are respectively: a constant part S_0 going up to the static waterline on the hull which is equivalent to the mean wetted surface, and an oscillating part $s(t)$ between S_0 and the wave profile along the body. This is apparent in the preceding Figure 3-1. Note that in our case of zero or very low forward speed, the oscillating surface $s(t)$ does not contribute to quantities of first-order. It will be now presented the extraction of the time dependence from $s(t)$.

After combining equations (3.33) and (3.7) it follows that:

$$\begin{aligned}\vec{F} = &-\iint_{S_0} (p^{(0)} + \varepsilon p^{(1)} + \varepsilon^2 p^{(2)})(\vec{n} + \varepsilon \vec{N}^{(1)}) dS + \\ &-\iint_{s(t)} (p^{(0)} + \varepsilon p^{(1)} + \varepsilon^2 p^{(2)})(\vec{n} + \varepsilon \vec{N}^{(1)}) dS = \\ &= \vec{F}^{(0)} + \varepsilon \vec{F}^{(1)} + \varepsilon^2 \vec{F}^{(2)} + O(\varepsilon^3)\end{aligned} \tag{3.38}$$

In this way we derive the hydrostatic force $\vec{F}^{(0)}$, the first-order oscillatory fluid force $\vec{F}^{(1)}$ and the second-order force $\vec{F}^{(2)}$.

Hydrostatics describes fluids in a calm state, when there is not observed relative movement between different molecules of the fluid. The hydrostatic force is the stationary contribution to the power series of forces and is the application of

Archimedes' law. It results from the integration of the hydrostatic pressure $p^{(0)}$ over the mean wetted surface S_0. The total hydrostatic force and moment is equilibrated by the weight of the floating body.

$$\vec{F}^{(0)} = F_3^{(0)} = \rho g \iint_{S_0} X_3{}^{(0)} \vec{n} dS = (0,0,\rho g V) \tag{3.39}$$

where V represents the displaced volume.

The total first-order oscillatory fluid force arises from the integration of the first-order pressure $p^{(1)}$ over the mean wetted surface S_0 and normal vector $\vec{n}$, as well as from the integration of the static pressure $p^{(0)}$ over S_0 and normal vector $\vec{N}$ so that there is always a first-order product, being preceded by ε.

$$\vec{F}^{(1)} = -\iint_{S_0} (p^{(1)}\vec{n} + p^{(0)}\vec{N}^{(1)}) dS = -\iint_{S_0} -\rho g X_3{}^{(1)} \vec{n} dS + \iint_{S_0} \rho \Phi_t{}^{(1)} \vec{n} dS + \vec{R}^{(1)} \cdot (0,0,\rho g V) \tag{3.40}$$

The first two terms represent the total first-order fluid force relative to the body axes $G\text{-}x_1\text{-}x_2\text{-}x_3$. They correspond to the hydrostatic restoring force [first term] and to the first-order wave exciting force and the hydrodynamic reaction force (added mass and damping force) [second term]. The third term is the hydrostatic contribution to pressure being multiplied by the matrix of first-order angular displacements. This term is also relative to the body axes.

The total second-order force $\vec{F}^{(2)}$ comes out on the one hand after integrating all the products of pressure p and normal vector $\vec{N}$, which contribute to second-order forces, over the constant part S_0 and on the other hand after integrating all first-order pressures over the oscillating surface $s(t)$.

$$\vec{F}^{(2)} = -\iint_{S_0} (p^{(1)}\vec{N}^{(1)} + p^{(2)}\vec{n}) dS - \iint_{s(t)} p^{(1)}\vec{n} dS \tag{3.41}$$

Taking into consideration that:

$$\vec{N}^{(1)} = \vec{R}^{(1)} \cdot \vec{n} \tag{3.42}$$

And since angular displacements are identical for all surface elements dS, the **first part of the first integral** is transformed to:

$$-\iint_{S_0} p^{(1)}\vec{N}^{(1)} dS = \vec{R}^{(1)} \cdot (-\iint_{S_0} p^{(1)}\vec{n} dS) \tag{3.43}$$

The entire equation is a consequence of the choice of the axes $G\text{-}x_1'\text{-}x_2'\text{-}x_3'$ to which the second-order force is referenced. It demonstrates that after a rotation relative to $G\text{-}x_1'\text{-}x_2'\text{-}x_3'$ a first-order fluid force relative to the body axes can create a second-order force contribution relative to $G\text{-}x_1'\text{-}x_2'\text{-}x_3'$ system of axes. Furthermore, an

example is given by Pinkster (1979b) for surge drifting force. He reports that after a rotation even a vertical first-order force can give rise to a longitudinal second-order component.

Likewise, the first-order component of the hydrostatic force acting on the body relative to the body axes, is considered to be a second-order force if acting on $G\text{-}x_1'\text{-}x_2'\text{-}x_3'$.

If this component is added to equation (3.43):

$$\vec{R}^{(1)} \cdot \left\{ -\iint_{S_0} p^{(1)} \vec{n} dS + \vec{R}^{(1)} \cdot (0,0,\rho g V) \right\} = \vec{R}^{(1)} \cdot \vec{F}^{(1)} \tag{3.44}$$

Where $\vec{F}^{(1)}$ is the total first-order fluid force including all the first-order components of equation (3.40). As $\vec{F}^{(1)}$ is the total first-order force it can be also expressed through the Newton's law:

$$\vec{F}^{(1)} = M \cdot \ddot{\vec{X}}_g{}^{(1)} \tag{3.45}$$

From which it follows that:

$$\vec{R}^{(1)} \cdot \vec{F}^{(1)} = \vec{R}^{(1)} \cdot (M \cdot \ddot{\vec{X}}_g{}^{(1)}) \tag{3.46}$$

The **second part of the first integral** in equation (3.41) involves a straightforward integration of the **hydrodynamic pressure** over the mean submerged part of the hull as given by Bernoulli for $p^{(2)}$.

The **second integral** over the oscillating surface $s(t)$ is solved after making use of equation (3.35) for $p^{(1)}$ and the following equation for the surface element dS. This step imposes some geometrical restrictions, like a vertical ship hull at the free surface.

$$dS = dX_3 \cdot dl \tag{3.47}$$

Right after, we rely on the dynamic condition on the water surface in order to approximate $\Phi^{(1)}{}_t$ at the static waterline of the vessel which is near to z=0:

$$-\rho \Phi_t{}^{(1)} = \rho g \zeta^{(1)} \tag{3.48}$$

where $\zeta^{(1)}$ is the first-order wave elevation

Therefore after combining the preceding equations it follows that:

$$-\iint_{s(t)} p^{(1)} \vec{n} dS = -\int_{WL} \int_{X^{(1)}_{3_{WL}}}^{\zeta^{(1)}} (-\rho g X_3 + \rho g \zeta^{(1)}) \vec{n} \cdot dX_3 dl \tag{3.49}$$

The relative wave height is the wave height as measured from the vessel:

$$\zeta_r^{(1)} = \zeta^{(1)} - \mathrm{X}_{3_{WL}}^{(1)} \tag{3.50}$$

where $\mathrm{X}_{3_{WL}}^{(1)}$ is the first-order vertical motion of a point on the hull at the waterline.

Consequently, the final expression for the integral is simplified in the following form:

$$-\int_{WL} \frac{1}{2}\rho g(\zeta_r^{(1)})^2 \vec{n} dl \tag{3.51}$$

Basically, this contribution is connected with the statement that near the surface the pressure in the waves can be approximated by the hydrostatic pressure. The aforementioned equation reveals that the hydrostatic pressure increase at both the mean waterline on the hull and the additional area where the pressure acts is proportional to the relative wave height. The integral around the time dependent oscillating surface has been transformed to a line integral around the **static waterline of the vessel**. Additionally, by introducing the relative wave height an equation completely relative to the motion of the vessel has been obtained.

The working out of equation (3.41) can be written as:

$$\vec{F}^{(2)} = -\int_{WL} \frac{1}{2}\rho g(\zeta_r^{(1)})^2 \vec{n} dl - \iint_{S_0} \left\{ -\frac{1}{2}\rho \left|\vec{\nabla}\Phi^{(1)}\right|^2 - \rho\Phi^{(2)}{}_t - \rho(\vec{\mathrm{X}}^{(1)} \cdot \vec{\nabla}\Phi^{(1)}{}_t) \right\} \vec{n} dS + \\ + R^{(1)} \cdot (M \cdot \ddot{\vec{X}}_g^{(1)}) \tag{3.52}$$

3.8 Contribution of the different components of the mean second-order wave exciting forces

There are five components in equation (3.52). Pinkster through his computations analyses the behavior of each component in sign and in magnitude. These results are presented in the following Figure 3-2 and refer to the mean surge drifting force on a rectangular barge and a semi-submersible. In Figure 3-3 Pinkster illustrates a comparison between these different contributions and the total mean horizontal drifting force. These results concern the three-dimensional case of a free floating hemisphere in infinitely deep water.

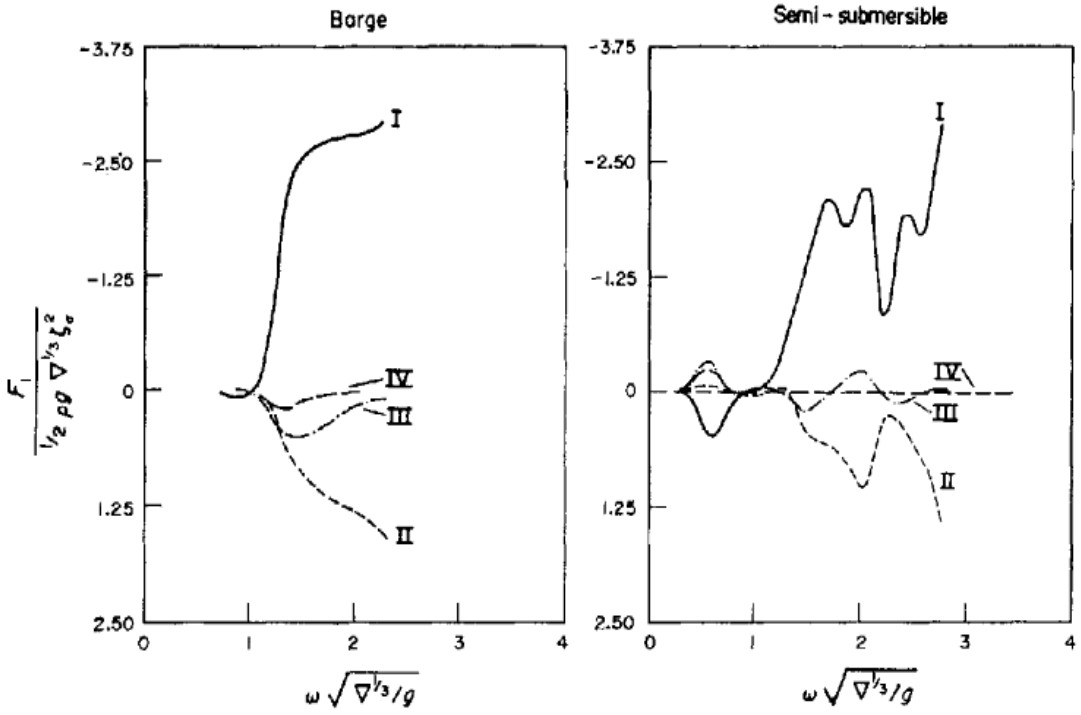

Figure 3-2: Components of the computed mean surge drifting force [Fig. from Pinkster (1979b)].

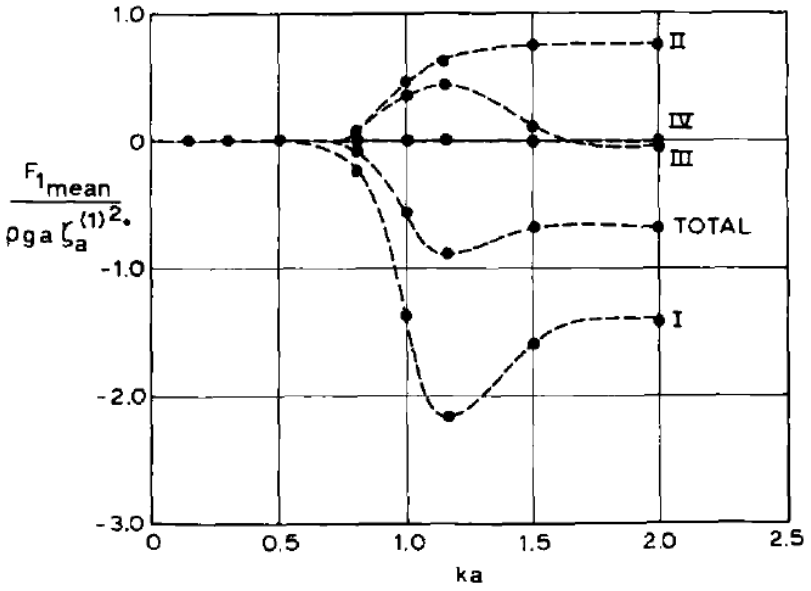

Figure 3-3: Components of the computed mean second-order horizontal drift force [Fig. from Pinkster (1979b)].

It is observed that contribution I, due to the relative wave elevation, is preponderant while the other contributions tend to reduce the effect of contribution I. In the case of the sphere this contribution is twice larger in magnitude than the total force and has always the same sign with it. It expresses a pressure increase and its sign coincides with the direction of propagation of the waves.

As it comes out from the example of the sphere, contribution II, which is the effect of the square of the velocity, is different in sign but equivalent in magnitude to the total. It represents a pressure decrease and what is remarkable is that it corresponds to a mean force component which, contrary to intuition, is directed into the waves.

The following contribution, due to the second-order potential $\Phi^{(2)}$, is not taken into consideration in the calculation of the mean drift forces in regular waves.

The following term, which is a mixed product of pressure gradient and first-order motion, will be termed as contribution III. It is quite complicated to predict the exact sign of this term. The sign depends on the phase angles of both quantities. This component is linked with the motions of the body and the pressure gradients. In the case of the sphere, it is smaller in magnitude and acts differently than the total force. At very high wave frequencies where the wavelengths are small, the motion of the vessel tends to zero and consequently this is also the case for the force component. At low frequencies, the pressure gradients tend to nullification and so does the force. This is apparent in all examples.

Contribution IV is the last term which incorporates the products of angular motions and body accelerations. In the example of the sphere, it is zero because there are no angular motions. Generally speaking, it is only in intermediate frequencies that this component takes a non-zero value which depends on the phase between the first-order included components. Similarly to contribution III, in high frequencies where the waves are considered to be short, the hull tends to immobilization and at low frequencies accelerations tend to zero.

Noteworthy is the fact that finally at high wave frequencies, as it is proved by all examples, only contributions I and II remain.

In Figure 3-4, the computed mean vertical wave drifting force is presented for the same structures presented in Figure 3-2. It is depicted that the mean vertical force on the barge is downwards while on the semi-submersible it is upwards. On the presumption that both vessels have vertical walls at the waterline, contribution I is zero. Contribution II and also partly contribution III and contribution IV give rise to the mean vertical wave drifting force. The peak in the mean vertical drift response function takes place at the natural pitch and heave frequency.

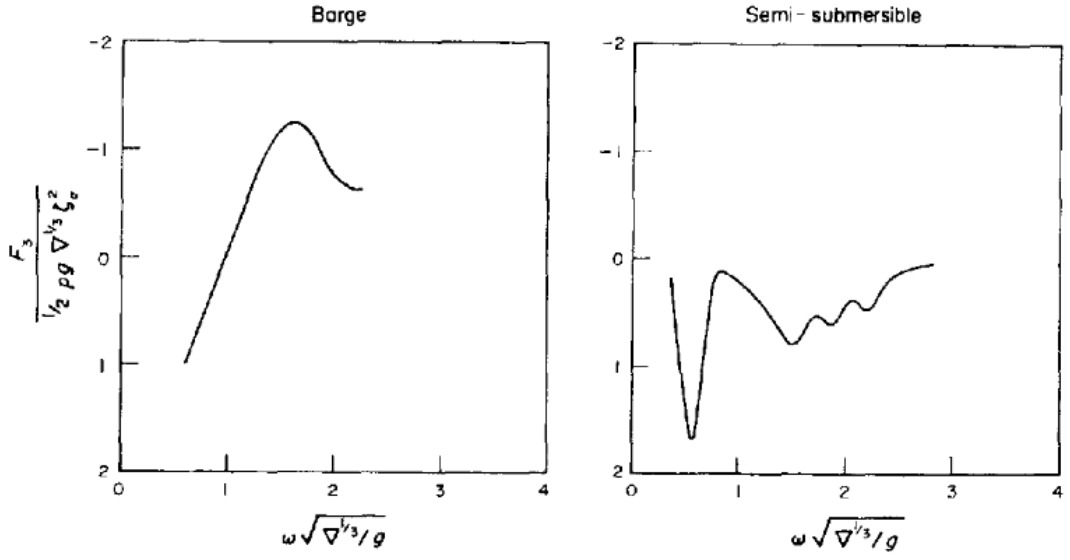

Figure 3-4: Components mean heave drifting force [Fig. from Pinkster (1979b)].

3.9 Second-order wave moment

The moment of the fluid about the axes of G-x_1'-x_2'-x_3' system follows from:

$$\overrightarrow{M} = -\iint_S p \cdot (\overrightarrow{X} \times \overrightarrow{N}) dS \tag{3.53}$$

The adopted procedure for obtaining the moments is similar to the procedure we followed for obtaining the forces.
The final formulae for the drift forces and drift moments are almost equivalent. The differences are that translational motion is replaced by the rotational motion, and the normal $\vec{n}$ by $\vec{x}\times\vec{n}$:

$$\overrightarrow{M}^{(2)} = -\int_{WL} \frac{1}{2}\rho g(\zeta_r^{(1)})^2(\vec{x}\times\vec{n})dl + R^{(1)}\cdot(I\cdot\ddot{\vec{X}}_g^{(1)}) +$$
$$-\iint_{S_0}\left\{-\frac{1}{2}\rho\left|\vec{\nabla}\Phi^{(1)}\right|^2 - \rho\Phi_t^{(2)} - \rho(\vec{X}^{(1)}\cdot\vec{\nabla}\Phi_t^{(1)})\right\}\cdot(\vec{x}\times\vec{n})dS \tag{3.54}$$

Equations (3.52) and (3.54) include the **total second-order loads** acting on a vessel; the wave exciting force in the absence of motions, the hydrodynamic and hydrostatic reaction force. Generally, we focus more on the second-order wave exciting force so the dependence on the other components has to be eliminated. In our case, in which we have not taken into account the second-order displacement, there are no second-order terms of hydrostatic reaction forces. The hydrodynamic reaction force is hidden in the total second-order potential $\Phi^{(2)}$, in the specific term of $\Phi_R^{(2)}$. It has been already noted the difficulty in the determination of the second-order potential. However, in the calculation of the mean drift forces the contribution due to $\Phi^{(2)}$ is zero in regular waves and we have no interest towards this potential in this problem. In the following sections it will be shown that in practice for irregular waves in finite depth a simple approximation of these second-order potential contributions can be used. To sum up, what we get if we neglect $\Phi^{(2)}$ is a wave exciting force and moment, but without the components of $\Phi^{(2)}$ that do contribute to the wave force in irregular waves.

3.10 Quadratic transfer functions for the mean and slow-drift (or low frequency) wave drifting force in irregular waves

The expressions for the second-order wave exciting forces and moments obtained by the direct integration method on the wetted surface of a body may give an insight into the mechanism by which the waves and vessels interact to produce the second-order force, but their form is quite complicated for practical applications. In this section, an attempt is made to formulate the forces under consideration by means of **time independent** quadratic transfer functions (QTF) for the mean and low frequency force and moment components. This will also allow the transition from time domain to frequency domain. Generally, frequency-domain methods are very useful in the preliminary design stage since they are computationally more efficient although time-domain analysis is indispensable for the final design purpose.

We start with low frequency second-order forces and furthermore we are going to clarify how we get mean wave forces in irregular sea-state.

Considering the different components of equation (3.52), the **total quadratic function** also consists of contributions due to first-order and second-order quantities. We focus on first-order quantities and as we are interested in the **low frequency forces**, the low frequency part of the longitudinal force's component due to the first-order contribution of the relative wave elevation is treated.

$$F_1^{(2)} = F_1(t) = -\int_{WL} \frac{1}{2}\rho g(\zeta_r^{(1)})^2(\mathrm{t},l)\cdot n_1(l)\cdot dl \tag{3.55}$$

where:

$(\zeta_r^{(1)})^2(\mathrm{t},l)$ = time dependent relative wave elevation in a point l along the waterline

$n_1(l)$ =direction cosine of a length element dl in longitudinal direction

The goal is to separate the double dependence of ζ_r on time and on a specific point l along the waterline into two components: a time independent part which includes the dependency on this specific point along the waterline and a time dependent part.

The treatment of low frequency components infers that the corresponding environment is an irregular wave system. A simple approach is to decompose this wave system to a discrete spectrum of regular waves. It is assumed that the waves are long-crested. Thus, the first-order wave elevation of the incoming, undisturbed, long-crested waves with respect to the mean position of the centre of gravity of the floating body is a sum of regular wave components:

$$\zeta^{(1)}(t) = \sum_{i=1}^{N} \zeta_i^{(1)} \cos(\omega_i t + \varepsilon_i) \tag{3.56}$$

The square of the wave elevation is:

$$\left\{\zeta^{(1)}(t)\right\}^2 = \sum_{i=1}^{N}\sum_{j=1}^{N} \zeta_i^{(1)}\cdot\zeta_j^{(1)} \cos(\omega_i t + \varepsilon_i)\cos(\omega_j t + \varepsilon_j) \tag{3.57}$$

The low frequency part of the square of the wave elevation is derived by applying the identity $\cos(x)\cdot\cos(y) = \frac{1}{2}\left[\cos(x-y)+\cos(x+y)\right]$:

$$\left\{\zeta^{(1)}(t)\right\}^2 = \sum_{i=1}^{N}\sum_{j=1}^{N} \frac{1}{2}\zeta_i^{(1)}\cdot\zeta_j^{(1)} \cos\left\{\left(\omega_i-\omega_j\right)t + \left(\varepsilon_i-\varepsilon_j\right)\right\} \tag{3.58}$$

The first-order relative wave elevation at a point l along the waterline can be written as:

$$\zeta_r^{(1)}(t,l) = \sum_{i=1}^{N} \zeta_i^{(1)}\cdot\zeta_{r_i}^{(1)'}(l)\cos\left\{(\omega_i t + \varepsilon_i + \varepsilon_{r_i}(l)\right\} \tag{3.59}$$

$\zeta_i^{(1)}$ = amplitude of i-th regular wave component

ω_i = frequency of i-th component

ε_i = random phase uniformly distributed over 0-2π

$\zeta_{r_i}^{(1)'}(l)$ = time independent transfer function of the amplitude of the first-order relative wave elevation

$\varepsilon_{r_i}(l)$ = phase angle of the relative wave elevation related to the undisturbed wave crest passing the centre of gravity. It has the role of a phase transfer function.

Combination of equations (3.55), (3.57) and (3.59) gives as a result:

$$F_1^{(2)}(t) = \sum_{i=1}^{N}\sum_{j=1}^{N} \zeta_i^{(1)} \cdot \zeta_j^{(1)} \cdot P_{ij} \cdot \cos\left\{\left(\omega_i - \omega_j\right)t + (\varepsilon_i - \varepsilon_j)\right\} +$$
$$+ \sum_{i=1}^{N}\sum_{j=1}^{N} \zeta_i^{(1)} \cdot \zeta_j^{(1)} \cdot Q_{ij} \cdot \sin\left\{\left(\omega_i - \omega_j\right)t + (\varepsilon_i - \varepsilon_j)\right\} +$$
$$+ \text{high frequency terms} \qquad (3.60)$$

The coefficients P_{ij} and Q_{ij} can be interpreted as transfer functions for the low frequency loads. The word "transfer function" means that these coefficients are independent of wave amplitudes and of time and thus they can be calculated independently of the sea state. Briefly, the calculation of these transfer functions requires the knowledge of the first-order amplitude and phase transfer functions as a function of the wave frequency. More specifically, as denoted by the coexistence of the subscripts i and j, P_{ij} and Q_{ij} are a function of two wave frequencies ω_i and ω_j:

$$P_{ij} = \int_{WL} \frac{1}{4}\rho g \zeta_{r_i}^{'(1)} \zeta_{r_j}^{'(1)} \cos\left\{\varepsilon_{r_i}(l) - \varepsilon_{r_j}(l)\right\} n_1 dl \qquad (3.61)$$

.

$$Q_{ij} = -\int_{WL} \frac{1}{4}\rho g \zeta_{r_i}^{'(1)} \zeta_{r_j}^{'(1)} \sin\left\{\varepsilon_{r_i}(l) - \varepsilon_{r_j}(l)\right\} n_1 dl \qquad (3.62)$$

If we take the low frequency part of the square of the wave elevation as it is given in equation (3.58), it is found that P_{ij} and Q_{ij} give respectively the part which is in-phase and out-of-phase with the low frequency part of the square of the incident waves. In other words, they provide us with the in- and out-of phase low frequency oscillating part of the second-order wave exciting forces when the body is exposed to a wave train constituted by two regular waves.

In similar ways, we can find the other contributions which depend on first-order quantities. The total in-phase and out-of-phase transfer functions are calculated by summation of all contributions. There is also a second-order contribution to the low frequency part of the longitudinal component of $F^{(2)}$ due to $\Phi^{(2)}$. In *Chapter 3.13*, it is presented Pinkster's simplifying formula for estimating $\Phi^{(2)}$ and for evaluating the quadratic transfer functions due to the second-order potential in relation to the QTFs obtained for the first-order relative wave height.

The most basic sea state which generates low frequency wave drifting forces is depicted. It consists of two frequencies:

$$\zeta^{(1)}(t) = \sum_{i=1}^{2} \zeta_i^{(1)} \cdot \cos(\omega_i t + \varepsilon_i) =$$
$$= \zeta_1^{(1)} \cdot \cos(\omega_1 t + \varepsilon_1) + \zeta_2^{(1)} \cdot \cos(\omega_2 t + \varepsilon_2) \qquad (3.63)$$

The wave drifting force in this case is:

$$F^{(2)}(t) = \sum_{i=1}^{2}\sum_{j=1}^{2} \zeta_i^{(1)} \zeta_j^{(1)} P_{ij} \cdot \cos\left\{\left(\omega_i - \omega_j\right)t + \left(\varepsilon_i - \varepsilon_j\right)\right\} +$$
$$+ \sum_{i=1}^{2}\sum_{j=1}^{2} \zeta_i^{(1)} \zeta_j^{(1)} Q_{ij} \cdot \sin\left\{\left(\omega_i - \omega_j\right)t + \left(\varepsilon_i - \varepsilon_j\right)\right\} =$$
$$= \zeta_1^{(1)^2} \cdot P_{11} + \zeta_2^{(1)^2} \cdot P_{22} +$$
$$+ \zeta_1^{(1)} \zeta_2^{(1)} (P_{12} + P_{21}) \cos\left\{\left(\omega_1 - \omega_2\right)t + \left(\varepsilon_1 - \varepsilon_2\right)\right\} +$$
$$+ \zeta_1^{(1)} \zeta_2^{(1)} (Q_{12} - Q_{21}) \sin\left\{\left(\omega_1 - \omega_2\right)t + \left(\varepsilon_1 - \varepsilon_2\right)\right\} \qquad (3.64)$$

There are two constant components in this equation. Each one illustrates the force which would be found if the wave group consisted of a single regular wave. In irregular sea-state, these are the representatives of the **mean wave force** in the total second-order force containing both constant and low frequency parts. A remarkable fact is that although the total force is a non-linear phenomenon, the constant or the mean second-order force acts as a first-order force. The superposition principle, which suggests that in an environment of two or more wave disturbances each disturbance can be propagated in space independently of the others, is valid. Consequently, the mean wave force in a wave group consisting of a superposition of regular waves is the sum of the mean forces acting on each of the constituent waves.

$$F_{mean}^{(2)} = \sum_{i=1}^{N} \zeta_i^{(1)^2} \cdot P_{ii} = \sum_{i=1}^{N} \zeta_i^{(1)^2} \cdot P(\omega_i, \omega_i) \qquad (3.65)$$

This formula is explained by the fact that in an irregular sea-state the only time independent terms describing a time-average occur when $i = j$. Hence, in both regular and irregular waves the mean wave drift force can be expressed as a function dependent on one frequency. Another interesting comment coming out from Pinkster's analysis that we have pursued, is that the quadratic transfer function of the mean wave force $P(\omega_i, \omega_i)$ appears to be a special case of the general $P(\omega_i, \omega_j)$ characterizing the force in regular wave groups.

Apart from the constant parts, low frequency parts which are a function of the difference frequency $\omega_1 - \omega_2$ are also present in equation (3.64). It is observed that the amplitudes of the in-phase transfer functions depend on the sum of the in-phase quadratic transfer functions P_{12} and P_{21}. Similarly, the amplitudes of the out-of-phase functions depend on the difference of the corresponding transfer functions. Contrary to the mean force, the transfer functions for low frequency components do not appear in isolation but are joined in pairs. As this is the case, these components may be chosen at random so that for instance:

$$P(\omega_i, \omega_j) \neq P(\omega_j, \omega_i)$$

However, as it is known a priori that they appear in pairs, they can be rearranged so that the following symmetry relations are valid: the in-phase component $P(\omega_i,\omega_j)$ takes the form of a matrix which is symmetrical about the diagonal while the out-of-phase $Q(\omega_i,\omega_j)$ is asymmetrical about the diagonal:

$$P(\omega_i,\omega_j) = P(\omega_j,\omega_i) \tag{3.66}$$

$$Q(\omega_i,\omega_j) = -Q(\omega_j,\omega_i) \tag{3.67}$$

and

$$T_{ij} = T_{ji}, \text{ where } T_{ij} = \sqrt{P_{ij}^{\ 2} + Q_{ij}^{\ 2}} \tag{3.68}$$

where T_{ij} is the amplitude of the quadratic transfer function.

3.11 Frequency domain representation of the mean and low frequency wave drifting force

Equations (3.64) and (3.65) describe the low-frequency and mean second-order wave exciting forces that arise from first-order quantities in irregular waves as a function of time for discrete values of the frequencies ω_i and ω_j.

The irregular waves are characterized by a spectral density or energy density $S(\omega_i)$ where:

$$S(\omega_i)d\omega_i = \frac{1}{2}\zeta_i^{(l)^2} \tag{3.69}$$

The transition from a discrete to a continuous representation is possible through correlation between equations (3.65) and (3.69):

$$F_{1_{mean}}^{(2)} = 2\int_0^\infty S(\omega)P(\omega,\omega)d\omega \tag{3.70}$$

Similarly it can be shown that the spectral density of the low frequency oscillating part of the wave drifting force follows from:

$$S_F(\mu) = 8\int_0^\infty S(\omega_1)S(\omega_2)\left[T(\omega_1,\omega_2)\right]^2 d\omega_2 \tag{3.71}$$

where $\omega_1 - \omega_2 = \mu$ is the low frequency and $T(\omega_1,\omega_2)$ is the amplitude of the quadratic transfer function as given by equation (3.68).

Equation (3.72) can also take the following form:

$$S_F(\mu) = 8\int_0^\infty S(\omega+\mu)S(\omega)\left[T(\omega+\mu,\omega)\right]^2 d\omega \tag{3.72}$$

3.12 Newman's approximations

A second-order contribution to the **slowly varying forces** stems from the existence of the second-order potential. Instead of analyzing the quantities which depend on $\Phi^{(2)}$, reference will be made once again to Newman's approximations applicable to the case of deep water. Newman (1974) focuses on the same component analyzed by Pinkster which is the low frequency contribution of the component arising from the relative waveheight. Some restrictions are introduced and Newman proves that the low frequency transfer functions can be formed in terms of the mean forces transfer functions. Thereby, we remain in the mean second-order force problem in regular waves and there is no need to solve for $\Phi^{(2)}$ as required in a sea state of irregular waves.

Newman stresses out the fact that we can observe slowly varying forces between all components of the spectrum. It is very important to study the slowly varying forces in a framework of a complete analysis especially in the case where a low resonant frequency exists. If this is the case, it is likely that the moored vessel with the low natural frequency resonates with the ω_i-ω_j components of the sea.

Newman formulates the wave elevation's expression which comes out by a discrete spectrum of unidirectional waves. To first-order the force arises directly from the wave elevation if we appeal to the first-order transfer function. There is also the analogous expression for the second-order force thanks to second-order transfer functions, which contains both sum and difference frequency components. The transfer functions corresponding to the difference frequency components are identical to those mentioned in the analysis of Pinkster but here they also incorporate the phase transfer function. Newman concentrates on the difference loads:

$$f(t) = \mathrm{Re}\sum_m \sum_n A_m A_n^* F_{mn} e^{i(\omega_m - \omega_n)t} \tag{3.73}$$

where an asterisk $(*)$ indicates the complex conjugate and F_{mn} is the transfer function for the difference frequency. F_{mn} represents the **total transfer function** including both the in-phase (real part) and the out-of-phase (imaginary part) terms with the low frequency part of the square of the incident waves quadratic transfer functions.

Newman takes the time-average of this force:

$$\overline{f} = \frac{1}{2}\mathrm{Re}\sum_m A_m A_m^* F_{mm} \tag{3.74}$$

The time independent terms are dominated by $m = n$. Hence, the time-average is described by F_{mm}. Newman introduces his first assumption; since these expressions are preceded by the real designation and as long as they include no other imaginary term, the imaginary part of F_{mm} has no sense. F_{mm} is supposed to be real. In a physical sense, this transfer function can now describe the second-order steady force acting on the vessel in regular waves of unit amplitude and frequency ω_m.

Furthermore, the investigator studies the non-diagonal terms F_{mn} which represent the amplitude and phase of the difference-frequency force in a regime of two simultaneous waves with frequencies ω_m and ω_n. Firstly, a question of correlation between these transfer functions is posed. According to him, the most practical

solution is to ascribe to two off-diagonal terms, which are in the same time complex conjugates, an equal contribution to the total force:

$$F_{mn}=F_{nm}^{*} \tag{3.75}$$

This is exactly similar to the sum of equations (3.66) and (3.67) for P and Q, obtained by Pinkster.

Eventually, Newman attempting to express F_{mn} in terms of F_{mm} generalizes the idea of time average in the case of the "slowing varying force". At this point, his second assumption is imposed. For practical reasons, the time average of the slowly varying force is associated with those off-diagonal elements for which $\omega_m \cong \omega_n$; this hypothesis implies that the difference of frequencies has to be very small compared to the average:

$$|\omega_m - \omega_n| \ll \frac{1}{2}(\omega_m + \omega_n) \tag{3.76}$$

Furthermore, Newman's second assumption has also a physical meaning because a large frequency difference $\omega_m - \omega_n$ gives a smaller oscillation period which is further away from the resonance period of the structure.

As a result, the slowly varying force can only be linked to those terms which are very close to the principal diagonal for which $\omega_m \cong \omega_n$. In fact, we realize that if the difference frequency is sufficiently small, so that we do not depart too much from the diagonal, and supposing that F_{mn} are regular functions of the two frequencies, F_{mn} is simplified:

$$F_{mn} = F_{mm} + O(\omega_m - \omega_n) \tag{3.77}$$

This function turns out to depend only on the transfer function of the diagonal F_{mm} plus on a term which is attributed to the small existing difference between the frequencies. However, we must be cautious if F_{mm} exhibits pronounced maxima because this means that we are in the resonance area and therefore adjacent F_{mn} may present significantly different values. Equation (3.73) takes the following form:

$$\widetilde{f(t)} = \mathrm{Re}\sum_m \sum_n A_m A_n^{*} F_{mm} e^{i(\omega_m - \omega_n)t} + O(\omega_m - \omega_n) \tag{3.78}$$

What changes now at the formulation of the time-average problem of the forces under consideration is that the asymptotic approximation to the slowly varying force depends exclusively on the regular wave second-order transfer function F_{mm}. As a lot more is known about this transfer function in comparison with the off-diagonal terms F_{mn}, equation (3.78) can be exploited to offer us at least a simple approximation for the slowly varying second-order forces. In addition to this, under this asymptotic approximation with the support of F_{mm}, F_{mn} gets also the real character of F_{mm}. In total, it is observed that during Newman's approximations the quadratic transfer functions are real quantities and thus, they offer an estimation of the real part P.

Nevertheless, the double summation in equation (3.78) requires a large computational time. Newman overcomes this difficulty by substituting the double series with the square of an appropriate chosen single series.

Newman concludes that the quantitative accuracy of his approximations may vary from one case to another. Some knowledge of the off-diagonal second-order forces coming out from the simultaneous presence of two discrete wave systems is of primary importance in order to have a complete image of this approximate calculation. Because of the mysterious character of these forces, in most cases the present approximation is the best solution instead of complete ignorance of the phenomenon.

3.13 Approximation for the contribution of the second-order potential

Inevitably, there are some cases where Newman's argument is annulated. In *Chapter 2.4,* we have already justified the two preconditions (deep water and ω_i close to ω_j) that ensure the validity of Newman's argument in a case of free waves. An important case of invalidation is when referring to mooring systems in shallow water because they are stiffer than deep water ones and the difference of frequencies is higher. Bowers (1976) is based on his scale model results of a barge in irregular head waves and points out that, as the natural surge frequency is increased by increasing the stiffness of the mooring system, the impact of $\Phi^{(2)}$ on the low frequency drifting force also increases. A general assumption is that when natural frequencies are low owing to the large effective mass in relation to the stiffness of the mooring system, the second-order potential can be neglected whereas in the opposite case the contribution due to this potential may be important. It seems that in a great number of LNG terminals, which are near-shore terminals, the second-order potential contribution to the quadratic transfer functions cannot be neglected.

We have already reported the difficulty to solve for $\Phi^{(2)}$ in the complete second-order problem due to the complexity of the non-homogeneous second-order free surface condition (equation (3.15)). Pinkster (1979b) makes an attempt to provide us with an indication of the magnitude of the contribution of $\Phi^{(2)}$ to the low frequency wave drifting forces. He invokes an approximative method based on linear potential theory which is practical for both two and three dimensions as well as for a case of shallow water.

Pinkster states that in equation (3.26) which offers the general form of $\Phi^{(2)}$, $\Phi^{(2)}{}_{ww}$ is the dominant term concerning the low frequency second-order force due to $\Phi^{(2)}$. $\Phi^{(2)}{}_{ww}$ stands for the second-order potential associated with the undisturbed incoming first-order wave potential. This statement implies that $\Phi^{(1)}{}_{d}$ and $\Phi^{(1)}{}_{R}$ are small relative to $\Phi^{(1)}{}_{w}$. In practice, in the sophisticated inhomogeneous free surface condition (3.15) this assumption allows us to substitute $\Phi^{(1)}$ for the terms involving the first-order velocity potential of the undisturbed incoming waves.

Moreover, Pinkster presents the form of the first-order velocity potential arising from the undisturbed incoming regular wave group of two regular waves. Hereafter $\Phi^{(i)}{}_{w}$ will be replaced by $\Phi^{(i)}{}_{I}$:

$$\Phi^{(1)}{}_I = -\sum_{i=1}^{2} \frac{\zeta_i g}{\omega_i} \frac{\cosh k_i (X_3 + h)}{\cosh k_i h} \sin(k_i X_1 + \omega_i t + \varepsilon_i) \tag{3.79}$$

Then the **low frequency component** of $\Phi^{(2)}$ that comes out from the same wave group is as follows:

$$\Phi^{(2)}{}_I = -\sum_{i=1}^{2}\sum_{j=1}^{2} \zeta_i \zeta_j A_{ij} \frac{\cosh\{(k_i - k_j)(X_3 + h)\}}{\cosh(k_i - k_j)h} \sin\{(k_i - k_j)X_1 + \\ +(\omega_i - \omega_j)t + (\varepsilon_i - \varepsilon_j)\} \qquad , \ \omega_i \geq \omega_j \tag{3.80}$$

Bowers denotes that A_{ij} is a coefficient which is a function of the frequencies ω_i, ω_j and the waterdepth *h*.

The expression (3.80) for $\Phi^{(2)}{}_I$ describes **long waves** which are introduced by the presence of the regular wave group. In the following Figure 3-5 it is indicated that the phase of these long waves in comparison with the short wave group's phase presents a trough where the wave group develops its maximum wave height. The potential $\Phi_I{}^{(2)}$ represents an accompanying long wave to the bichromatic sea-state, inducing a decrease (set-down) of the mean free-surface. By what means are we going to calculate the contribution of $\Phi^{(2)}{}_I$ to the second-order low-frequency forces?

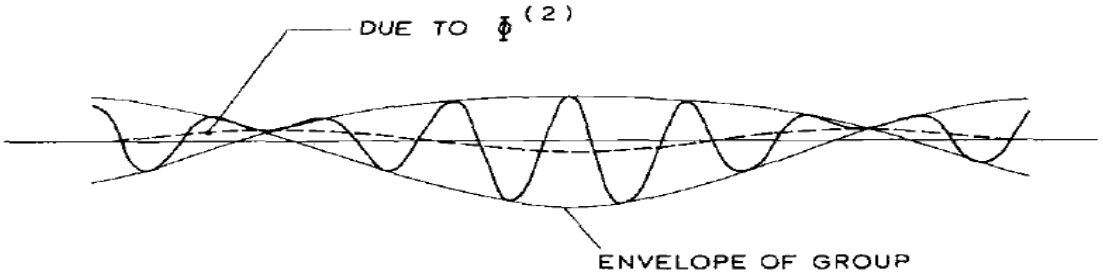

Figure 3-5: Wave due to the second-order potential of a wave group [Fig. from Pinkster (1979b)]

According to the second assumption of Pinkster, the long waves linked to this potential can be regarded as separate waves. The potential of a separate wave does not satisfy the boundary condition on the body which for the simplified case, is assumed to be equivalent to the normal first-order boundary condition. The validity of the normal first-order boundary condition implies that all the first-order contributions in the right hand side of equation (3.21) is zero. In this way, the separate waves introduce a diffraction potential which is described by a motionless body in the presence of undisturbed incoming waves. The $\Phi_d{}^{(2)}$ is considered to be a simple, ordinary potential because it has been already shown that it satisfies the homogeneous free surface condition of equation (3.28). This potential needs only to verify the equation of continuity, the boundary condition at the sea-floor, the radiation condition and the homogeneous free surface condition:

$$g\Phi^{(2)}{}_{d\,x_3} + \Phi^{(2)}{}_{d\,tt} = 0 \tag{3.81}$$

From the last condition the dispersion relationship arises:

$$\omega^2 = kg \tanh kh \tag{3.82}$$

Through equation (3.80) we realize that the undisturbed incoming waves are characterized by a wave number equal to k_i-k_j and a wave frequency equal to ω_i-ω_j. These waves do not follow the dispersion law. If the frequency of the incoming waves is ω_i-ω_j, the diffracted waves' frequency will be the same. However, the wave number of the diffracted waves will not be equal to k_i-k_j but will result from the application of the dispersion relationship:

$$\left(\omega_i - \omega_j\right)^2 = kg \tanh kh \tag{3.83}$$

The third simplification is applied according to which the diffraction waves are allowed to have the same wave number k_i-k_j as the incoming waves. This is permitted only for the diffracted waves which are further away from the body. Near the body, the situation cannot change because the boundary condition at the body still has to be satisfied.

The difficulty level of the problem under consideration has been lowered. It is required the calculation of the low frequency $F^{(2)}$ caused by a wave described by (3.80) while assuming that the diffracted waves have the same wave number and frequency as the incoming waves. The procedure of solution suggests the correlation between the expressions of $\Phi_I^{(1)}$ and $\Phi_I^{(2)}$, or the transition from $F^{(1)}$ to $F^{(2)}$. $F^{(1)}$ acts in the environment of a regular wave with wave number equal to k. In order to produce the wave number of the low-frequency $F^{(2)}$ caused by two regular waves which is equal to $k_i - k_j$ we set:

$$k = k_i - k_j \tag{3.84}$$

We are situated in an ordinary gravity field with g as the constant of gravity. In this case, the wave frequency ω of $F^{(1)}$ obeys the dispersion law. We change ω for $\omega_i - \omega_j$ by choosing another value for the constant of gravity:

$$g_{ij} = \frac{\left(\omega_i - \omega_j\right)^2}{\left(k_i - k_j\right)\tanh\left(k_i - k_j\right)h} \qquad , \ \omega_i \geq \omega_j \tag{3.85}$$

The low-frequency part of $F^{(2)}$ is proportional to the constant of gravity. The first-order velocity potential of equation (3.79), which is responsible for $F^{(1)}$, is also proportional to the constant of gravity. Therefore, in order to express $F^{(2)}$ through $F^{(1)}$ the following correlation factor is used:

$$n_{ij} = \frac{g_{ij}}{g} \tag{3.86}$$

To this end, the transformed potential of the first-order regular wave given by equation (3.79) changes to:

$$\Phi_I^{(1)} = -\sum_{i=1}^{2} \frac{\zeta_a g_{ij}}{\omega_i - \omega_j} \frac{\cosh\left\{\left(k_i - k_j\right)(X_3 + h)\right\}}{\cosh\left(k_i - k_j\right)h} \sin\left\{\left(k_i - k_j\right)X_1 + \right.$$
$$\left. + \left(\omega_i - \omega_j\right)t + \left(\varepsilon_i - \varepsilon_j\right)\right\} \qquad , \ \omega_i \geq \omega_j \qquad (3.87)$$

For the completion of the transformation we merely need to relate the amplitude of the preceding equation (3.87) with the amplitude of equation (3.80):

$$\frac{\zeta_a g_{ij}}{\omega_i - \omega_j} = \zeta_i \zeta_j A_{ij} \qquad , \ \omega_i \geq \omega_j \qquad (3.88)$$

Equation (3.89) expresses that the first-order wave amplitude must be selected in a way that it verifies:

$$\zeta_a = \zeta_i \zeta_j \frac{A_{ij}\left(\omega_i - \omega_j\right)}{g_{ij}} \qquad , \ \omega_i \geq \omega_j \qquad (3.89)$$

The low-frequency $F^{(2)}$ is also proportional to the wave amplitude. Thus, equation (3.89) depicts the second correction factor imposed on $F^{(1)}$ in order to provide us with $F^{(2)}$. In total we get:

$$F^{(2)}{}_{ij} = n_{ij} \frac{\zeta_i \zeta_j A_{ij}\left(\omega_i - \omega_j\right)F^{(1)}}{g_{ij}} \qquad , \ \omega_i \geq \omega_j \qquad (3.90)$$

After combining (3.90) with (3.86) **the low-frequency part of $\mathbf{F^{(2)}}$ owing to $\mathbf{\Phi_I^{(2)}}$** is obtained**.** We have obviated the computation of $\Phi^{(2)}$ itself:

$$F^{(2)}{}_{ij} = f_{ij} \cdot F^{(1)} \qquad (3.91)$$

where

$$f_{ij} = \frac{\zeta_i \zeta_j A_{ij}\left(\omega_i - \omega_j\right)}{g} \qquad , \ \omega_i \geq \omega_j \qquad (3.92)$$

To this end, one would worry if they are still valid the foregoing quadratic transfer functions for the low frequency wave drifting forces defined by equation (91). In order to comply with the definition of the quadratic transfer functions due to first-order relative wave height, the in- and out-of-phase transfer functions of the force component due to the second-order $\Phi_I^{(2)}$ become:

$$P_{ij} = \frac{1}{2} P^{(2)}{}_{ij} \qquad , \ \omega_i \geq \omega_j \qquad (3.93)$$

$$P_{ij} = P_{ji} \tag{3.94}$$

$$Q_{ij} = \frac{1}{2} Q^{(2)}{}_{ij} \qquad , \ \omega_i \geq \omega_j \tag{3.95}$$

$$Q_{ij} = -Q_{ji} \tag{3.96}$$

Where $P^{(2)}{}_{ij}$ and $Q^{(2)}{}_{ij}$ stand for the in-phase and out-of-phase components of the second-order wave force as determined by equation (3.91).

At this point it is reported that Newman's preconditions are also well explained by means of Pinkster's analysis. According to the analytical expression of $\Phi_{\mathrm{I}}{}^{(2)}$ (equation (3.80)), $\Phi_{\mathrm{I}}{}^{(2)}$ is a function of $(\omega_m - \omega_n)$ and $(k_m - k_n)$, and consequently this potential's contribution vanishes when the difference of frequencies goes to zero. As the water depth decreases there remains a factor $(\omega_m - \omega_n)$ and the contribution of $\Phi_{\mathrm{I}}{}^{(2)}$ at the difference frequency can no longer be neglected.

Pinkster's approximation is exact in cases where the contributions to $\Phi^{(2)}$ of the first-order diffraction and body motions are negligible, so that the $\Phi_I{}^{(2)}$ component is indeed dominant. In general, it is more likely that this requirement is satisfied by vessels like semi-submersibles rather than by ordinary ships or barge shaped structures. Noteworthy in Pinkster's remarks is the statement that when the first-order diffraction and body motion effects grow, the total $F^{(2)}$ will be dominated by first-order phenomena so that the increase in the error of the component owing to $\Phi^{(2)}$ is of small importance relative to the total force.

Moreover, Pinkster presents a specific example where the foregoing approximation gives accurate results. We study the horizontal low frequency wave drifting force arising from $\Phi^{(2)}$, acting on a vertical wall in deep water. In such a problem, total reflection is observed. Therefore, the first-order incoming waves and the first-order outgoing waves are identical. The total second-order potential consists of the contribution of the undisturbed incoming waves and the outgoing diffraction waves. In this case we may have diffraction which is not included in Pinkster's approximation but the formula remains accurate. The reason for this is that since the outgoing component is equal to $\Phi_I{}^{(2)}$, the approximation can well predict both of them.

4. EXAMPLE OF AN LNG-CARRIER MOORED AT A JETTY IN A COMPLEX BATHYMETRY AND DEVELOPMENT OF A CORRECTION FACTOR TO THE QUADRATIC TRANSFER FUNCTIONS

Concerning motions and mooring loads of an LNG- Carrier moored at a jetty in a complex bathymetry area the results from the paper of Weiler et al. (2009) are remarkable. The Yemen LNG Company was planning to design and construct a near-shore LNG plant in the Republic of Yemen. Deltares in Delft together with Marin conducted a study to compare the hydrodynamic scale model tests, in the $40\times40\,m$ basin in Delft, with the computer simulations derived by the software TERMSIM from Marin. The scope of their project was to determine the limiting environmental conditions for loading and safe mooring of the LNG carriers in this very hard to be simulated environment.

The natural periods in the horizontal motions surge, sway and yaw are typically in the range of 30 to 100 sec and this means that both the linear wave response as well as the second-order slow-drift motion must be accounted for in the design of the berthing system. In the formulation of the problem, it must be also considered that the bathymetry around the jetty is very complex. Moreover, the environmental conditions at this area are characterized by monsoon seasons and by a strong sea breeze. A cape near the jetty also influences the incoming wave conditions. The carrier has to stay at the berth almost 24 hours to complete the loading operation and so it will have to face the wave conditions created by the sea breeze blowing during the afternoon. The sea breeze will give rise to a so- called young sea dominated by short-crested (multidirectional) waves. This is why Deltares suggested that short-crested waves should be incorporated in the test conditions. In general, different combinations of tests proceeded: with wind and without wind, and in both short-crested and long-crested waves.

Concerning the short-crested waves, the experiments showed that Deltares' input lead to greater motions and mooring loads compared with long-crested wave conditions. Furthermore, through the comparison of the six motions spectra arising from model tests and simulations (Figure 4-1), it is observed that the greatest discrepancies are found for the surge, sway and yaw responses. For these motions, as we have justified in the beginning of our study, the low-frequency motions are dominant. The numerical simulations assuming long-crested waves (primary waves and low-frequency waves), seem to overestimate the loads. The difference in surge is eventually attributed to the wave loading or the response of the ship on the sloping bathymetry. For sway and yaw the shifts in the peak frequencies can be correlated with differences in added mass. Besides, there is also observed a great difference in roll response. This is ascribed to the differences in sway and yaw.

The genre of these discrepancies does not give away an obvious reason for this variance. An ultimate solution to this problem can be presented by means of the comparison of the quantity of energy between the two different procedures. However, it seems that despite the larger low-frequency wave energy in the basin, the vessel manifests smaller motions compared to numerical simulations. The paper does not explain this contradiction.

Finally, the suggested explanation is that it is the **distribution of energy** which creates the disagreement and not the quantity of energy itself. In the basin the low-frequency energy is spread over a wider range of directions. The basin possesses

a non-uniform bottom with a slope whose steepness is not the same between the two sides of the vessel and there may be a different behavior of the long wave energy predicted by the simulations (flat bottom expressions). Besides, in the simulations the low-frequency waves are co-linear with the primary waves and this may lead to larger vessel responses. In addition, it is possible that a part of the low frequency energy in the basin does not lead to vessel motions and is defused in the interaction of waves with the headland or with the shallow water area near the location of the plant.

In their conclusion, the researchers report that since the condition of short-crested waves excites larger ship motions and mooring loads, it is important to check whether this condition has to be integrated in a problem where local wind gives rise to waves. They also stress out that actually, a conventional numerical code may be inadequate as far as the evolution of low-frequency waves over the bathymetry is concerned. In such a complex bathymetry the assumption of long crested waves with low frequency bound waves (or locked) in the same direction is a very simplifying assumption.

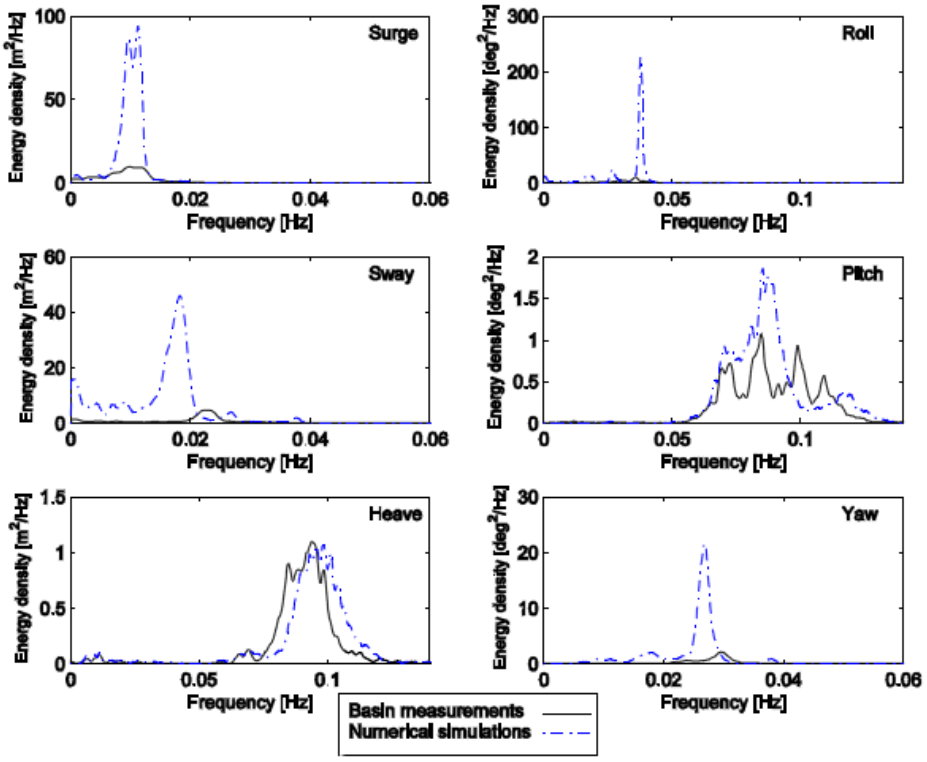

Figure 4-1: Motion spectra from model tests and simulations [Fig. from Weiler et al. (2009)].

From Weiler et al. (2009) we got aware of the failure of the flat bottom expressions to depict a variable bathymetry and to properly estimate the low frequency loads. A mild bottom slope to first-order waves can be very steep to the second-order accompanying long waves. The regular wave drift forces can still be accurately calculated by the flat bottom assumption, whereas, the second-order long waves **shoal up** on the varying bathymetry and not on the limit predicted by the constant depth model. Hence, they are not developed to the full extent following from the flat bottom theory, unless the slope is negligible. Wave shoaling, in simple words, is the effect according to which surface waves increase in wave height when they enter area of shallower water. This is explained by the conservation of energy flux. In the same time, the phases of the various frequency components sometimes give rise to

velocities significantly different from those predicted by the linear finite-depth dispersion velocity. In total the shape of individual shoaling waves changes from an almost symmetrical profile in deep water to a shape with sharp crests and broad, flat troughs in shallow water.

Another significant argument mentioned in Molin et al. (2011) is that the phase relationship of the second-order long waves with the short waves envelope also does not agree with the flat bottom model. The local sea state is not unidirectional and this is attributed either to the long-crested wave system being affected by the variable bathymetry, or to the incoming wave system due to local wind (young seas) being short-crested.

Molin et al. (2011) give a response to Weiler et al. (2009) by introducing a correction factor to the quadratic transfer functions. It is assumed that the incoming wave system initially is and remains long-crested and thus the angular spreading phenomenon is not considered. Molin et al. (2011) focus on the effect of shoaling, which affects the wave both in magnitude and in phase.

If the water depth can no longer be considered as deep, we have to include $\Phi^{(2)}$ in the problem. According to Pinkster $\Phi^{(2)}$ can be approximated by $\Phi_I^{(2)}$ in the calculation of the low frequency second-order force and therefore the correction due to the effect of shoaling refers to this component of the second-order potential. Molin et al. (2011) actually exploit equation (3.60) arising from the integral over the waterline, to import a correction for $\Phi_I^{(2)}$. It is stated that in flat bottom, in a bichromatic wave system, the associated acceleration with the second-order incident potential is 90° out of phase with the short wave envelope. So it seems hat $\Phi_I^{(2)}$ mostly contributes to the out-of phase imaginary part Q of the QTFs. Therefore, in the determination of the low frequency loads when shoaling in varying bathymetry takes place, it is the imaginary part Q which has to be altered. The longwave is reduced in amplitude but is also shifted. Therefore, because of the phase lag the QTF takes the following form:

$$f_-^{(2)}(\omega_i,\omega_j) = P(\omega_i,\omega_j) + iQ(\omega_i,\omega_j)\times R(\omega_i,\omega_j)e^{i\alpha(\omega_i,\omega_j)} = \\ = P - QR\sin\alpha + iQR\cos\alpha \qquad (4.1)$$

with $R \le 1$. As a result, the modulus of the QTF is decreased in comparison with its flat bottom reference value. Furthermore, depending on the value of the phase lag α, it can even get a lower value than the Newman's approximation P alone. The values of R and α depend on the bathymetry profile, from the deep water region to the terminal.

Furthermore, Molin et al. (2011) put forward the problem of the a priori determination of the impact of shoaling in the correction factor in comparison with the flat bottom model. In a bathymetry formed by a constant depth zone with a following rectilinear ramp, the following main parameters are selected: the initial depth, the bottom slope, the mean wave period and the resonant period of the mooring system. It appears that the initial depth is not a critical parameter contrary to the wave and beat periods. Practically, it is concluded that as the bottom slope, the wave period and the beat period increase, the R coefficient gradually decreases and the phase shift α increases. Hence, the low-frequency second-order loads will be significantly lower compared to the values obtained by the flat bottom model.

5. FAR-FIELD METHOD

Another way to obtain expressions for mean wave forces and moments in **regular waves** is to refer to the potential flow theory known as far-field method. Actually this method applies the Newton's second law, or in other words the fundamental equation of conservation of linear and angular momentum in the fluid. The law of conservation of momentum states that if no external force acts on a closed system of objects, the momentum of the closed system remains constant. Actually, through this principle the forces on the structure can be related to the forces on exterior fixed or moving control surfaces and to the rate of change of the fluid momentum between the control surfaces and the body.

A three-dimensional case is studied and thus a control volume Ω needs to be defined in order to proceed with our analysis. Let Ω be the volume bordered by the surface S_B, S_{FS}, S_D and S_∞. S_B depicts the instant wetted surface of the body, S_{FS} the real free surface, S_D the surface of the bottom which is assumed to be horizontal and S_∞ a non-moving vertical cylindrical surface with large radius away from the body. It is remarkable that S_∞ does not need to be far away from the body. The total enclosing control surface S does not need to follow the fluid motion. As system of reference, it has been selected the system $0\text{-}x_1\text{-}x_2\text{-}x_3$ which is fixed in space with z=0 being the plane of the calm water surface and the z-axis positive upwards. The body is considered to be excited by a plane periodic wave, propagating in water of finite depth h.

The linear and angular momentums inside Ω are expressed by the following vectorial forms:

$$\vec{M}(t) = \iiint_{\Omega} \rho \vec{V} d\omega \tag{5.1}$$

$$\vec{H}(t) = \iiint_{\Omega} \rho (\vec{r} \times \vec{V}) d\omega \tag{5.2}$$

where $\vec{V} = \vec{\nabla}\Phi$ is the fluid's velocity and ρ the fluid's density.

By means of the definition of a derivative and taking into account that the rate of change of the system's momentum can be decomposed to a part depending on the rate of change of the momentum of the fluid in the control volume and to a part depending on the rate of the net outflow of the momentum through the control surface S it is obtained:

$$\frac{d\vec{M}}{dt} = \frac{d}{dt}\iiint_{\Omega} \rho \vec{V} d\omega = \rho \iiint_{\Omega} \frac{\partial \vec{V}}{\partial t} d\omega + \rho \iint_{S} \vec{V} U_n dS \tag{5.3}$$

where U_n is the normal component of the velocity of the surface S itself in which the positive normal direction has been defined to be out of the fluid.

Actually the first term of equation (5.3) denotes the non-permanent flow in which the vector of the fluid's velocity may change over time while the control volume remains invariable, whereas the second term stands for the rate of net outflow in the non-

constant surface which may change over time. A non-constant surface in time means that the area S(t) is not identical with the area S(t+Δt). However, Δt should be small.

Right after, we make use of the Euler equation of motion and for an incompressible fluid it can be state:

$$\frac{\partial \vec{V}}{\partial t} + \vec{V} \cdot \vec{\nabla}\vec{V} = -\vec{\nabla}\left(\frac{p}{\rho} + gz\right) \tag{5.4}$$

Then, the Gauss' theorem-divergence theorem is applied in order to transform the volume integral into a surface integral. The divergence theorem is a conservation law which states that the total volume of all sinks and sources, the volume integral of the divergence, is equal to the net flow across the volume's boundary:

$$\iiint_{\Omega} \vec{\nabla} \circ \mathrm{X} d\omega = \iint_{S} \vec{n} \circ X dS \tag{5.5}$$

Here X can be a scalar, vector or tensor and $\circ$ denotes a dot or cross or an ordinary multiplication or nothing. It is assumed that X has continuous derivatives in Ω.
The outcome of the combination of (5.3), (5.4) and (5.5) is:

$$\frac{d\vec{M}}{dt} = -\iint_{S} \left[(p + \rho g z)\vec{n} + \rho \vec{V}(V_n - U_n) \right] dS \tag{5.6}$$

where $V_n = \vec{n} \cdot \vec{\nabla}\Phi$ is the normal component of the fluid velocity at the surface S.

In all the preceding equations $\vec{n}$ is specified to be a unit vector normal to the corresponding surface S. More precisely, with respect to the real free surface $S_{FS,}$ this vector is almost parallel to the unit vertical vector pointing outwards from the fluid. This is valid in an environment of small amplitude harmonic waves. Regarding the body surface S_B, $\vec{n}$ is oriented into the body. In the sea-bottom surface, $\vec{n}$ is identical with the vertical unit vector but in an opposite direction, pointing outwards from the control volume. Finally, concerning S_∞ $\vec{n}$ coincides with the horizontal unit radial vector and its direction is outwards the fluid.

The total force exerted on the body, following from the pressure integration, is as follows:

$$\vec{F}(t) = \iint_{S_B} p\vec{n} dS \tag{5.7}$$

According to the body boundary condition mentioned already:

$$V_n = U_n \tag{5.8}$$

Consequently, if terms of equation (5.6) are rearranged, thanks to equations (5.7) and (5.8) the force on the body is acquired:

$$\vec{F} = -\frac{d\vec{M}}{dt} - \rho g \iint_{S_B} z\vec{n}dS - \iint_{S-S_B} \left[(p + \rho g z)\vec{n} + \rho \vec{V}(V_n - U_n) \right] dS \qquad (5.9)$$

Equation (5.9) can be generalized to incorporate the fluid moment $\vec{G}$ on the body. It is practical to make use of notifications $i = 1,2,3,4,5,6$ in order to express separately every axis component of the fluid force $\vec{F} = (\mathrm{F}_1, \mathrm{F}_2, \mathrm{F}_3)$ and of the fluid moment $\vec{G} = (F_4, F_5, F_6)$. In a similar manner,

$\vec{M} = (M_1, M_2, M_3)$ = linear momentum of fluid inside S

$\vec{H} = (M_4, M_5, M_6)$ = angular momentum of fluid inside S

$\vec{n} = (n_1, n_2, n_3)$

$\vec{r} \times \vec{n} = (n_4, n_5, n_6)$ (where r is the position vector relative to the origin of the coordinate system $0\text{-}x_1\text{-}x_2\text{-}x_3$ which is fixed in space)

$\vec{V} = (V_1, V_2, V_3)$ = fluid velocity

$\vec{r} \times \vec{V} = (V_4, V_5, V_6)$

Starting from the definition of the angular moment (equation (5.2)), if we proceed in parallel steps we can prove the validity of equation (5.9) also for i= 4, 5, 6. Within the scope of finally determining the steady mean wave drift forces we calculate the time averages of all terms over one period of oscillation. The time average of $\frac{d\vec{M}}{dt}$ is zero since the movement is periodical and an increase of momentum in the control volume from the one circle to the other cannot be flourished.

$$\overline{F_i} = -\rho g \overline{\iint_{S_B} n_i z dS} - \overline{\iint_{S-S_B} \left[(p + \rho g z) n_i + \rho V_i (V_n - U_n) \right] dS} \quad \text{, i= 1..6} \qquad (5.10)$$

Concerning the horizontal motions i= 1, 2, 6, the terms containing z can be neglected as they offer no net contribution when associated with n_i, i= 1, 2, 6. For the vertical motions this is not the case and this is why their analysis is more complicated.

Equation (5.10) is simplified by analyzing the boundary conditions on the control surfaces that make up $S\text{-}S_B$:

-On the fixed surface $S_{\infty,}$ the velocity of the control volume is equal to zero $U_n = 0$.

-On the material surface $S_{FS,}$ bounded by S_B and $S_{\infty,}$ $V_n = U_n$ and p=0.

In order to justify the last equation it is underlined that on the free surface the pressure is equal to the atmospheric pressure p_0 (dynamic condition). In a previous section when developing Bernoulli equation we have mentioned that p_0 can be set equal to zero without loss of generality. Therefore, it can be assumed that p=0 on the free surface.

-On the fixed surface S_D, the requirement that no fluid particles may cross this boundary renders the normal component of both the surface's velocity and the fluid's velocity equal to zero: $U_n = V_n = 0$

After taking into account this theoretical background, the following equation for the horizontal force is established:

$$\overline{F_i} = -\overline{\iint_{S_\infty} [\, p n_i + \rho V_i V_n \,] dS} \ , \ i = 1, 2, 6 \tag{5.11}$$

Equation (5.11) was derived by Maruo (1960) for the cases i= 1, 2 and Newman (1967) expanded it to the significant case of mean wave-drift yaw moment case of i=6.

Equation (5.11) together with the aforementioned equations, provide us with the total mean wave force. It goes without saying that in order to take the mean drift force, merely the arising second-order terms need to be taken into consideration. Concerning the potential, merely the knowledge of the first-order potential gives an adequate solution as far as the mean wave drift forces are concerned.

In the same equation the pressure can be calculated evoking Bernoulli's equation. However, we must not leave behind the time dependence of S_∞ due to the time-varying wave elevation at S_∞. In order to carry out computations and especially under the scope of calculating the time average it is important to separate the time-dependent and time-independent terms. It is practical to divide S_∞ into two parts: C_∞ and S_1^∞. This is exactly what we have also put into practice in the near-field method in which the total force $\vec{F}^{(2)}$ is consisted of an integral of pressure over the constant surface S_0 and a pressure integral over the oscillating surface *s(t)*. The first part C_∞ denotes the integration from $z = -\infty$ to $z = 0$. In this case, second-order terms have to be kept in the integrand in order to obtain the components of the second-order force $\vec{F}^{(2)}$. The second part S_1^∞ includes the surface between the mean free-surface level z=0 and the instantaneous position ζ_∞ of the free surface. This part of the total water surface comes up only in the case of surface-piercing bodies. Since ζ_∞ is a first-order quantity, we need exclusively first-order quantities in the integral. Finally after applying the same simplifications used in near-field method an equation identical to equation (3.49) is derived.

Equation (5.11) takes the following form:

$$\overline{F_i} = -\iint_{C_\infty} \left\{ n_i \overline{p} + \rho \overline{V_i V_R} \right\} dS - \frac{1}{2} \varepsilon^2 \rho g \oint_{S_1^\infty} \overline{\zeta^2}_1 n_i dl \tag{5.12}$$

$$\text{with } \overline{p} = -\frac{1}{2} \varepsilon^2 \rho \left\{ \overline{\Phi^2}_{1x} + \overline{\Phi^2}_{1y} + \overline{\Phi^2}_{1z} \right\} \tag{5.13}$$

The hydrostatic pressure integrates to zero over C_∞ and thanks to the potential's periodicity the potential time derivatives do not contribute to the mean value of the pressure.

It is remarkable that the contribution due to the oscillating part of the wave elevation is the same in both methods and is proportional to the first-order wave elevation.

It is also important to mention that equation (5.11) is applicable to a two-dimensional case as well. In such a case S_∞ stands for the sum of the surface elements included between the verticals $S_{-\infty}$ and S_∞, which are the vertical control surfaces for negative and positive horizontal coordinates respectively.

Mavrakos (1995) came to a proof of the same equation but originating from the equation of the hydrodynamic force exerted on the body.

$$\vec{F} = \iint_{S_B} p\vec{n}_B dS \tag{5.14}$$

Mavrakos invokes the divergence theorem and the fact that p=0 on the free surface:

$$\iiint_{\Omega} \vec{\nabla} p d\omega = \iint_{S_B + S_{FS} + S_D + S_\infty} p\vec{n} dS = \iint_{S_B} p\vec{n}_B dS + \iint_{S_D} p\vec{n}_D dS + \iint_{S_\infty} p\vec{n}_\infty dS \tag{5.15}$$

A reformulation of (5.15) gives:

$$\iint_{S_B} p\vec{n}_B dS = \iiint_{\Omega} \vec{\nabla} p d\omega - \iint_{S_\infty} p\vec{n}_\infty dS - \iint_{S_D} p\vec{n}_D dS \tag{5.16}$$

From (5.14) and (5.16) the force $\vec{F}$ can be derived:

$$\vec{F} = \iiint_{\Omega} \vec{\nabla} p d\omega - \iint_{S_\infty} p\vec{n}_\infty dS - \iint_{S_D} p\vec{n}_D dS \tag{5.17}$$

From Bernoulli it is obtained:

$$\vec{\nabla} p = -\rho g \vec{\nabla} z - \rho \vec{\nabla} \Phi_t - \frac{1}{2} \rho \vec{\nabla} \left| \vec{\nabla} \Phi \cdot \vec{\nabla} \Phi \right| \tag{5.18}$$

The first term of equation (5.17) takes the following form:

$$\iiint_{\Omega} \vec{\nabla} p d\omega = -\rho \iiint_{\Omega} \vec{\nabla} (gz + \frac{1}{2} \left| \vec{\nabla} \Phi \cdot \vec{\nabla} \Phi \right| + \Phi_t) d\omega \tag{5.19}$$

The first and second terms of equation (5.19) are transformed by accounting for the divergence theorem and the last term is rewritten after making use of the momentum theorem as described above and the definition of the linear momentum in the control volume Ω:

$$\rho g \iiint_{\Omega} \vec{\nabla} z d\omega = \rho g \iint_{S} z\vec{n} dS \tag{5.20}$$

$$\frac{1}{2} \rho \iiint_{\Omega} \vec{\nabla} (\vec{\nabla} \Phi \cdot \vec{\nabla} \Phi) d\omega = \rho \iint_{S} \frac{\partial \Phi}{\partial n} \vec{\nabla} \Phi dS \tag{5.21}$$

$$\begin{aligned} &\frac{d\vec{M}}{dt} = \rho \iiint_{\Omega} \vec{\nabla} \Phi_t d\omega + \rho \iint_{S} \vec{\nabla} \Phi (\vec{U} \cdot \vec{n}) dS \Leftrightarrow \\ &\rho \iiint_{\Omega} \vec{\nabla} \Phi_t d\omega = \frac{d\vec{M}}{dt} - \rho \iint_{S} \vec{\nabla} \Phi (\vec{U} \cdot \vec{n}) dS \Leftrightarrow \\ &\rho \iiint_{\Omega} \vec{\nabla} \Phi_t d\omega = \rho \frac{d}{dt} \iiint_{\Omega} \vec{\nabla} \Phi d\omega - \rho \iint_{S} \vec{\nabla} \Phi (\vec{U} \cdot \vec{n}) dS \end{aligned} \tag{5.22}$$

Furthermore, we exploit once again the boundary condition at S_D and S_∞ and we get rid of the term containing U_n at these surfaces.

$$\rho\iiint_{\Omega}\vec{\nabla}\Phi_t d\omega=\rho\frac{d}{dt}\iiint_{\Omega}\vec{\nabla}\Phi d\omega-\rho\iint_{S_B+S_{FS}}\vec{\nabla}\Phi(\vec{U}\cdot\vec{n})dS \tag{5.23}$$

Upon substituting (5.18), (5.19), (5.20), (5.21) and (5.22) in equation (5.17) the force can be expressed in the form:

$$\begin{aligned}
\vec{F}&=-\rho\iiint_{\Omega}\left\{g\vec{\nabla}z+\vec{\nabla}\Phi_t+\frac{1}{2}\vec{\nabla}\left|\vec{\nabla}\Phi\cdot\vec{\nabla}\Phi\right|\right\}d\omega+\rho\iint_{S_\infty+S_D}\left\{gz+\Phi_t+\frac{1}{2}\left|\vec{\nabla}\Phi\cdot\vec{\nabla}\Phi\right|\right\}\vec{n}dS=\\
&=-\rho\iiint_{\Omega}\left\{g\vec{\nabla}z+\frac{1}{2}\vec{\nabla}\left|\vec{\nabla}\Phi\cdot\vec{\nabla}\Phi\right|\right\}d\omega-\rho\frac{d}{dt}\iiint_{\Omega}\vec{\nabla}\Phi d\omega+\rho\iint_{S_B+S_{FS}}\vec{\nabla}\Phi(\vec{U}\cdot\vec{n})dS+\\
&\quad+\rho\iint_{S_\infty+S_D}\left\{gz+\Phi_t+\frac{1}{2}\left|\vec{\nabla}\Phi\cdot\vec{\nabla}\Phi\right|\right\}\vec{n}dS\Rightarrow\\
\vec{F}&=-\rho g\iint_{S}z\vec{n}dS-\rho\iint_{S}\frac{\partial\Phi}{\partial n}\vec{\nabla}\Phi dS-\frac{d\vec{M}}{dt}+\rho\iint_{S_B+S_{FS}}\vec{\nabla}\Phi(\vec{U}\cdot\vec{n})dS+\\
&\quad+\rho\iint_{S_\infty+S_D}\left\{gz+\Phi_t+\frac{1}{2}\left|\vec{\nabla}\Phi\cdot\vec{\nabla}\Phi\right|\right\}\vec{n}dS
\end{aligned}\tag{5.24}$$

In addition we take into consideration the boundary condition at the vertical surface S_∞, where $\vec{n}$ is identical with the horizontal unit vector. Therefore, $z\cdot\vec{n}_\infty=0$:

$$\begin{aligned}
\vec{F}&=-\rho g\iint_{S_{FS}+S_B+S_D}z\vec{n}dS-\rho\iint_{S}\frac{\partial\Phi}{\partial n}\vec{\nabla}\Phi dS-\frac{d\vec{M}}{dt}+\rho\iint_{S_B+S_{FS}}\vec{\nabla}\Phi(\vec{U}\cdot\vec{n})dS+\\
&\quad+\rho\iint_{S_\infty+S_D}\left\{gz+\Phi_t+\frac{1}{2}\left|\vec{\nabla}\Phi\cdot\vec{\nabla}\Phi\right|\right\}\vec{n}dS
\end{aligned}\tag{5.25}$$

According to the boundary conditions, we substitute $\frac{\partial\Phi}{\partial n}$ for $(\vec{U}\cdot\vec{n})$ in the surfaces S_{FS} and S_B and furthermore we apply the boundary condition at the sea bottom S_D where $U_n=V_n=0$:

$$\begin{aligned}
\vec{F}&=-\rho g\iint_{S_{FS}+S_B+S_D}z\vec{n}dS+\rho\iint_{S_D}\left(gz+\Phi_t+\frac{1}{2}\left|\vec{\nabla}\Phi\cdot\vec{\nabla}\Phi\right|\right)\vec{n}_D dS-\frac{d\vec{M}}{dt}+\\
&\quad+\rho\iint_{S_\infty}\left\{\left[gz+\Phi_t+\frac{1}{2}\left|\vec{\nabla}\Phi\cdot\vec{\nabla}\Phi\right|\right]\vec{n}_\infty-\frac{\partial\Phi}{\partial n_\infty}\vec{\nabla}\Phi\right\}dS
\end{aligned}\tag{5.26}$$

As previously mentioned the terms containing z offer no net contribution in horizontal motions and furthermore $n_{D,x}=n_{D,y}=0$ and $n_{\infty,z}=0$.

$$F_x = -\frac{dM_x}{dt} + \rho \iint_{S_\infty} \left\{ \left[gz + \Phi_t + \frac{1}{2} \left| \vec{\nabla}\Phi \cdot \vec{\nabla}\Phi \right| \right] n_{\infty,x} - \frac{\partial \Phi}{\partial n_\infty} \Phi_x \right\} dS \tag{5.27}$$

$$F_y = -\frac{dM_y}{dt} + \rho \iint_{S_\infty} \left\{ \left[gz + \Phi_t + \frac{1}{2} \left| \vec{\nabla}\Phi \cdot \vec{\nabla}\Phi \right| \right] n_{\infty,y} - \frac{\partial \Phi}{\partial n_\infty} \Phi_y \right\} dS \tag{5.28}$$

The preceding equations (5.27) and (5.28) are in agreement with equations (5.11). Mavrakos (1988, 1995) provides us also with an equation for F_z:

$$\begin{aligned}
F_z &= -\rho g \iint_{S_{FS}+S_B+S_D} z n_z dS + \rho \iint_{S_D} \left(gz + \Phi_t + \frac{1}{2} \left| \vec{\nabla}\Phi \cdot \vec{\nabla}\Phi \right| \right) n_{D,z} dS - \frac{dM_z}{dt} + \\
&+ \rho \iint_{S_\infty} \left(-\frac{\partial \Phi}{\partial n_\infty} \Phi_z \right) dS = \\
&= -\rho g \iint_{S_{FS}+S_B} z n_z dS + \rho \iint_{S_D} \left(\Phi_t + \frac{1}{2} \left| \vec{\nabla}\Phi \cdot \vec{\nabla}\Phi \right| \right) n_{D,z} dS - \frac{dM_z}{dt} + \\
&+ \rho \iint_{S_\infty} \left(-\frac{\partial \Phi}{\partial n_\infty} \Phi_z \right) dS = \\
&= -\rho g \iint_{S_{FS}+S_B} z n_z dS - \iint_{S_D} (p + \rho g z) n_{D,z} dS - \frac{dM_z}{dt} + \\
&+ \rho \iint_{S_\infty} \left(-\frac{\partial \Phi}{\partial n_\infty} \Phi_z \right) dS
\end{aligned} \tag{5.29}$$

From the final form of F_z (equation (5.29)), it is apparent that the application of the momentum approach for predicting the mean heave and the roll and pitch moments leads to expressions that include unattractive integrations to be carried out over the free-surface and the sea-bottom in the case of finite depth water. Mavrakos in his analysis also denotes that the corresponding expression for the moments can be derived in a similar way. All equations referring to forces and moments are exact under the assumption of irrotational flow.

The total mean forces are calculated by the time average of equations (5.27), (5.28) and (5.29). As previously mentioned, assuming periodic first-order solutions, implies that the mean values in time of the rate of change of linear and angular momentum vanish. We have non-linearities resulting from two reasons: the non-linear terms introduced by the Bernoulli equation and the integrations to be carried out on the control surfaces $S_{FS}(t)$, $S_B(t)$, $S_D(t)$, $S_\infty(t)$. Equations (5.27) and (5.28) connected with the horizontal forces are developed similarly to equation (5.12) by separating $S_\infty(t)$ into two parts. Concerning the vertical drift force, all integrals over $S_{FS}(t)$, $S_B(t)$, $S_D(t)$ and $S_\infty(t)$ need to be decomposed into two parts.

As already mentioned, equation (5.11) is also valid for a two-dimensional case. Maruo (1960) elaborated this equation to derive a useful formula for the horizontal drift force exerted on a two-dimensional surface piercing body in incident regular beam deep-water waves. The body can be either fixed or free oscillating around a mean position. There is no current and the body has no constant speed.

Three potentials are required for the determination of the environment around the body. The velocity potential for the incident waves is described by the following form:

$$\varphi_I = -\frac{\zeta_a}{k} e^{kz} \sin(\omega t - ky + \delta) \tag{5.30}$$

The presence of the body disturbs the wave-field and is responsible for the potential of the reflected waves:

$$\varphi_R = -\frac{A_R \omega}{k} e^{kz} \sin(\omega t + ky + \varepsilon) \tag{5.31}$$

A combination of the incident waves and the waves generated at $y \to \infty$ by the body creates the velocity potential of the transmitted waves which is written as:

$$\varphi_T = -\frac{A_T \omega}{k} e^{kz} \sin(\omega t - ky + \gamma) \tag{5.32}$$

In all three cases ζ_a, A_R, A_T stand for the amplitude of these waves.

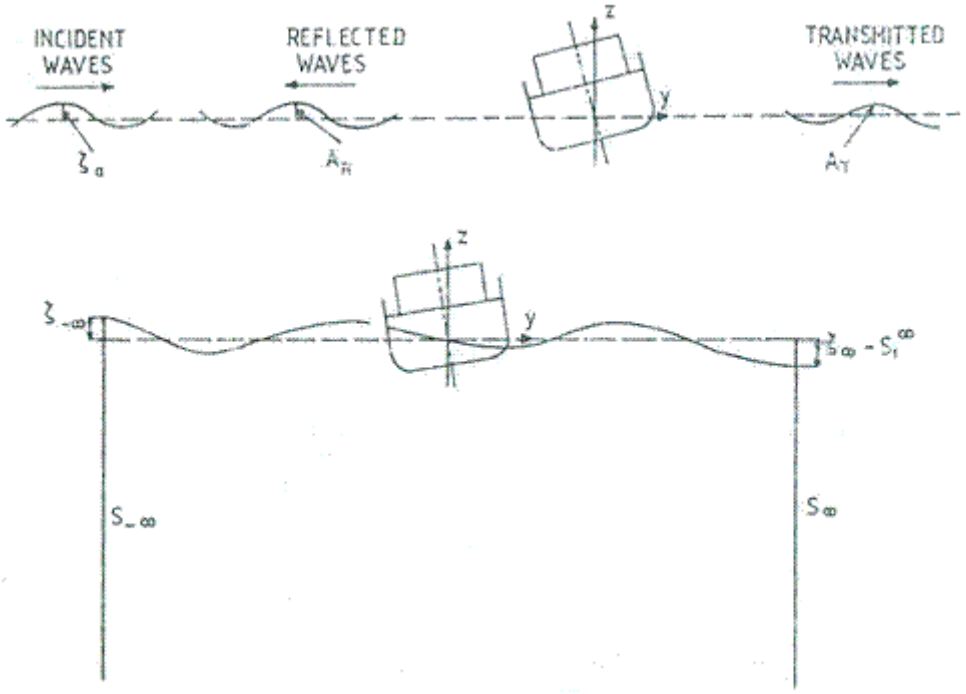

Figure 5-1: Definition of control surfaces and wave systems in the analysis of drift forces on a two-dimensional body [Fig. from Faltinsen (1990)].

Moreover, equation (5.12) is used. A 2-D case is studied therefore the surface S_∞ is limited by two vertical planes at $y = \pm\infty$. The line integral over S_1^∞ is replaced by $\overline{\zeta_1^2}\Big|_{+\infty} - \overline{\zeta_1^2}\Big|_{-\infty}$. The horizontal drift force takes the following form:

$$\overline{F_2} = \frac{1}{4}\rho g\left[\zeta_a{}^2 + A_R{}^2 - A_T{}^2\right] \tag{5.33}$$

Longuet-Higgins (1977) generalized equation (5.33) to finite waterdepth. In this case, the right hand side should be multiplied by $\left(1+\frac{2kh}{\sinh 2kh}\right)$, where h is the waterdepth.

If it is assumed that the average energy flux is zero through S_B, the inward mass transport must be equal to the outward mass transport:

$$\zeta_a{}^2 = A_R{}^2 + A_T{}^2 \tag{5.34}$$

This statement introduces the requirement that there is no work done (or absorbed) by the body during one period of oscillation; the body cannot be an active wave power device.

At this moment, the elegant equation of Maruo for the second-order horizontal mean wave drift force can be obtained:

$$\overline{F_2} = \frac{1}{2}\rho g A_R{}^2 \tag{5.35}$$

According to Maruo's formula the wave-drift force will always act in the wave propagation direction. Due to condition (5.34), Maruo's formula is firmly linked with the existence of energy-flux equilibrium.

It has been stated that A_R is the amplitude of the reflected waves. If the body is fixed, the reflected waves can be computed by the diffraction potential only. In other words, the incoming waves are disturbed exclusively by the presence of the restrained body. If the body is buoyant and free to move, A_R also encompasses the disturbance caused by the movements of the body. Reflection potential in this case includes both the diffracted waves and the motion-generated waves moving to the left. In both cases, the average force in a potential flow model is described by the amplitude of the waves that travel in the direction against the incident waves and is connected with **a structure's ability to generate waves**.

To this end, the effect of the wavelength's magnitude on Maruo's formula is considered. On the one hand, for long wavelengths relative to the cross-sectional dimensions, the body becomes "invisible" and does not disturb the wave field. Hence, the reflected wave amplitude and consequently the average drift force become negligible. On the other hand, if the wavelengths are very short in reference with the dimensions of the body, the incident waves are totally reflected from a surface-piercing body with vertical hull surface in the wave zone. It is therefore obvious that the amplitude of the reflected waves is equal to the amplitude of the incident waves and this fact gives rise to an important **asymptotic value**:

$$A_R \to \zeta_a \quad \text{and} \quad \overline{F_2} \to \frac{1}{2}\rho g \zeta_a{}^2 \ \text{as} \ \lambda \to 0 \tag{5.36}$$

This asymptotic value is valid whether the body is restrained or free. It is also valid for a submerged body.

Maruo's formula depicts clearly the drift force dependence on resonance. In the vicinity of the resonance frequencies, the amplitude of the reflected waves is likely to be large and this formula offers an explanation to the common peak of wave drift forces in this area. However, it is not necessary that the resonance occurs in the same degree of freedom as the horizontal drift force. In particular, due to heave resonance the amplitude of reflection is likely to be large and the horizontal wave drift force may exhibit a peak around this resonance frequency. This is also confirmed by the experimental results presented in *Chapter 9*.

6. FACTORS AFFECTING DRIFT FORCES IN MAGNITUDE AND IN SIGN

6.1 Effects of diffraction and of different wave-directions

From the aforementioned it is obvious that the magnitude of wavelengths is a matter that also affects the importance of the diffraction effects. When the waves are short, the wave-diffraction effects are dominant whereas when the waves are long the body motion effects become critical and tend to cancel the diffraction effects. Hence, it must be noted that both diffraction's and motions' effects must be accounted for in the calculation of the drift forces.

The diffraction phenomenon is also affected by the direction of waves. Salvesen (1974) in his theory for steady force on ship like forms neglects diffraction waves in **head waves** and obtains accurate results. Furthermore, Bowers (1976) does not take into consideration diffraction effects in drift force's calculations in head sea and acquires good agreement with experimental results. However, according to Faltinsen (1972), Maruo and Sasaki (1974), and Ursell (1975) diffraction of head waves is a complex phenomenon because it does not concern exclusively the small frontal area of the ship. The incident waves are diffracted all along the length of the ship gradually from bow to stern.

It has been stated that the diffraction effects, which depend on the direction of the waves, contribute to the drift force. Hence, it is logical that the wave propagation direction influences also the drift forces. In the potential flow model, wave-drift force is considered to be always in the wave propagation direction. This is valid for head waves but other wave headings may affect the direction and the magnitude of the force. Calculations presented by Faltinsen et al. (1979) illustrate that for the smallest wavelength the transverse drift force has greater magnitude for beam sea waves, while for the largest wavelength drift forces vanish in beam waves and are larger in wave headings between 45° and 135° (see Fig. 6-1). In the same figure it is demonstrated that the transverse drift force is more amplified when the wavelength is smaller. It is therefore inferred that diffraction effects may be the dominant cause of drift force compared with the effect of the ship's motions.

Besides, different parts of a structure may cause the generation of various waves. These waves are superposed and for some wavelengths and headings they can result in small wave drift forces. An illustrative example is a Tension Leg Platform (TLP). Each column acts as an independent wave generator, therefore in total one column may tend to intensify or invalidate the other.

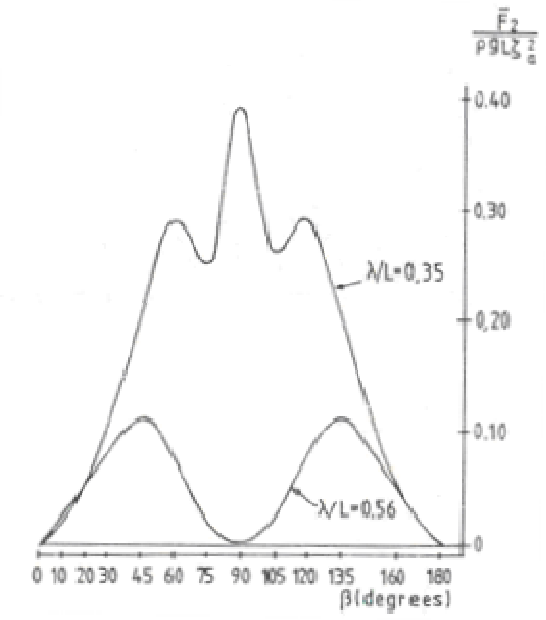

Figure 6-1: Transverse drift force $\bar{F}_2$ on a ship as a function of wave heading β for two wavelengths λ. Infinite water depth(L=ship length, β=0º in head seas, ζ_a=wave amplitude of the incident waves) [Fig. from Faltinsen (1990)]

6.2 Viscous effects on mean drift forces and negative drift forces

So far, we have analyzed the two main approaches (*near-field* and *far-field* methods) which offer calculation methods for the drift forces due to potential effects (potential drift forces). In the following, reference will be made to the fourth category mentioned in *Chapter 2.3* including the calculation of the contribution of the viscous effects in the mean drift forces (viscous drift forces).

In a framework of idealization, the viscous phenomena are often neglected. However, we must be cautious especially when referring to potential flow theory and develop a sense on when these phenomena are not negligible. When there is significant loss of energy owing to viscosity, the potential theory is invalidated. For example, due to these phenomena Maruo's formula which is based on potential flow theory may be cancelled. In addition, viscosity is strongly present in roll movement and especially near the roll resonance. Thus, it is necessary to take into consideration viscous effects while calculating roll resonance amplitudes. For example, a common way to take into account viscous effects in a potential flow theory is the implementation of correction terms into the equations of motion. This is applied in the proposed theoretical model described in *Chapter 8*.

According to Dev (1994) the viscous effects must be accounted for when the behavior of semi-submersibles or tension leg platforms (TLPs) is analysed. This is due to the geometry of this kind of semi-submersibles, which is characterized by surface piercing column structures. The viscosity effects are more intense in a low frequency range. In fact, diffraction and viscosity effects act as competitive phenomena. Concerning ships and very large floating structures, cases in which diffraction effects are dominant to the total forces, especially at moderate to low wave periods, the potential drift force is significant. In low frequency range where

diffraction effects are feebler for slender bodies, the impact of viscous effects becomes more important and the second-order force may be also due to viscous effects. This impact becomes even greater if the waves co-exist with currents due to their non-linear interactions. To sum up, the importance of the viscous effects can be influenced by three parameters:

1. the type of structure
2. the frequency range
3. the presence of currents

It is deduced that in some cases the sum of the potential and viscous phenomena may be essential for a more accurate estimation of the drift forces. In the following graph presented by Dev (1994), it is depicted that especially in lower frequencies the measured mean drift forces are higher than those calculated by the potential model. After adding the viscous effects in the calculation of the drift forces, the experimental and theoretical results seem to be in better agreement notably in the low frequency range (see Fig. 6-2).

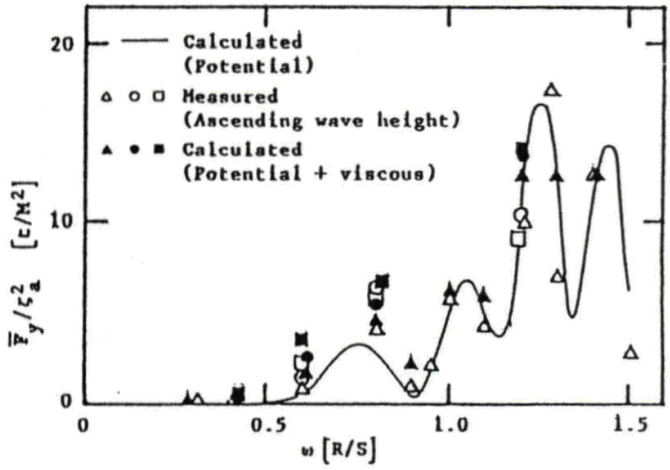

Figure 6-2: Mean drift force in regular beam waves [Fig. from Dev (1994)].

Several authors have investigated the viscous effects in the mean drift force. The majority of these scientists have developed a theory based on the drag force term of Morison's equation and on the relative motion concept. However, not much attention has been paid to the values of the mean drag coefficients for variant flow fields and only horizontal relative velocity has been taken into consideration. Furthermore, in bibliography the mean drift force due to waves has been mainly attributed to the wave elevation up to the instantaneous sea level whereas the wave-current interaction effects have been mostly analyzed merely up to the mean water level.

Dev (1994) calculates the viscous contribution to drift forces by applying the linear Airy theory. Dev considers constant velocity in the wave crest in order to obviate the ambiguous validity of the linear theory up to the instantaneous water line. In the calculation of the viscous mean drift force due to the waves only, Dev calculates the mean drift force up to the splash zone (from the mean waterline up to the actual sea level). Concerning the viscous drift force emanating from the contribution of both waves and current, he studies both components of splash and submerged zones (from the mean waterline down to the bottom of the cylinder).

The viscous drag force according to Morison's equation together with Lorentz hypothesis formulate the mean viscous drift force in the splash zone **for a unit length cylindrical section** in *waves only:*

$$\bar{F}_D = \frac{4}{(3\pi)} \rho \cdot C_{D0} \cdot D \cdot \zeta_a{}^2 \cdot \omega^2 \frac{1}{T} \int_0^T \int_0^\zeta \cos \omega t dz dt = \frac{2}{(3\pi)} \rho \cdot g \cdot k \cdot C_{D0} \cdot D \cdot \zeta_a{}^3 \qquad (6.1)$$

Thus it is proved that the mean drift force on the splash zone, which is the major source of the viscous contributions in waves without currents, is a function of the **cube of the wave height** in regular waves and that for a constant wave height it would be a function of the square of the wave frequency. While the wave amplitude increases, the drift forces caused by viscous effects become gradually more important. It is deduced that while the potential mean drift-force is, when non-dimensionalized, independent of the wave height, the total viscous and potential mean drift force is a function of the wave height (see Fig. 6-3, Fig. 6-4). Therefore, the viscous mean drift forces in irregular waves should not be considered as quadratic transfer functions.

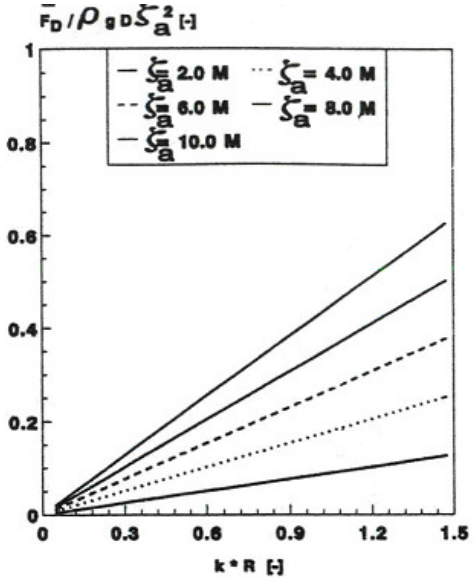

Figure 6-3: $\bar{F}_D$ **versus** $k * R$ **in waves only for different wave amplitudes [Fig. from Dev (1994)].**

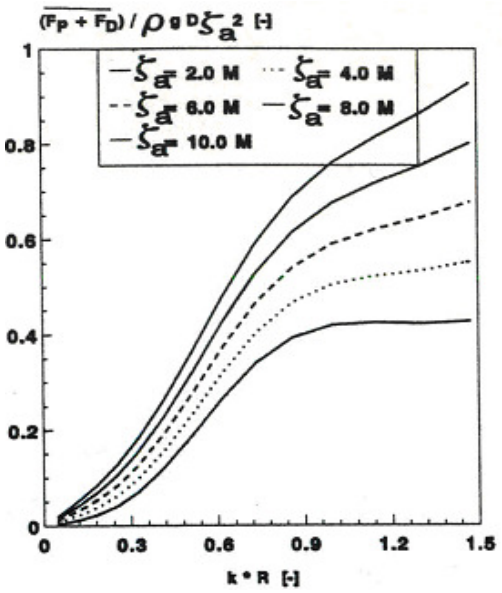

Figure 6-4: $\overline{F}_T$ versus $k*R$ in waves only for different wave amplitudes [Fig. from Dev (1994)].

In order to study the combined effect of waves and currents, a forward velocity simulating the effect of currents is added to the Morison's formula. In this case, the mean viscous drift force is evaluated at both the submerged and the splash zone. The magnitude of the forward velocity with respect to the wave particle's velocity influences the final form of the viscous drift forces. In Dev's results it is depicted that the wave-current interaction is much more pronounced at or immediately below the mean water level. This interaction increases with the increase of wave frequencies for a constant wave height. It is observed that the draft also influences the drift forces; an increment in draft leads to a feebler interaction (see Fig. 6-5).

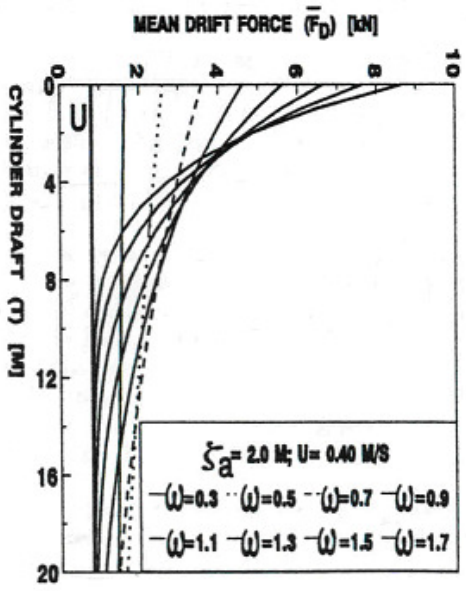

Figure 6-5: $\overline{F}_D$ over *T* in waves and currents for different wave frequencies [Fig. from Dev (1994)].

It is remarkable that the viscosity phenomenon additionally to its contribution to the force's magnitude may also influence the drift forces' direction. At this point, the new term of positive and negative drift force is introduced. The positive force refers to a force in the propagation direction of the incident waves whereas the negative drift force is the force acting in the opposite direction. According to ideal-fluid theory a body undergoes a positive average drift force. This is obvious from Maruo's formula (see equation (5.35)). Concerning the near-field approach, owing to the various terms contributing to the second-order wave forces, it is more difficult to deduce that the horizontal mean drift force is always positive. However, in *Chapter 3.8* it is accentuated that the contribution due to the relative wave height is the dominant term in the calculation of the horizontal drift forces. This term coincides always with the wave propagation direction. In addition according to the theory outlined in *Chapter 2.1*, a fluid particle in a regime of free waves is always in the direction of wave propagation.

In order to investigate the mechanism which formulates the direction of the viscous drift forces, reference will be made to the longitudinal viscous drift force of a pontoon type construction. In this case, a longitudinal viscous drift force is formed by the combined contribution of the normal drag force and the relative velocity, between a strip of the platform and the incident wave field, in the direction of the vertical normal vector. The longitudinal force arising from a vertical force's contribution is due to the rotation of the pontoon in reference to the selected earth fixed co-ordinate system. Noteworthy is the fact that depending on the phase angles between the platform motions and the wave motions, viscous effects may induce a force causing the platform to move against the waves. The time average of this longitudinal viscous drift force is one of the contributions to mean wave forces arising from drag forces [Faltinsen (1990)].

In bibliography, there have been reported negative force examples attributed to viscous phenomena. Particularly, Huse (1977) makes reference to a negative drift force on a platform observed in model tests at the Norwegian Ship Model Tank (see Fig 6-6). There are reported results of two platforms: a platform having a vertical cylinder as its underwater body and a pontoon-type (semi-submersible) platform. The drift force is presented as a function of the variable $\frac{\omega}{\omega_r}$, where ω is the radian frequency of the regular incident waves and ω_r is the pitch resonance frequency. The pontoon-type construction experiences negative drift forces in a narrower area of frequencies compared with the other construction. As already stated, the relation between these two parameters seems to define the sign of the drift force. According to Huse (1977), there is a physical explanation for the pontoon platform: "Whenever it has a nonzero pitch angle, the crossflow drag on the pontoons produces a horizontal component of force. Whether this causes a positive or negative drift force depends on the phase of the pitch motion with respect to the incident waves." His assessment, which is also confirmed by his experimental results, proves that when the frequency ω is higher than the pitch resonance frequency ω_r a negative drift force is observed. Huse does not provide us with an adequate theoretical explanation of the vertical cylinder's behavior.

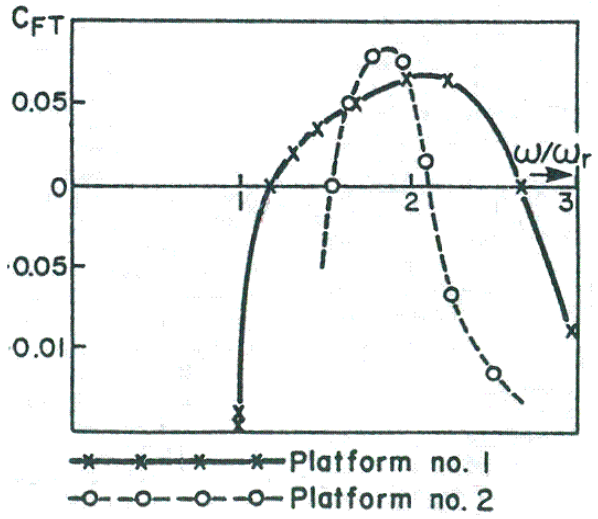

Figure 6-6: Mean drift force measured in regular waves (positive C_{FT} referring to negative drift force) [Fig. from Ogilvie (1983)].

7. EXPERIMENTAL PART

The experimental part of the research project took place in the wave flume of Ecole Centrale Marseille (ECM). The ECM's wave-tank is a glass-windowed structure of 18 m length, 65 cm width and 1.5 m height, containing fresh water.

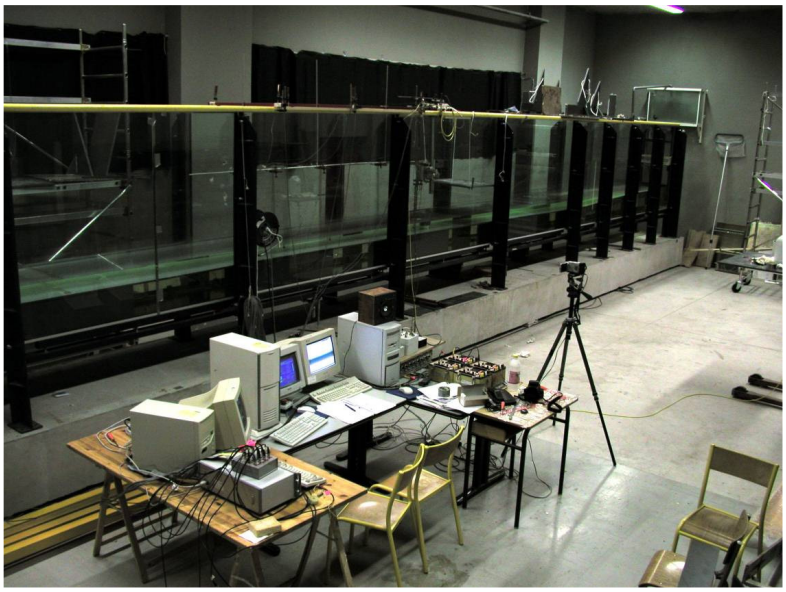

Figure 7-1: ECM's canal.

The model applied to our experiments was a rectangular barge with square bilges with 64.5 cm length, 30 cm width, and a draft of 6 cm. Experiments were conducted by exposing the model in regular beam waves. The length of the barge coincided with the width of the canal.

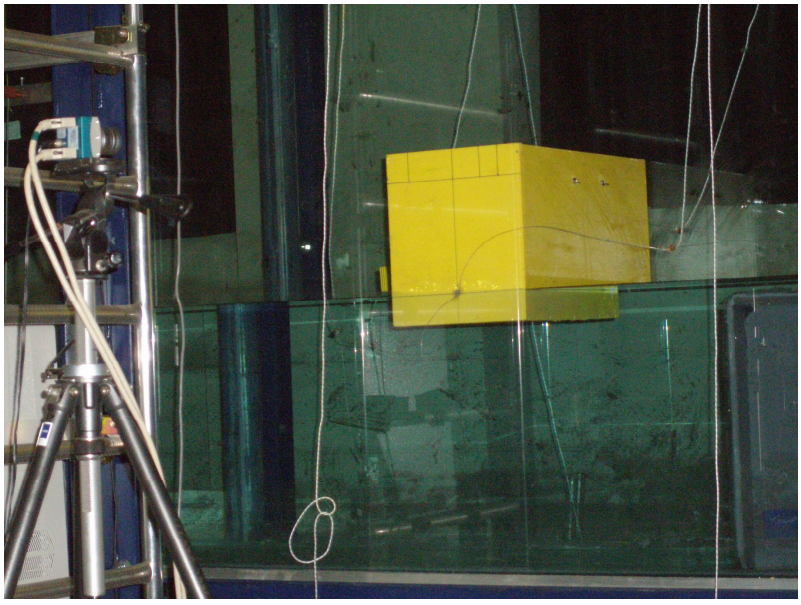

Figure 7-2: The model.

In this work, the two-dimensional problem is studied, by considering three out of the six degrees of freedom of a floating structure; a vertical movement (heave), a horizontal movement (sway) and a rotational movement (roll). For this type of floating models, there is the possibility that the barge's natural period coincides with the wave period. In this case of resonance, the amplitude exhibits a maximum value which depends on the damping capacity of the system. Reader should be aware that there are two sources of damping: the radiation damping and the damping caused by viscous phenomena. The former is suggested in the case of heave and sway, while the latter is dominant in the roll response, where strong viscous effects are observed, as for example the separation of the flow over the bilges of the barge.

Experiments consisted of four steps. First of all, the floater was moored with a variable spring system and there was no obstacle downstream. Various experiments were conducted in order to verify that there is good agreement between the experiments and the model, and additionally to study the impact of the variant number of springs. Furthermore, the floater was set free and was placed just ahead of an abrupt depth transition. The setup in the third step was similar to the previous' step except that the depth transition was modified to form a vertical wall. The distance between the barge and the wall was variable (Fig. 7-3). During this step, video techniques with a vertical laser light sheet were utilized (Fig. 7-4). We added a laser aiming to study more thoroughly the free surface elevation and the interaction between the rectangular model and the wall including the phenomenon of piston mode resonance. Last but not least, in the final series of experiments the moored rectangular barge was installed in front of the wall. The mooring line allowed the placement of the barge near to the wall. The mooring was returned upwards by a pulley system (Fig. 7-5). The wave steepness $\varepsilon = \frac{H}{\lambda}$ was fixed at various values for each series of experiments.

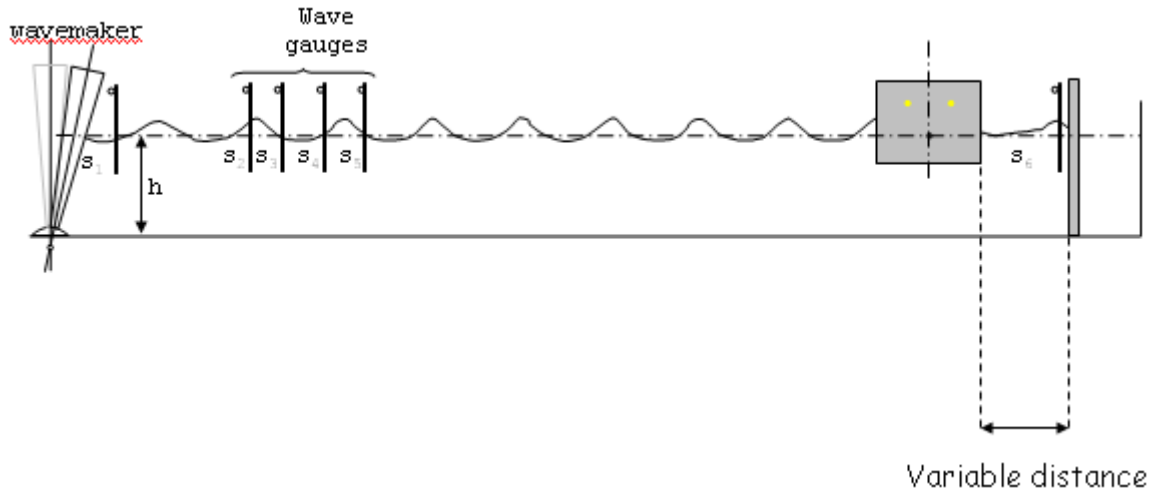

Figure 7-3: Freely drifting barge in front of a wall.

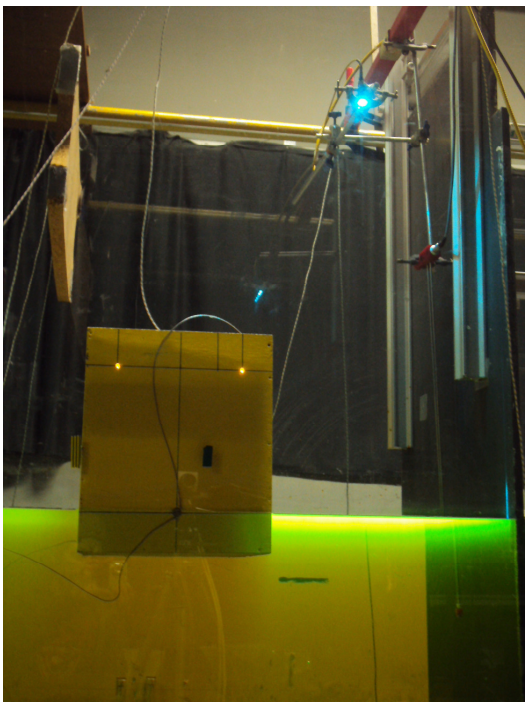

Figure 7-4: Vertical laser light sheet.

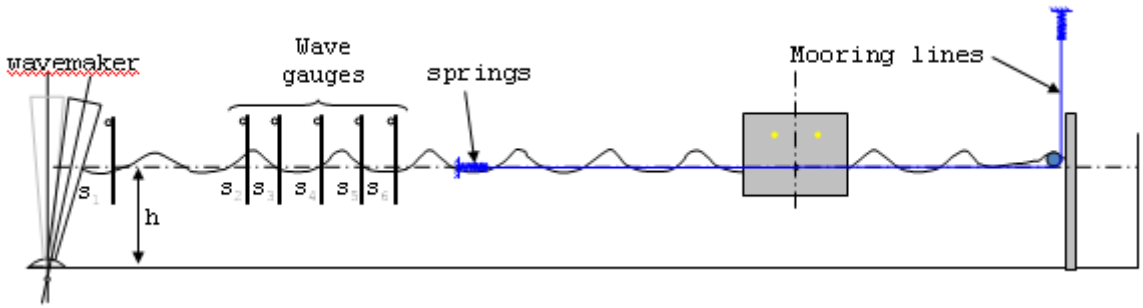

Figure 7-5: Rectangular barge moored in front of a wall.

Presentation of the equipment

1. The **wave-maker** is of flap type possessing a rotation axis lowered by 40 cm in reference to the bottom of the canal. It allows the generation of focused waves, regular, irregular and transient seas in variable water depth from 25 cm to 1 m.

Figure 7-6: Flat type wave-maker at ECM's canal.

2. The time evolution of the free surface elevation is recorded by **wave gauges**. In the beginning of the experiments, the instrumentation consisted of 8 wave gauges along the canal (5 gauges ahead of the barge and 3 gauges after it). When the wall was inserted in the experiments' instrumentation, 6 wave gauges (5 gauges ahead of the barge and 1 gauge after it) were used (Fig. 7-3) when the barge was free, while 6 gauges upstream the barge were used when it was moored (Fig. 7-5). The gauges which are used in the ECM's canal are resistive gauges of the Churchill Control model. Each gauge is constituted of 2 rigid and parallel cables made of steel, of 50 cm length, 1.5 mm diameter and 12.5 mm separation distance. A gauge when plunged into a liquid delivers a current which is proportional to its depth of immersion. In order to avoid the polarisation of the sensor on the surface of the cable, the gauge is inserted into a high frequency oscillating circuit.

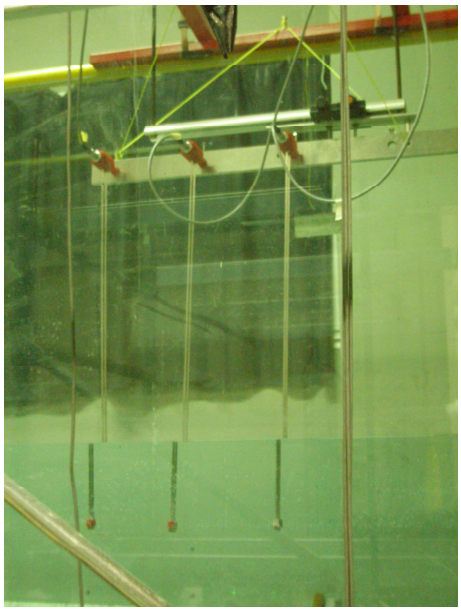

Figure 7-7: Wave gauges at ECM's canal.

An alternating current (AC)-continuous voltage converter provides us directly with the relation between the immersion depth of the gauge and the voltage at the exit of the converter. During the experiments, the response of all gauges was effectively linear, dominated by a constant sensitivity [cm/Volt].

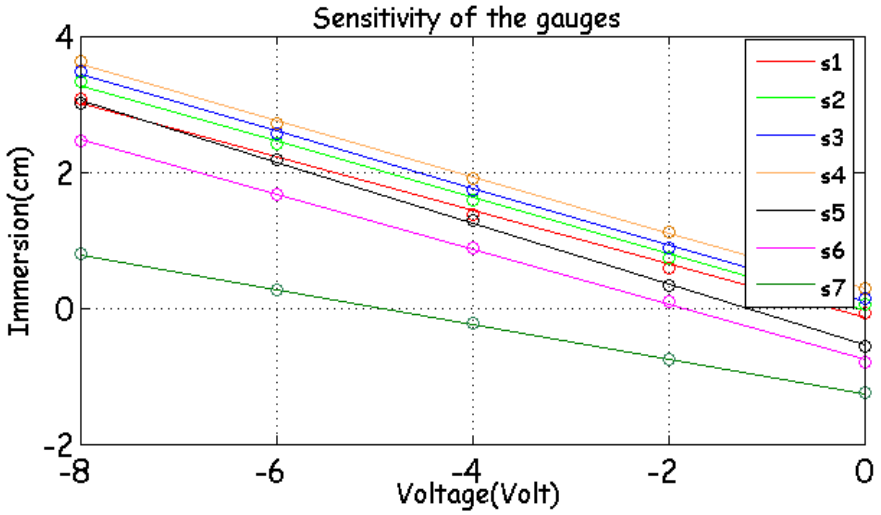

Figure 7-8: Linear response of the wave-gauges.

The gauges ahead of the barge allow us to separate the incident wave component from the reflected component, by following the method of quadratic error minimization. This method minimizes the quadratic error between measurements and theory. Concerning the gauges after the barge, they allow the calculation of the transmitted wave component. As a result, we can derive the coefficients of reflection $\left(R = A_R / A_I\right)$ and transmission $\left(T = A_T / A_I\right)$ of the experiments. Additionally, the precise value of the incident wave amplitude is critical for the forthcoming experimental calculation of the transfer functions RAOs (Response Amplitude Operators) for all degrees of freedom of the rectangular barge. In the final series of experiments, the placement of the barge near the wall does not allow the installation of a gauge after the barge. Thus, in this case the coefficient of transmission cannot be obtained.

3. In order to measure the movement of the barge, a system consisted of two **electroluminescent diodes** located on the barge and a **numerical video-camera** was used.

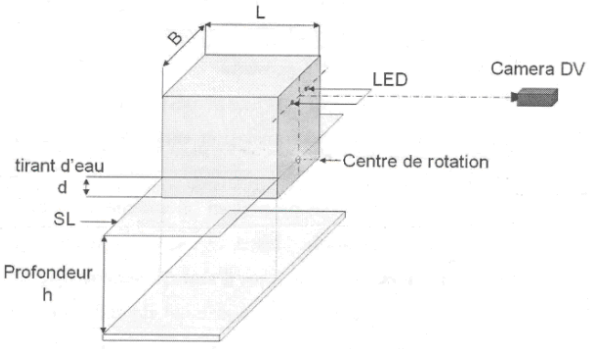

Figure 7-9: System electroluminescent diodes-numerical video camera.

The camera was a Mikrotron Eosens model with a resolution of 1280X1024 pixels^2 and a frame rate of 50 Hz. During the trials, the lights in the laboratory were turned off in order to produce total black images except the light emitted by the diodes. By this means, a technique of **automatic detection of the diodes** can be used. Furthermore, the procedure is based on the sequential matlab programs:

traite_barge: the images derived from the camera's software, are imported in the program in the form of a table of 720 columns, 576 lines and 3 colours (red, green, blue). The intensity of each colour is defined by a value between 0 and 255. Therefore, each element of the matrix corresponds to three values describing the intensity of the three colours. Due to the diodes' light properties only the red value is considered. The program iterates through video frames to create a new table sequence for the different values of luminosity. The function `contour()` offers the possibility of drawing isovalue lines. In our case, we are interested to closed curves which are surrounding each of the two diodes. By selecting luminosity value, the function `contour()` finally creates the corresponding matrix. This matrix represents the circle which is characterized by the specific luminosity. Hence, it includes all position co-ordinates (x, y) of the circle. To continue with, the mean position $[\text{posx}, \text{posy}] = [\text{mean}(\text{x}), \text{mean}(\text{y})]$ is calculated for every step in time, which actually refers to the centre of the circle for every step in time. To end with, through this procedure we obtain the position of both light-emitting diodes (LEDs) as a function of time, given in the tables *posx* and *posy*.

traite_data: this program is composed of two parts: the part *gauge* and the part *LED*.

To begin with, the first part of the program (*gauge*) involves the processing of the signals of the gauges, in order to provide us with the amplitude of the incident wave A_I and the reflection/transmission coefficients as a function of time. These coefficients are presented as a percentage of the amplitude of the incident wave.

The second part *LED* calculates the three motions of the barge (: heave, sway and roll) from the position of the diodes LED1 and LED2. In Figure 7-10 the model's initial position and a random position of the barge during its response to the waves are presented.

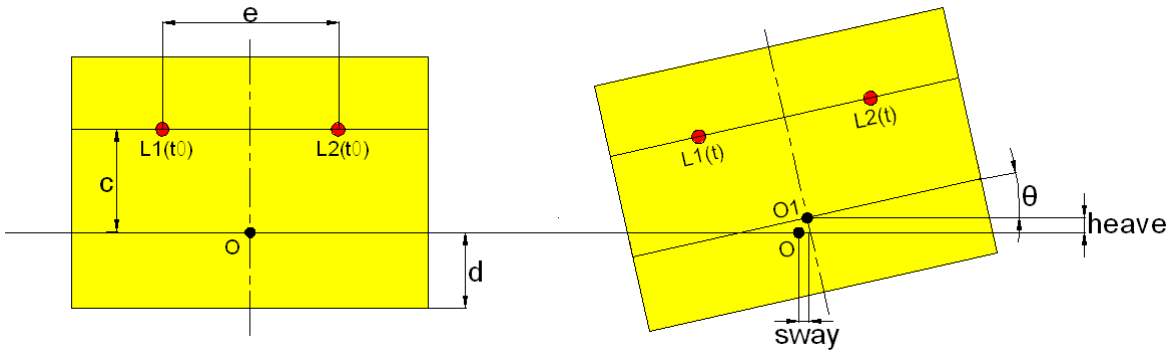

Figure 7-10: The barge in movement [Fig. from Kimmoun and Molin (2007)]

The movements of the floater are given by $\overrightarrow{OO_1}$, which is the vector of the displacement of the barge's centre of rotation. This vector can be decomposed as follows:

$$\overrightarrow{OO_1} = \overrightarrow{OL_1(t_o)} + \overrightarrow{L_1(t_0)L_1(t)} + \overrightarrow{L_1(t)O_1} \tag{7.1}$$

where t_0 corresponds to $\theta = 0$ and t to the random angle θ. The angle θ, which actually is the angle of roll, is geometrically given by the angle between the vector $\overrightarrow{L_1(t)L_2(t)}$ and the horizontal.

In Equation (7.1), we can derive the vectors $\overrightarrow{OL_1(t_o)}$ and $\overrightarrow{L_1(t)O_1}$ from the geometry of the problem. For this purpose, we need the horizontal distance between the two LEDs (e), the vertical distance between the LEDs and the centre of careen (c), as well as the random angle θ. In our problem, $e = 0.2m$ and $c = 0.23m$. Moreover, $\overrightarrow{\mathrm{L}_1(t_0)\mathrm{L}_1(t)}$ is directly given by $[posx_1, posy_1]$. Thus, firstly, we produce the value of roll and right after the values of sway and heave can be derived.

$$\theta = \tan^{-1}\left(\frac{(posy_2 - posy_1)}{(posx_2 - posx_1)}\right) \tag{7.2}$$

$$\text{sway} = \text{posx}_1 + \frac{e}{2}\cdot\cos(\theta) + c\cdot\sin(\theta) \tag{7.3}$$

$$heave = \text{posy}_1 + \frac{e}{2}\cdot\sin(\theta) - \text{c}\cdot\cos(\theta) \tag{7.4}$$

It is reported that the solutions of each iteration are influenced by the propagation of the disturbance owing to the wave maker. In order to avoid this disturbance it is preferable to filter the solutions. Thus, a low-pass filter is adopted.

To continue with, the drift movement has to be computed. The drift movement is a low frequency movement which is superposed to the movement of sway in the wave period [Kimmoun and Molin (2007)]. Therefore in order to measure the drift movement, the oscillation caused by the movement of sway has to be ignored. In order to obviate the contribution of the roll angle which is involved in the computation of sway, we select the horizontal movement of the second LED $(posx_2)$ to represent the drift movement instead of the sway movement itself. For the experiments where the barge was moored, a low pass Butterworth filter is adopted in order to eliminate the oscillation of the data $(posx_2)$. The cut-off frequency of the filter is computed by the matlab function `buttord()`. In the application of `buttord()`, the natural frequency of the mooring system (which is a function of the number of springs) determines the passband/stopband corner frequencies of the butterworth filter. For the rest of the trials where the barge was set free we consider solely $(posx_2)$ as the first estimation of the drift movement.

Afterwards, for all the movements we make use of the Short Time Fourier Transform (STFT) with a sliding window of 2T with a lag of T/10 between two successive windows. While Fourier Transform determines the main components of a sinusoidal movement, Short Time Fourier Transform (STFT) provides us with a superior time-frequency analysis. STFT is a mathematical procedure which permits

under certain circumstances the more rapid execution of the Fourier transformation. Thus, the latter was utilized in our program. As a result, in the graphs of sway, heave, roll and drift the amplitudes of the sinusoidal movement are derived as a function of the corresponding time. For each period *T*, instead of calculating a total average of the movement, thanks to STFT we obtain the more representative parameter of the average of the **amplitudes** that corresponds to the temporal interval between t_{deb} and t_{fin}. This procedure is repeated for each wave period, resulting the mean amplitude's values as a function of period *T*.

In order to better comprehend the physical phenomenon and the selection of a specific t_{deb} and t_{fin}, we are going to analyze the behavior of the coefficient of reflection. Four discrete areas are observed in the diagram of the coefficient of reflection as a function of time. To begin with, we observe a disturbed area characterized by several pronounced maxima caused by the omnipresence of the wave-maker. After the elimination of the disturbances, the coefficient of reflection tends to decrease until it reaches the last gauge. The second area starts since the waves pass from the last gauge, reach the model and get reflected on it, and ends when they pass for a second time from all the gauges. In this area (see Fig. 7-11), which starts at about 20 sec, the coefficient of reflection starts to increase steadily. Right after, we enter in an area (~25 sec) with no gauges where the reflection is constant; this is the area between the first gauge and the wave-maker. The waves cover this distance twice in an opposite direction. In the end of this area (~45-55 sec) the coefficient of reflection tends to decrease until it reaches the last gauge. Finally, in the fourth area the waves reach for second time the model and the coefficient of reflection starts to increase again. Numerous reflections take place in this area. In the following graph, a coefficient of reflection, taken from the first series of experiments, is plotted.

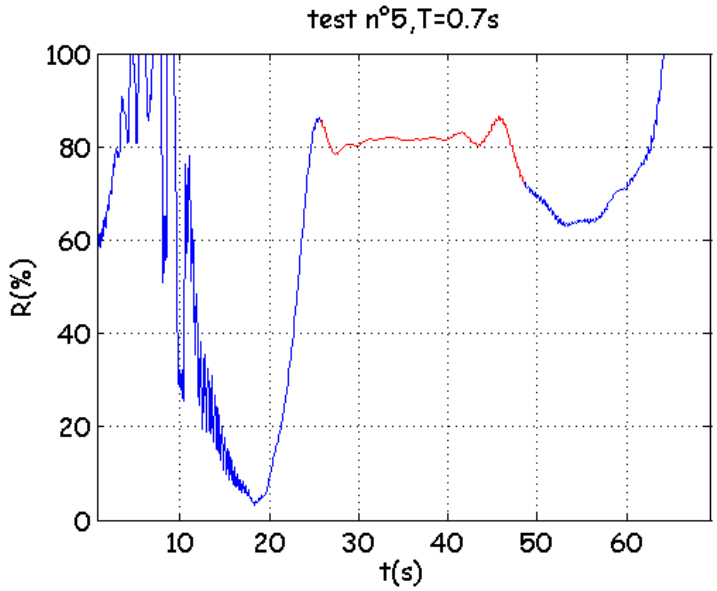

Figure 7-11: Coefficient of reflection.

Concerning the coefficient of reflection, as characteristic area is considered the constant reflection area. This area is plotted in red color in Figure 7-11. For the responses of sway, heave and roll we consider the representative temporal distance between t_{deb} and t_{fin} (which is equal to 2T) to be located in the end of the second area, in which the coefficient of reflection starts to increase (Fig. 7-12). Regarding the drift

movement, we refer to a characteristic temporal distance, wider than 2T, which is situated in the third area of constant reflection (Fig. 7-13). For the drift, the temporal interval is wider because it is difficult to reach a stable state for this movement. In the following Figures 7-12, 7-13 the characteristic area is also plotted in red color.

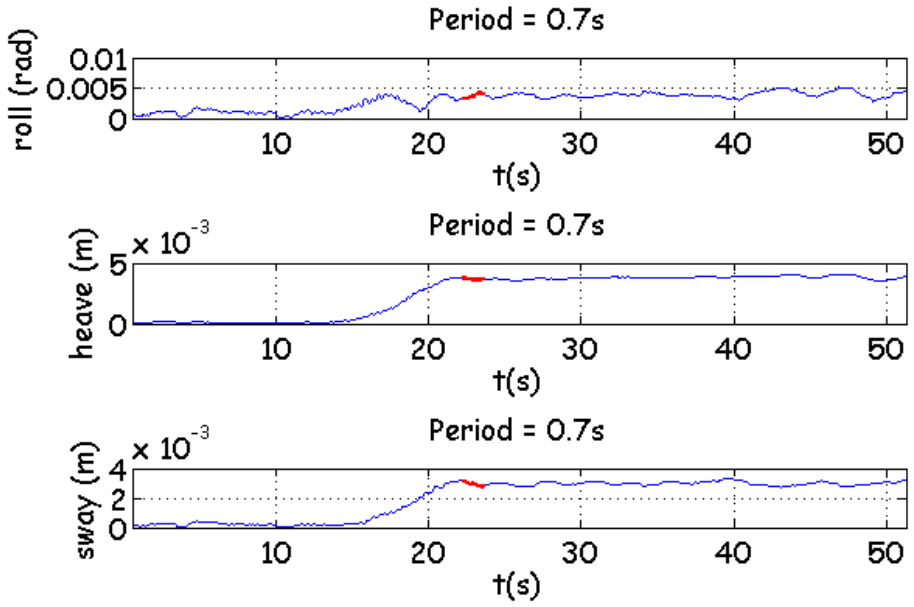

Figure 7-12: Diagrams of roll, heave and sway.

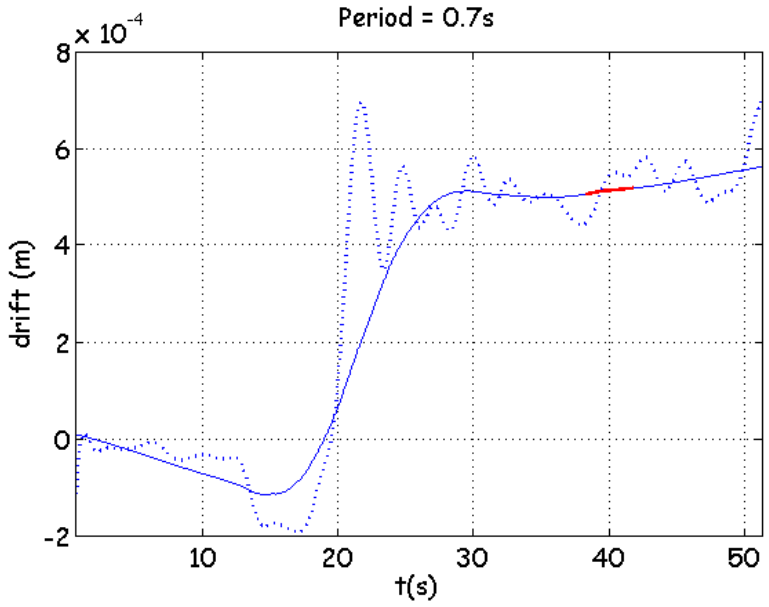

Figure 7-13: Diagram of drift.

In Figure 7-13, the blue dotted line is the drift movement calculated by the STFT. It is noticed that there still exists some oscillation. In order to remove it, the matlab function `smooth()` is applied. In particular, data is smoothed with the method Robust Loess (quadratic fit). The number of points used to compute the smoothed curve is 50% of the total number of the data points. The outcome of the application of the function `smooth()` is marked with the continuous blue line in Figure 7-13.

As we have already stated, this procedure can be repeated for each wave period. Therefore, after the completion of both parts (*gauge, LED*), diagrams of each experimental series as a function of the wave period T are obtained. In total, we can plot the RAOs of sway, heave and roll, the normalized drift force, the drift force, the coefficients of reflection and transmission and the steepness as a function of the wave period. These diagrams can be directly compared with the theoretical model.

Concerning the drift force, it can be approximated only in the case where the model is moored. If this is the case, the drift force is simulated with the force given by the Hooke's Law. The force's magnitude is $F_{drift} = k \cdot x_{drift}$, where k is the spring rate and x_{drift} is the mean drift movement between t_{deb} and t_{fin} that we have already estimated. If the barge is set free the drift force cannot be measured because the reference position continuously varies.

Reference will be made to the extraction of the RAOs which depict the movement of the barge. RAOs are effectively transfer functions used to determine the effect that a sea state will have upon the motion of a ship through the water. In linear theory, the barge's response to a monochromatic wave corresponds to a movement of the same period as the wave with amplitude proportional to the wave's amplitude. If the free surface elevation is given by:

$$\eta(t) = \Re\left(A_I \cdot e^{-i\omega t}\right) \tag{7.6}$$

Then the movement of the structure in the corresponding degree of freedom k (k=2, 3, 4) is the following:

$$X_k(t) = \Re\left(x_k \cdot e^{-i\omega t}\right) = \Re\left(A_I \cdot f_k(\omega) \cdot e^{-i\omega t}\right) \tag{7.7}$$

where $f_k(\omega)$ is the Response Amplitude Operator of the movement X_k. In linear theory, the RAO is obtained by the ratio of the response's amplitude to the amplitude of the waves. More specifically, the RAOs of sway, heave and roll are calculated as follows:

$$\tilde{x}_k = \frac{x_k}{A_I} \quad k = 2, 3 \tag{7.8}$$

$$\tilde{x}_k = \frac{x_k}{A_I \cdot k_0} \quad k = 4 \tag{7.9}$$

where x_k in our case is the mean value of the amplitudes corresponding to the degree of freedom k and calculated for the time interval between t_{deb} and t_{fin}, A_I is the incident wave amplitude obtained by the part *gauge* of the program and k_0 stands for the wave number which satisfies the equation of dispersion.

The drift force is normalized as in the following form:

$$\tilde{F}_{drift} = \frac{F_{drift}}{\rho \cdot g \cdot A_I^{\,2} \cdot L} = \frac{k \cdot x_{drift}}{\rho \cdot g \cdot A_I^{\,2} \cdot L} \tag{7.10}$$

where L corresponds to the length of the barge (L = 0.645 m)

4. During the video-techniques, we used an Ion-Helium source with an optical fibre to generate the laser sheet, associated with fluorescein in water. The matlab program utilised is **display_SL** which plots two graphs for each experiment; the first depicting the wave elevation in the gap between the barge and the wall as a function of time in a 3-D graph and the second picturing the wave elevation as a function of the distance between the barge and the wall in a 2-D graph.

5. The existence of an **absorption beach** is very important to ensure the reestablishment of a calm sea state after every trial (see Fig. 7-14). Nevertheless, during the first experiments, a part of the ramp had slipped out of the water. There was more reflection and less absorption. This fact may explain some discrepancies.

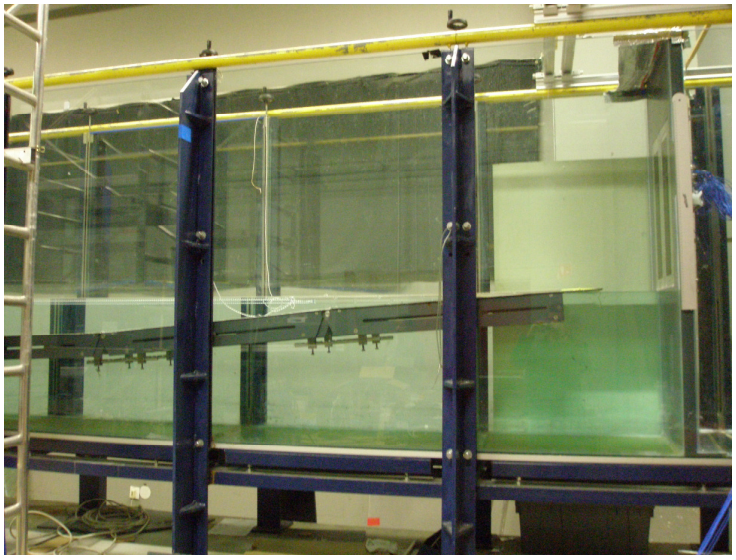

Figure 7-14: Absorption beach.

8. LINEAR NUMERICAL MODEL – STEP METHOD

The ultimate scope of an experimental series is the optimization of a numerical model which simulates as precisely as possible the physical phenomenon in an extent that experiments are no longer indispensable. Noteworthy is the fact that this optimization process is an iterative procedure that uses as a feedback mechanism the comparison between reality and theory.

There exist diverse numerical methods to depict the environment and the linear wave response of floating bodies within the scope of potential flow theory. A very practical and accessible family of numerical models in a varying bathymetry problem is the idealization of the sea-floor as a succession of steps. This is called the *step method* and it is not a new method. It has been frequently used in coastal engineering (for example we refer to Kirby and Dalrymple (1983)) but in absence of a floating structure. In our case we additionally introduce a floating body in the environment.

This macroelement method is based on the discretization of the flow field around the structure using rectangular elements (sub-domains). In these successive rectangular sub-domains the velocity potential can be analytically expressed as two propagative modes plus two series of evanescent modes emanating from the boundaries. The method of separation of variables is used in order to express this velocity potential in all sub-domains. The unknown coefficients are determined by matching the potentials and the horizontal velocities at the vertical boundaries of the sub-domains. The arising complex linear systems are numerically solved through the corresponding numerical code. Moreover, the solution of the equation of movement provides us with the amplitude of motions in all three degrees of freedom. Therefore, the potential in the entire area of the fluid domain can be obtained. According to Liu (2010b), a drawback of the step method is that it is restricted to a two-dimensional case whereas an advantage is that it allows us to treat also the case of a varying bathymetry with no limitation on the bottom slope. Therefore the bottom slope can be locally vertical.

The numerical code is practical when the barge is moored. It has not been validated in the case where the model is free to respond to the movement of the waves. This is a complex problem because it implies the solution of the model's equations of movement in time. Thus, graphs which present a direct comparison between the experiments and the model are going to be plotted merely for the 1st and 4th series of experiments, where the barge is moored. The numerical code proceeds to the calculation of the drift forces. In total two characteristic graphs can be derived. The first depicts the normalized response amplitudes, including the normalized drift force and the normalized response amplitudes of the free surface elevation at a point situated in the gap between the body and the vertical transition as a function of the wave period. The second plots the normalized response amplitudes as a function of the distance from the vertical transition (for the experiments where a vertical obstacle exists). Theoretically, a collection of infinite graphs of the first type, each one been plotted for a different distance corresponding to the exact position of the barge as a function of time, provides us with the complete solution of the free barge problem. The other graph is also very important because it shows clearly the dependence of the drift force on the distance between the barge and the vertical transition. In addition to this, through the RAO of the free-surface elevation as a function of the variable distance, the impact of the sloshing modes on the free-surface elevation can be also depicted.

To this end, the basic steps of the applied method adjusted to our case are going to be described. The environment is described as a water layer restrained by two horizontal boundaries: the upper limit is the free-surface and the lower limit is a rigid bottom. The problem of the 1st series of experiments is considered to be a flat bottom problem. In order to geometrize the problems of the 2nd, 3rd and 4th series of experiments, an abrupt vertical transition which has the form of a step and a wall were added to the geometry of the numerical model. Each sub-domain is characterized by a constant depth. The varying bathymetry consists in the different water depth between the upwave and the downave regions. Concerning the case with the vertical wall the downwave water depth is equal to zero. This problem can be also considered as a flat bottom problem. The applied model is the rectangular body which has been already described in the experimental part of our study except that in the numerical code the barge is supposed to be characterized by a unit length.

Similarly to the experiments, the two-dimensional problem is studied and therefore the body possesses three degrees of freedom. Cartesian coordinates *(x, z)* are used. Due to the fact that horizontal axis is denoted by *x* instead of *y* that was used in the experimental part, the degrees of freedom are the following: *surge*, *heave*, and *pitch*. Needless to mention, both problems are equivalent. The axis *z* is directed vertically upwards from the undisturbed free surface and the axis *x*, whose direction coincides with the length of the canal, is oriented towards the right-hand side. The point of origin of the system coincides with the undisturbed free surface in the longitudinal position where the vertical transition begins. The surface of the rigid bottom is described by $z = -h(x)$ where:

$$h(x) = \begin{cases} h_1, x < 0 \\ h_2, x > 0 \end{cases} \tag{8.1}$$

The fluid domain D is decomposed in four sub-domains D_m, $m = 1..4$. D_1 is the sub-domain situated in the area between $x<x_1$ and $h = h_1$, D_2 is the sub-domain characterized by $(x_1 < x < x_2) \bigcup (h = h_1)$ which includes the floating body and D_3, D_4 are the sub-domains described respectively by $(x_2 < x < x_3 = 0) \bigcup (h = h_1)$ and $(x>0) \bigcup (h = h_2)$. In the flat bottom problems, the number of sub-domains is reduced to three with $h = h_1$. (see Fig. 8-1)

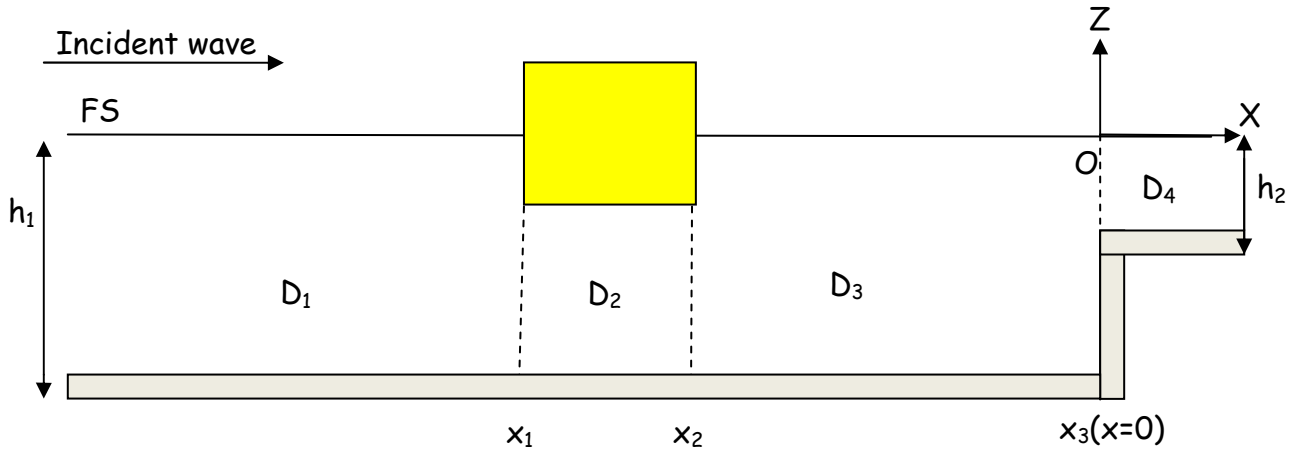

Figure 8-1: Geometrical configuration of the numerical 2-D problem concerning the case with the abrupt vertical transition.

In the framework of the potential theory, the fluid is assumed to be incompressible and inviscid and the flow is considered to be irrotational. The wave spectrum in the region D is represented by monochromatic harmonic incident waves along x axis, propagating from the left-hand-side towards the right-hand side. In order to refer to perturbation analysis, the steepness of the wave-field is assumed to be sufficiently small. Similarly, the motions of the fluid and the body are also supposed to be sufficiently small. Hence, the linearized boundary value problems are valid. Concerning the fluid, this approach of linearization suggests that we are interested to the mean position of the free surface and therefore we study an invariable fluid domain. The potential Φ is a function of three variables: two spatial variables and a time variable. The harmonic problem is studied in which the entire hydro-mechanical system is harmonically oscillating with angular frequency ω. Under these circumstances, the velocity potential takes the following form:

$$\Phi(x,z;t) = \Re\left\{\varphi(x,z)e^{-i\omega t}\right\} \tag{8.2}$$

where the function $\varphi(x,z)$ plays the role of the complex amplitude of the time harmonic velocity potential $\Phi(x,z;t)$.

The free-surface elevation is given in terms of the wave potential on the free surface as will be stated next. This is the dynamic condition on the free surface:

$$\eta(x,t) = -\frac{1}{g}\frac{\vartheta\Phi\left(x,z=0\right)}{\vartheta t} \tag{8.3}$$

The incoming incident first-order waves in the upwave area are the regular waves Airy governed by:

$$\varphi_0^{(1)}(x,z) = -i\frac{Ag}{\omega}\frac{\cos hk_0(z+h_1)}{\cos hk_0 h_1}e^{ik_0 x} \tag{8.4}$$

where A is the incident wave amplitude, g is the acceleration due to gravity, k_0 is the wave-number and $i=\sqrt{-1}$. The wave number k_0 satisfies the equation of dispersion which connects the wavelength $\lambda=\frac{2\pi}{k_0}$ and the wave period $T=\frac{2\pi}{\omega}$:

$$\lambda=\frac{gT^2}{2\pi}\tan h_1\frac{2\pi h_1}{\lambda}\Rightarrow\omega^2=gk_0\tanh k_0h_1 \tag{8.5}$$

Another advantage of the existing linearity is the validity of the superposition principle. Thus, it is possible the decomposition of the main problem to a series of elementary problems:

- a diffraction problem: this problem is described as the determination of the incident flow's perturbation due to the presence of the body restrained from movement.
- three problems of radiation: while the body is placed in calm water, the flow submitted to a forced oscillation in all three degrees of freedom has to be defined.

To formulate the diffraction and radiation problems, it is assumed that the transient phenomena have been damped. Therefore, concerning the diffraction problem some waiting time is required after the penetration of the body into the water. In the radiation problem, it is critical to wait some time after the beginning of the body's movement. At this point, both potentials can be considered as time harmonic functions of the same frequency as the incoming wave:

$$\begin{aligned}\Phi_{d_{(m)}}&=\Re\left\{\varphi_{d_{(m)}}e^{-i\omega t}\right\}\\ \Phi_{R_{(m)}}&=\Re\left\{\varphi_{R_{(m)}}e^{-i\omega t}\right\}\end{aligned} \tag{8.6}$$

The floating body is also assumed to perform a forced oscillation with frequency ω:

$$\vec{\xi}=\Re\left\{x_ke^{-i\omega t}\right\} \tag{8.7}$$

Moreover, the form of the boundary condition on the body contour in association with the assumption that the fluid is excited to movement only by the oscillation of the body, lead to the following linear decomposition of the total radiation potential:

$$\varphi_R(x,z)=\sum_{k=1,3,5}-i\omega x_k\varphi_{Rk}(x,z) \tag{8.8}$$

Hereafter the following modifications in the notation are valid:

$$\begin{aligned}\varphi_0(x,z)&=-i\frac{Ag}{\omega}\varphi_I(x,z)\\ \varphi_d(x,z)&=-i\frac{Ag}{\omega}\varphi_D(x,z)\end{aligned} \tag{8.9}$$

To this end, if we relate the validity of the superposition principle with expressions (8.8), (8.9), the potential $\varphi(x,z)$ can be expressed by the following form:

$$\varphi(x,z) = -i\frac{Ag}{\omega}(\varphi_1(x,z) + \varphi_D(x,z)) + \sum_{k=1,3,5} -i\omega x_k \varphi_{Rk}(x,z) \tag{8.10}$$

where $\varphi_D(x,z)$ denotes the complex amplitude of the diffraction potential due to the presence of the (fixed) body and the variable bathymetry and $\varphi_{Rk}(x,z), k=1,3,5$ denote the complex amplitudes of the radiation wave potentials arising from the forced body oscillation linked with the three degrees of freedom, i.e. *sway(k=1)*, *heave(k=3)*, *roll(k=5)*. $x_k, k=1,3,5$ stand for the complex amplitudes of the corresponding motions of the body.

In the **diffraction problem** the potential φ_D is governed by the five boundary conditions mentioned also in the theoretical part of our study: the Laplace equation, the two conditions of impermeability on the solid boundaries, the free-surface boundary condition and a radiation condition.

1. $\Delta\varphi_D = 0$ $\quad (x,z) \in D$ (8.11)

2. $\frac{\partial\varphi_D}{\partial n} = -\frac{\partial\varphi_I}{\partial n}$ on the body contour C_0 (8.12)

3. $\frac{\partial\varphi_D}{\partial z} = 0$ $\quad z = -h(x)$ (8.13)

4. $g\frac{\partial\varphi_D}{\partial z} - \omega^2\varphi_D = 0$ $\quad$ z=0 (8.14)

5. propagation of waves to infinity (8.15)

In the diffraction problem the radiation condition must ensure that in the upwave region D_1, the wave field consists in a reflected wave and in the downwave region, it consists in a transmitted wave.

Henceforward, the potential in sub-domains 1, 3 and 4 where there is no body presence will be termed *external potential*. In sub-domain 2 which includes the floating body the characteristic potential will be named as *internal potential*. Equations (8.10) to (8.14) as well as the radiation condition (8.15) are related in the method of separation of variables in order to define the form of the diffraction potential in all sub-domains.

More specifically, concerning the external diffraction problem the Laplace equation is firstly used in order to provide us with a general form of the diffraction potential. Moreover, the preceding equation is combined with the equation on the sea-floor. At this point, the radiation condition is applied. To continue with, the free-surface boundary condition determines the foregoing solutions. The latter condition provides us with two equations: the first one is the dispersion equation which yields one positive root whereas the second one is a group of infinite solutions. The evanescent modes are determined by this second group of infinite solutions. Therefore we can report that the presence of the evanescent modes is the result of the Laplace equation and is designated by the free-surface boundary condition.

Referring to the internal diffraction problem, at a first step the Laplace equation together with the equation on the sea-floor are applied. In this problem there is no need to impose a radiation condition. Finally, the body boundary condition yields an infinity of solutions which is used to determine the evanescent modes. To this end, all the velocity potentials have been expressed in the form of eigen-function expansions that arise from the Fourier series.

In the same way **the radiation problem** is designated by the following boundary conditions:

$$1.\ \Delta\varphi_{Rk} = 0 \qquad (x,z) \in D \tag{8.16}$$

$$2.\ \frac{\partial\varphi_{Rk}}{\partial n} = n_k = f_k \qquad \text{on the body contour } C_0 \tag{8.17}$$

$$3.\ \frac{\partial\varphi_{Rk}}{\partial z} = 0 \qquad z = -h(x) \tag{8.18}$$

$$4.\ g\frac{\partial\varphi_{Rk}}{\partial z} - \omega^2\varphi_{Rk} = 0 \qquad z=0 \tag{8.19}$$

5. propagation of waves to infinity (8.20)

In total, the parameters f_k $(k = 1,3,5)$ represent the components of the generalized normal vector on the body boundary. In our problem the components of the generalized normal vector n_k are the following:

$$\begin{aligned} n_1 &= n_x \\ n_3 &= n_z \\ n_5 &= \left(z - z_G\right)n_x - \left(x - x_G\right)n_z \end{aligned} \tag{8.21}$$

These vectors introduce the forcing of the system for each degree of freedom k. The verification of this equation gives rise to a particular potential solution for each radiation problem.

The difference between the diffraction and the radiation problem lies in the transformation of the boundary condition on the hull of the body. In addition to this, the formulation of the total problem does not prescribe an incident wave component in the radiation problem. In order to define the external potentials the condition of impermeability on the body surface is not used. Therefore, the downstream external potential remains invariable in both diffraction and radiation problems whereas the upwave external potential is modified due to the absence of the incident wave component. The condition on the body contour formulates the internal potential of the radiation problem. As already indicated, this potential obeys the Laplace's equation as well as the boundary conditions on the sea floor and on the body boundary. It is required that the particular solution of each radiation problem also verifies the above conditions. Thereby, as long as the problem is linear, the total internal potential is the sum of the internal potential obtained by the diffraction problem plus the particular solution corresponding to each degree of freedom k. To this end, the total solution fulfills the requirements of the radiation problem.

In both diffraction and radiation problems the application of the boundary conditions gives rise to the general analytical form of the potential as two propagative modes plus two series of evanescent modes. The propagative modes are described by a coefficient of transmitted wave amplitude and a coefficient of reflected wave

amplitude. There are also two coefficients that represent the amplitude functions for the evanescent modes ($n=1\to\infty$) at the boundaries. The effect of the evanescent modes is significant near the body and it decays exponentially with the distance from the boundary. Furthermore, an order of truncation for the series of the evanescent modes has to be selected.

Moreover, in order to get the complete expression of every potential in all problems, the calculation of the unknown Fourier coefficients is necessary. There are two conditions, applied at each boundary between adjacent regions, which will contribute in the calculation of the unknown coefficients. They ensure the continuity of the velocity potential:

- $\varphi_m = \varphi_{m+1} \qquad (x = x_m)$ (8.22)
- $\frac{\partial \varphi_m}{\partial x} = \frac{\partial \varphi_{m+1}}{\partial x} \ (x = x_m)$ (8.23)

We also take advantage of the orthogonality of the eigen-functions in order to furthermore simplify our problem. Thus, after solving complex linear systems, we end up getting the potentials φ_{Dm} and φ_{Rkm} in the successive domains in the form of Fourier series.

The next step is the calculation of the first-order hydrodynamic exciting loads $F_k \ (k=1,3,5)$ on the floating body by surface integration:

$$F_k(t) = \iint_{C_0} p^{(HYD)} n_k dS \tag{8.24}$$

where $p^{(HYD)}$ is the hydrodynamic pressure exerted on the wetted surface of the floating body C_0 and $n_k, k=1,3,5$, are the (non-zero) components of the generalized normal vector on the mean wetted surface of the floating body C_0, pointing inside the body.

Given the linear approach, the hydrodynamic pressure as expressed by Bernoulli is simplified as:

$$p^{(HYD)} = -\rho \frac{\partial \Phi}{\partial t} \tag{8.25}$$

In addition, the force arising from the harmonic problem can be expressed as follows:

$$F_k(x,z;t) = \Re\left\{ f_k(x,z) e^{-i\omega t} \right\} \tag{8.26}$$

The combination of (8.24), (8.25) and (8.26) gives:

$$\begin{aligned} f_k &= -i \frac{Ag}{\omega} \iint_{C_0} i\omega\rho\varphi' n_k dS \Rightarrow \\ f_k &= \iint_{C_0} Ag\rho\varphi' n_k dS \end{aligned} \tag{8.27}$$

In a 2-D problem (8.27) takes the following form:

$$f_k = \rho g A \int_{C_0} \varphi' n_k dl \tag{8.28}$$

The velocity potential φ' in equations (8.27) and (8.28) is the sum of the incident wave potential and the diffraction potential ($\varphi' = \varphi_I + \varphi_D$). The Froude-Kryloff forces together with the diffraction forces, as determined in *Chapter 2.5,* constitute the hydrodynamic exciting loads (exciting forces and moments).

Furthermore, reference will be made to the radiation forces and moments. These forces give rise to the hydrodynamic coefficients of added-mass and damping. The loads F_{Rk} arise from the integration of the pressure field emanating from the body's forced oscillation with amplitude x_k. We analyze these forces in order to define the hydrodynamic coefficients and in order to give insight into the mechanism the radiation forces act.

Similarly to equation (8.26) we write:

$$F_{Rk}(x,z;t) = \Re\left\{ f_{RK}(x,z) e^{-i\omega t} \right\} \tag{8.29}$$

Therefore:

$$\begin{aligned} f_{Rk} &= \iint_{C_0} i\omega\rho\varphi_R n_k dS = \\ &= \iint_{C_0} -(i\omega)^2 \rho x_k \varphi_{Rk} n_k dS \end{aligned} \tag{8.30}$$

In a 2-D problem:

$$f_{Rk} = -(i\omega)^2 \rho x_k \int_{C_0} \varphi_{Rk} n_k dl \tag{8.31}$$

The radiation loads can be furthermore analyzed by introducing the hydrodynamic coefficients. Henceforward the notation is modified as:

$$\Pi_{kl} = \rho \int_{C_0} \varphi_{Rkl} n_k dl \tag{8.32}$$

To this end,

$$f_{Rkl} = -(i\omega)^2 x_l \Pi_{kl} \tag{8.33}$$

This is the hydrodynamic radiation force of the fluid in direction *k* (in our case *k*=1, 3, 5), owing to the movement of the body in direction *l* (*l*=1, 3, 5).

$$\Pi_{kl} = \Pi_{kl}(\omega) = a_{kl}(\omega) + \frac{i}{\omega} b_{kl}(\omega) \tag{8.34}$$

where a_{kl} is the symmetric matrix of added-masses and b_{kl} is the associated matrix of damping coefficients. By combining equations (8.33) and (8.34) we get:

$$f_{Rkl} = \omega^2 x_l a_{kl}(\omega) + (i\omega) x_l b_{kl}(\omega) \tag{8.35}$$

From expressions (8.31) and (8.35) the following expression is derived:

$$\begin{aligned} &-(i\omega)^2 \rho x_l \int_{C_0} \varphi_{Rkl} n_k dl = \omega^2 x_l a_{kl}(\omega) + (i\omega) x_l b_{kl}(\omega) \Rightarrow \\ &\rho\omega^2 \int_{C_0} \varphi_{Rkl} n_k dl = \omega^2 a_{kl}(\omega) + (i\omega) b_{kl}(\omega) \end{aligned} \tag{8.36}$$

Reader should be aware that the matrices a_{kl} and b_{kl} are symmetric which means that:

$$a_{kl} = a_{lk} \text{ and } b_{kl} = b_{lk} \tag{8.37}$$

Based on expressions (8.8), (8.31) and (8.36) we can write:

$$f_{Rk} = \sum_{l=1,3,5} (-a_{kl}(\omega)\ddot{x}_l - b_{kl}(\omega)\dot{x}_l) \tag{8.38}$$

The above expression reveals that the response of the fluid to the movement of the body comprises:

- one term which is 180° out of phase with the acceleration, resulting in the augmentation of the inertia of the body
- one term which is 180° out of phase with the velocity. This term depicts the damping of the mechanical energy of the floating body, due to the dissipation of energy expressed by the propagation of waves. The damping coefficients follow solely from the wave making and they are not related with the damping due to phenomena of friction or viscosity.

Furthermore, the ensemble of these equations allows the formulation and the solution of the equations of motion of the floating body. The equations of motion are the working out of Newton's second-law:

$$\begin{aligned} &m\frac{d^2\vec{\xi}}{dt^2} = \int_{C_0} p\vec{n} dl \Rightarrow \\ &\sum_{l=1,3,5} \left(-M_{kl}\omega^2 + C_{kl}\right) x_l = f_k + f_{Rkl} \Rightarrow \\ &\sum_{l=1,3,5} \left\{\left(-M_{kl}\omega^2 + C_{kl}\right) x_l - f_{Rkl}\right\} = f_k \Rightarrow \\ &\sum_{l=1,3,5} \left\{\left(-M_{kl}\omega^2 + C_{kl}\right) x_l - \left(\omega^2 x_l a_{kl}(\omega) + (i\omega) x_l b_{kl}(\omega)\right)\right\} = \rho g A \int_{C_0} \varphi' n_k dl \Rightarrow \\ &\sum_{l=1,3,5} \left\{-(M_{kl} + a_{kl})\omega^2 - i b_{kl}\omega + C_{kl}\right\} x_l = \rho g A \int_{C_0} \varphi' n_k dl \end{aligned} \tag{8.39}$$

Where p is the total pressure exerted on the wetted surface C_0 of the floating body and x_l $(l = 1,3,5)$ stand respectively for heave, sway and roll complex amplitudes

This equation expresses the dynamic equilibrium between the inertial forces, the hydrodynamic responses, the hydrostatic restoring forces and the exciting loads. C_{kl} denote the restoring coefficients of the hydrostatic loads, and M_{kl} stands for the generalized inertial tensor.

In our problem we firstly calculate the contribution of the potential to the exciting loads and to the radiation forces (which include the dependence on the matrices a_{kl} and b_{kl}) from expressions (8.28) and (8.31) respectively:

$$P_k = \int_{C_0} \varphi' n_k dl \tag{8.40}$$

and

$$N_{kl} = \int_{C_0} \varphi_{Rkl} n_k dl \tag{8.41}$$

However, an extra term must be added to the radiation forces in order to model the dependency on viscous phenomena and to avoid excessive resonance [Kimmoun and Molin (2007)]. It has been indicated that the origin of the damping in the roll movement is mainly attributed to viscous phenomena (as it is the flow separation) which take place at the square bilges of the barge. In order to take into consideration these effects an extra term of dissipation which is a quadratic function of the velocity is adopted:

$$B_Q \cdot \dot{\theta} \cdot \left|\dot{\theta}\right| \tag{8.42}$$

where θ is the angle of the roll movement. Based on experimental considerations we express the coefficient B_Q in the following form:

$$B_Q = \frac{1}{2} \rho \cdot C_d \cdot B^4 \cdot L \tag{8.43}$$

where B describes the breadth of the barge, L the length of the barge, which in the present numerical mode is supposed to be equal to one, and C_d the coefficient of damping. In our case the value of C_d is considered to be between 0.1 and 0.2. However, it is obvious that this is a non-linear term introduced in a linear equation. It must be linearized for the harmonic problem. This linearization is possible if we apply the Lorentz hypothesis:

$$\dot{\theta}\left|\dot{\theta}\right| \simeq \frac{8}{3\pi} \omega \left\|\theta_0\right\| \dot{\theta} \tag{8.44}$$

where $\left\|\theta_0\right\|$ is the amplitude of roll.

From previous experiments in the wave flume of ECM it has been observed that in order to obtain a good agreement between the numerical model and the experiments, it was required to add a dissipation term also for the heave response. This term is introduced in the same way as the roll damping. The value selected for the heave damping is significantly superior to 1 and corresponds to the value obtained from many previous comparisons [Kimmoun and Molin (2007)].

Moreover, we define the non-zero elements of the matrices C_{kl} and M_{kl} that correspond to the geometry of our problem. Finally, the following system 3×3 (Eq. (8.45)) is derived. This system provides the complex amplitudes concerning the responses of the model to the three radiation problems.

$$\begin{aligned}&\sum_{l=1,3,5}\left\{\left(-M_{kl}\omega^2+C_{kl}\right)x_l-f_{Rkl}\right\}=f_k\Rightarrow\\&\sum_{l=1,3,5}\left\{\left(-M_{kl}\omega^2+C_{kl}\right)-\omega^2\rho N_{kl}\right\}x_l=\rho gAP_k\end{aligned}\tag{8.45}$$

Right after, the RAOs in the three degrees of freedom are calculated. They follow the same normalization as in the experimental part:

$$\tilde{x}_k=\frac{x_k}{A}\qquad k=1,\,3\tag{8.46}$$

$$\tilde{x}_k=\frac{x_k}{A\cdot k_0}\quad k=5\tag{8.47}$$

The total wave potential in each sub-domain including the diffraction potential and the three radiation potentials is obtained by the superposition formula (Eq. 8.10). To this end, the free surface elevation in each sub-domain can be also calculated by referring to expression (8.3). The RAO of the free surface is as follows:

$$\tilde{\eta}=\frac{\eta}{A}\tag{8.48}$$

The main scope of the conducted experiments and thus of the theoretical model is the drift force's calculation. As already mentioned, there are two well-known formulations for the calculation of the wave drift force: "*the far-field method*" and "*the near-field method*". In our problem, drift force is obtained through the far-field method's momentum considerations with two vertical cuts at upstream infinity and at downstream infinity.

A synopsis of the *far-field's* advantages and disadvantages is presented. A significant advantage of the method of reference is that the control surface can be extended to infinity. Furthermore, according to Liu (2010b) in a problem where the sea-floor is flat below the barge, the momentum method with the two control cuts in the flat region, presents higher numerical convergence in comparison with the direct integration method. However, three disadvantages are reported. Firstly, the far-field method allows the calculation of the three out of the six components of the drift forces. Moreover, when the interaction between different structures is studied, the far-field method does not allow the computation of the drift force exerted separately on each structure. Last but not least, through the far-field method merely the mean drift forces are calculated instead of the total mean and slow drift forces computed by the near-field method. Hence, it is common to put into practice both methods.

In the theoretical part of our study, we have already made reference to the expression for the mean horizontal drift forces as it is derived by the far-field method:

$$\overline{F_i}=-\iint_{C_\infty}\left\{n_i\overline{p}+\rho\overline{V_iV_R}\right\}dS-\frac{1}{2}\varepsilon^2\rho g\oint_{S_1^\infty}\overline{\zeta^2}_1 n_i dl\tag{8.49}$$

$$\text{with } \overline{p} = -\frac{1}{2}\varepsilon^2 \rho \left\{ \overline{\Phi^2{}_{1x} + \Phi^2{}_{1y} + \Phi^2{}_{1z}} \right\} \tag{8.50}$$

where C_∞ is the surface up to $z = 0$ and S_1^∞ is the remaining part between $z = 0$ and $z = \zeta$. V_i stands for the fluid velocity in direction i, V_R is the radial component of the fluid velocity on C_∞ and ζ_1 represents the first-order wave elevation.

In the numerical model, we make use of Maruo's formula [Maruo (1960]. This is an elaboration of the far-field method's expression (Eq. (8.49)) corresponding to a two-dimensional case. In a two-dimensional case C_∞ is a rectangular surface enclosing the body and S_∞ is limited by two vertical planes at $y = \pm\infty$. In our problem the upstream infinity $-\infty$ is located at the 1st sub-domain and the downstream infinity $+\infty$ is situated in the 3rd sub-domain no matter the geometry of the problem.

Following Maruo's formula, the mean horizontal drift force when the sea-floor is flat is obtained as:

$$F_d = \frac{1}{2}\rho g \frac{C_G}{C} A^2 \left(1 + R_1 R_1^* - T_3 T_3^*\right) \tag{8.51}$$

where C_G is the group velocity and C the phase velocity. R_1 denotes the complex coefficient of reflection in the upwave infinity and T_3 the complex coefficient of transmission in the downwave infinity. R_1^*, T_3^* represent their conjugates.

We point out that in a flat bottom problem the drift force is always positive. This is obvious by combining the flat bottom expression (Eq. (8.51)) with the expression describing the energy flux conservation $RR^* + TT^* \equiv 1$. If the barge is an active power device which consumes energy, the current form for the energy flux conservation is $RR^* + TT^* < 1$. We become aware of the fact that the drift force remains positive.

The problems with a vertical transition are also considered to be flat bottom problems as far as the formulation of the drift-force is concerned. This is due to the fact that the downwave region is still selected to be situated in the 3rd sub-domain. However, Eq. (8.51) is altered in order to include also the reflection caused by the vertical obstacle:

$$F_d = \frac{1}{2}\rho g \frac{C_G}{C} A^2 \left(1 + R_1 R_1^* - T_3 T_3^* - R_3 R_3^*\right) \tag{8.52}$$

Noteworthy is the fact that in the latter problems, governed by Eq. (8.52), the sign of the drift force can be also negative due to the reflection caused by the vertical obstacle. This is also confirmed by the experimental results which are going to be analyzed in the following chapter.

Nevertheless, through the above expressions (Eq. (8.51), (8.52)) the total mean force acting both on the body and on the sea-floor is derived. To be accurate, there is need to either isolate the body by considering a contour closer to it or to make use of the *"near-field method"*. But in the same time as mentioned by Liu (2010b) the *"near-field method"* encounters slow convergence problems owing to the singularity of the velocity potential at the square bilges.

The final results for the drift forces are normalized by $\rho g A^2$:

$$\tilde{F}_d = \frac{F_d}{\rho g A^2} \tag{8.53}$$

9. COMPARISON BETWEEN EXPERIMENTS AND THEORY

The main goal of the present experimental and theoretical investigation is to highlight the occurrence of negative drift force. In this context we are dealing with circumstances under which this force becomes negative, trying to explain whether the source of this phenomenon is potential or viscous. The incentive to our experimental research was given by Liu et al. (2010a), where negative drift forces in a case of a step or a wall downwave the flow are reported.

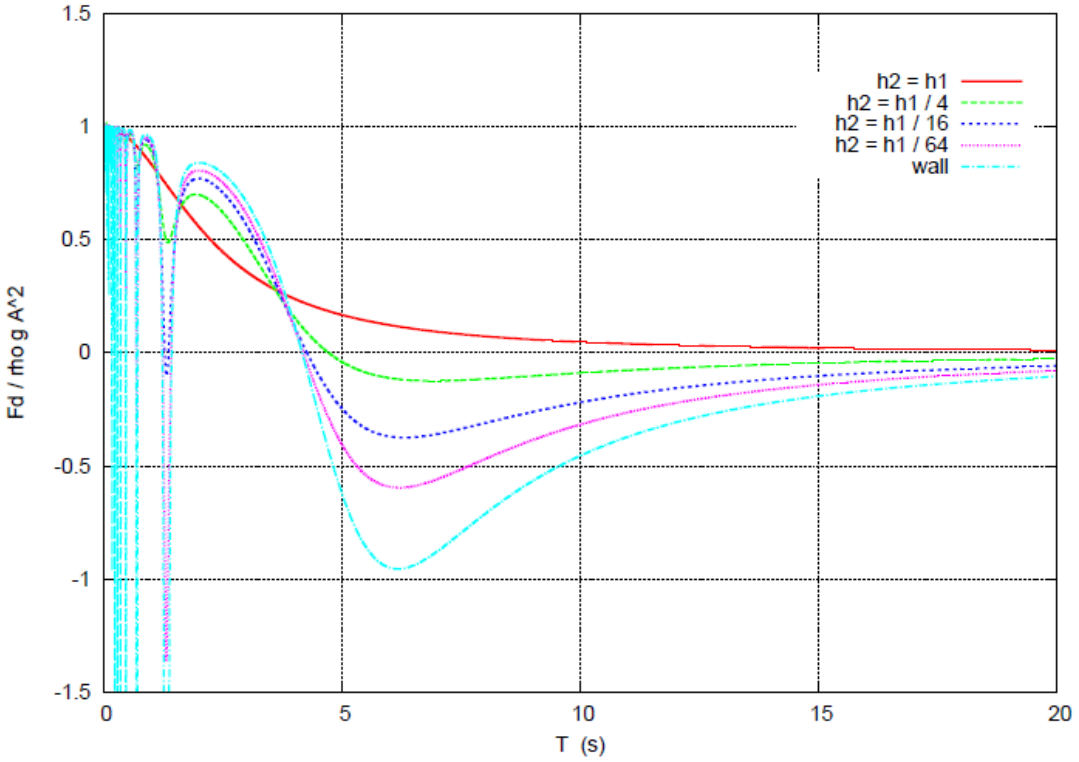

Figure 9-1: The drift force of the barge when the bathymetry is a submarine cliff with different heights [Fig. from Liu et al. (2010a)].

In Figure 9-1, the numerical results for an applied model of the following dimensions are presented: *length in the direction of the canal =1 m*, *distance barge-cliff = 2 m*, *draft = 0.4m*. The waterdepth h_1 of the weather side is equal to 0.8 m and in the lee side it is considered successively as equal to $h_1, \frac{h_1}{4}, \frac{h_1}{16}, \frac{h_1}{64}$ and right after as equal to nil (which is the case of the wall). The momentum method is used for the calculation of the drift force. It is shown that the drift force is always positive when $h_1 = h_2$ and presents multiple negative peaks in the low period range as approaching the case of the wall. According to Liu et al. (2010a) this is due to sloshing modes in-between the barge and the abrupt vertical transition. Concerning the drift force which becomes negative in greater periods than 4-5 sec, this is attributed to some kind of piston mode between the barge and the vertical transition.

In the following analysis, we must be aware of the existing non-linear phenomena which affect our system. Firstly, the flow separation at the square bilges

of the barge leading to vortex shedding is present in a case of roll or heave resonance. In order to take into consideration this effect, roll and heave damping coefficients have been added to the numerical model. Another non-linearity occurs when the fluid is entrapped in a small gap, for example when two floating bodies are in proximity. If this is the case, the fluid is characterized by an infinite number of resonance modes; a piston mode resonance in heave and an infinite number of sloshing modes. Flow separation may occur also due to these phenomena. Additionally, negative drift force may be observed due to this large amplitude motion of the fluid. In total, due to the flow separation the potential theoretical model notably over-predicts the responses. Last but not least, the wave-flume is not adequately long. Therefore there may be non-linear interactions as there is not enough time for equilibrium to be re-established. Consequently, the experimental results may be amplified in comparison with the numerical results.

At first, we are going to make an attempt to gain insight into the effect of the distance between the barge and the wall on the sign and the magnitude of the drift forces. Three cases of the theoretical model, governed by different distance between wall and barge, are presented. For the different cases, the distance between wall and barge, as measured from the right corner of the barge, is the following:

- Distance= 1.9 m
- Distance= 0.9 m
- Distance= 0.2 m

The waterdepth is equal to 0.513 m in all cases and the wave steepness is equal to 0.02. The RAOs of the considered degrees of freedom, the normalized drift force and the normalized free surface elevation at distance equal to -0.1 m from the wall are presented. The viscous damping in roll and heave, when included in the equations, take the following values: $C_{D\ \mathrm{roll}} = 0.1$ and $C_{D\ \mathrm{heave}} = 5$.

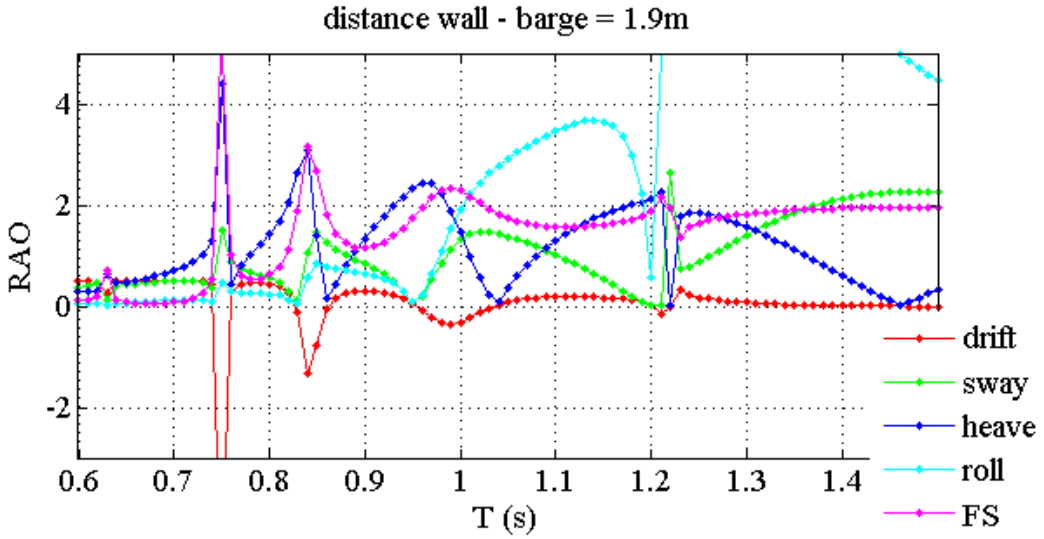

Figure 9-2: Barge 1.9 m from the wall with no dissipation terms in the equations.

It is observed that there are two particular cases where the drift force is equal to zero. In the first case, in certain periods (~0.86 sec, ~1.03 sec, ~1.22 sec, ~1.45 sec) in addition to the cancellation of the normalized drift force the RAO of heave response is also cancelled, while the RAOs of roll and sway exhibit maximum values.

In the second case, in the periods when the normalized drift force is cancelled, a cancellation of the roll and sway motions together with a maximum heave motion take place (~0.83 sec, ~0.95 sec). In all the preceding cases, the normalized free surface elevation crosses the value level of 2 except for the periodical interval between 0.7-0.8 sec when it takes a greater value due to the heave resonance. [Kimmoun et al. (2011)]

Moreover, we show that in this case the total maximum negative drift force occurs in the vicinity of the heave resonance (~0.75 sec) which also corresponds to a resonance of the free surface in the gap between the wall and the barge. Another local maximum of the negative drift force takes place at ~0.85 sec, which also coincides with a maximum of heave's RAO and of the normalized free surface. It is also observed that when local or total maxima of the negative drift force occur, the responses corresponding to all three considered degrees of freedom are significantly oscillating.

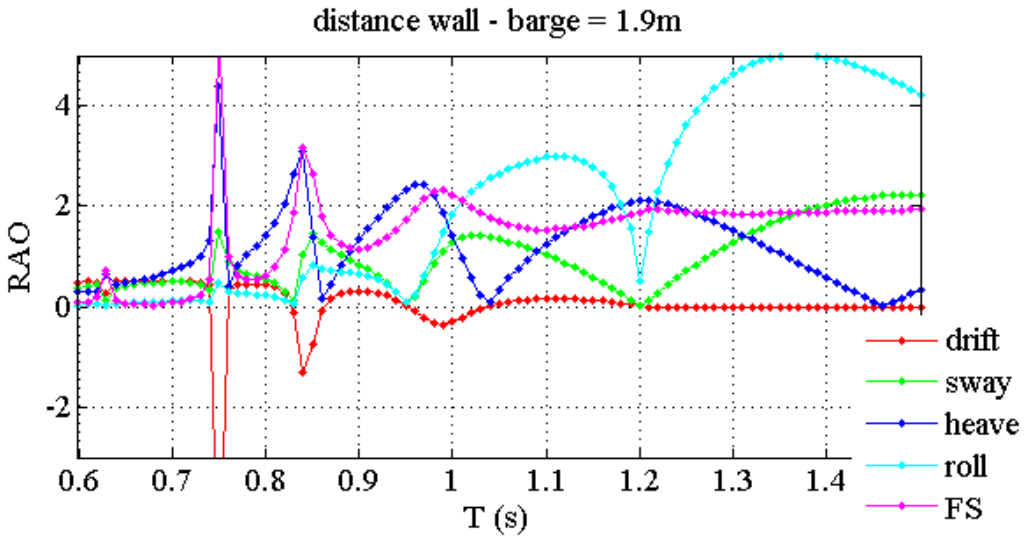

Figure 9-3: Barge 1.9 m from the wall with viscous damping in roll.

The roll dissipation term, which is added in the theoretical model in Figure 9-3, changes significantly the roll response. In particular, it reduces the magnitude of the roll's RAO between $T = 0.94$ sec and $T = 1.2$ sec and decreases considerably the roll resonance after $T = 1.2$ sec. The drift force is not affected by this dissipation term except that around $T = 1.2$ sec the small negative drift force peak vanishes.

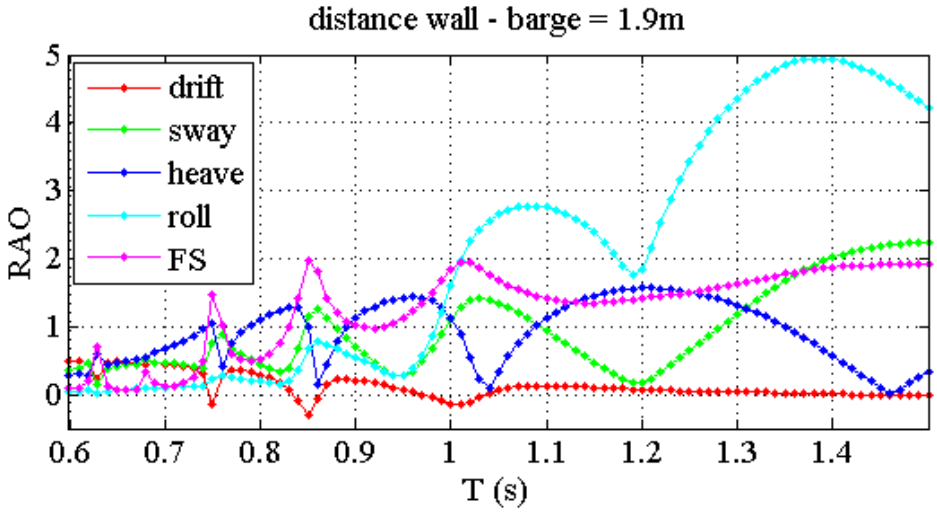

Figure 9-4: Barge 1.9 m from the wall with viscous damping in roll and heave.

Moreover, in Figure 9-4 both roll and heave dissipation terms are incorporated in the equations. The heave dissipation term changes significantly the heave response, the free surface elevation as well as the normalized drift force. All the maxima of heave's RAO have been attenuated and the normalized free surface never exceeds the value level of 2. Noteworthy is the fact that the heave dissipation term influences the drift force especially when it takes negative values and the negative peaks appear to be significantly minimized in magnitude.

In total, from the preceding Figures 9-2, 9-3, 9-4 it can be deduced that the viscous damping coefficients influence mostly the intensity of the responses without significantly displacing their maximum and minimum values.

To illustrate more sufficiently the response of the free surface elevation, the graphs of the normalized free surface elevation as a function of the distance from the wall are plotted. In the two following Figures 9-5, 9-6 the free surface elevation is depicted for the wave periods where the RAO of heave response is cancelled:

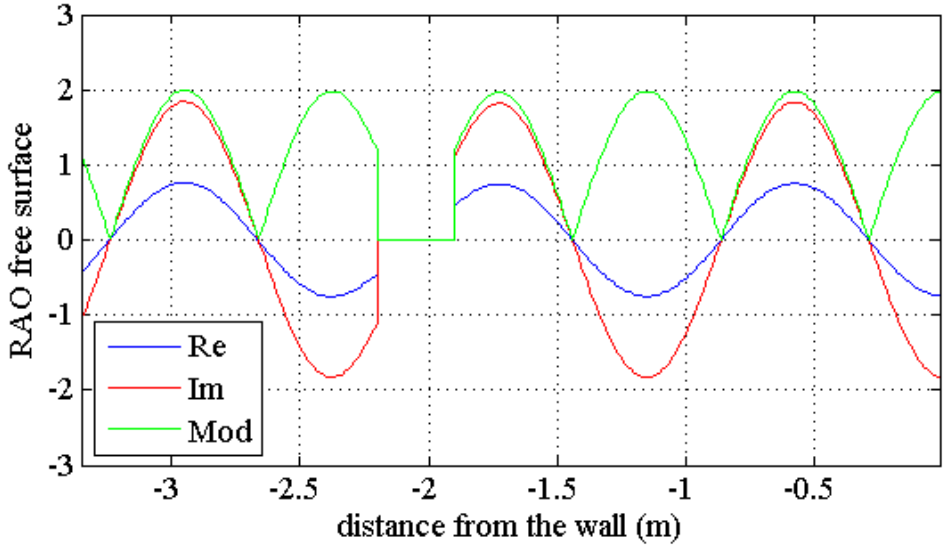

Figure 9-5: Free surface profile for *T*= 0.862 sec (zero heave) with viscous damping in roll.

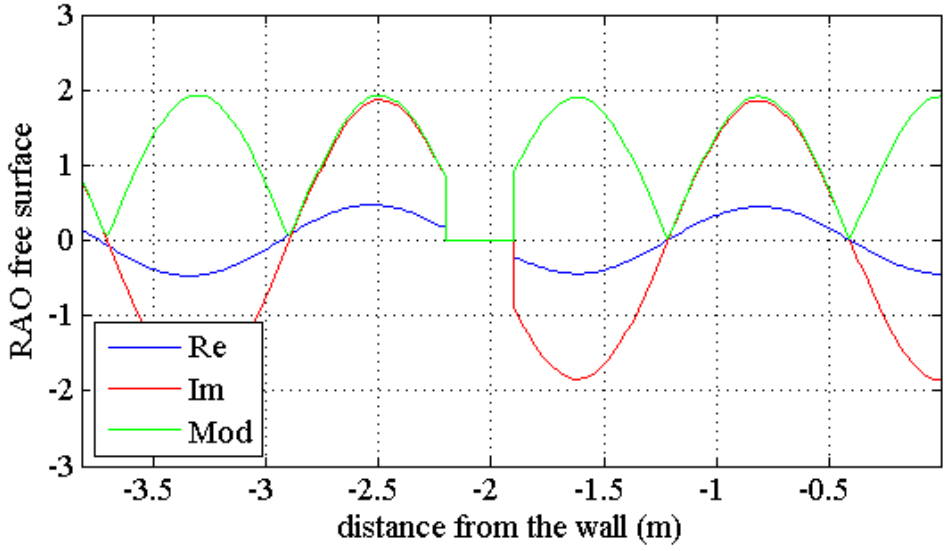

Figure 9-6: Free surface profile for *T*= 1.038 sec (zero heave) with viscous damping in roll and heave.

There is no difference between the cases with roll viscous damping and with both roll and heave viscous damping. When the drift force is nullified the body is considered to be invisible and it can be assumed that there in no wave reflected from the body. Hence, it is expected that the transmission coefficient is equal to 1, which means that the same incident wave (but with a phase lag) arrives at the wall and is reflected on it [Kimmoun et al. (2011)]. Therefore, the normalized free surface on the wall is expected to be equal to 2 in these cases of cancellation of the drift force.

In the same way, in the following Figures 9-7, 9-8 the free surface profile for the periods corresponding to the sway's and roll's cancellation is plotted. In Figure 9-7 the case of T = 0.828 sec is considered, which stands for a cancellation of sway and roll in Figure 9-3. In Figure 9-8, the case of T = 0.836 sec is studied. In this period, both sway and roll are nullified for the case with viscous damping in roll and heave.

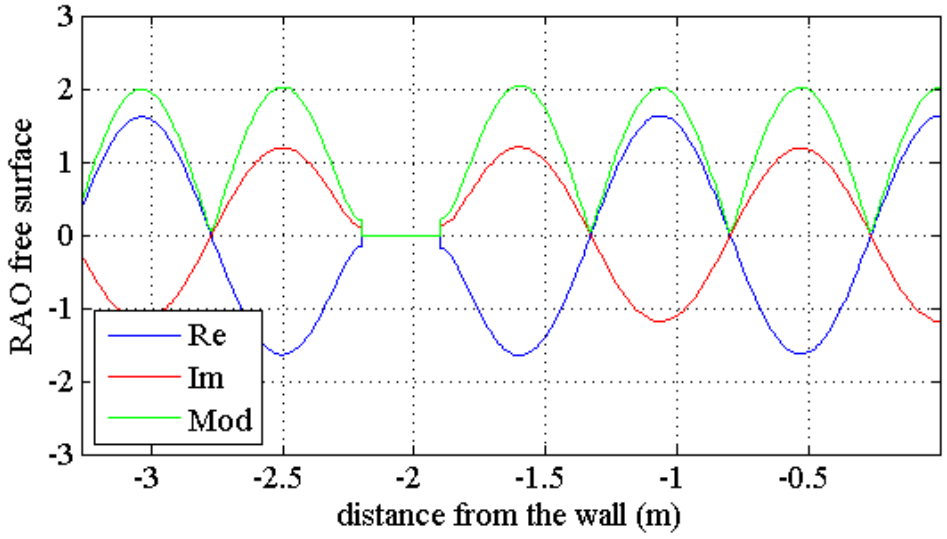

Figure 9-7: Free surface profile for *T*= 0.828 sec (neither sway nor roll) with viscous damping in roll.

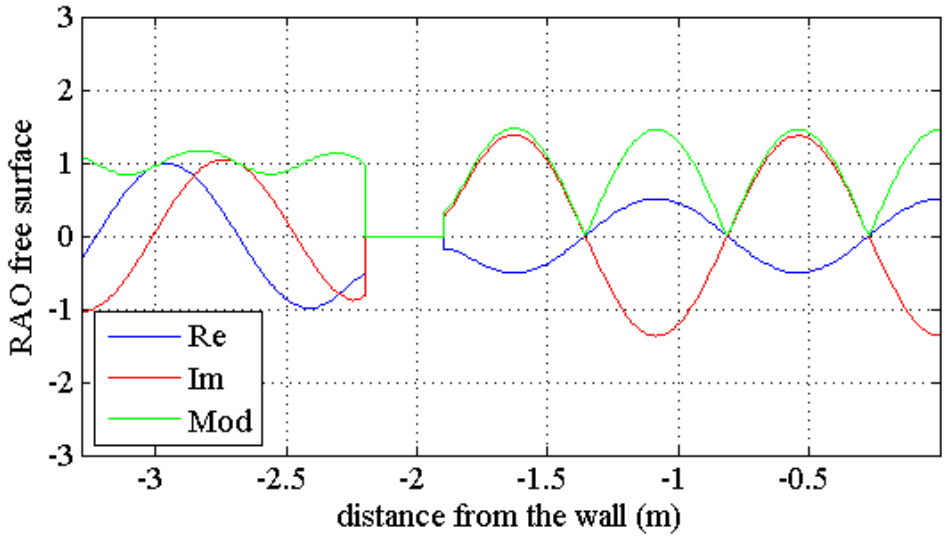

Figure 9-8: Free surface profile for *T*= 0.836 sec (neither sway nor roll) with viscous damping in roll and heave.

Figure 9-7 is in line with the theory we have already expressed. The presence of the body does not disturb the wave-field and additionally, the undisturbed incoming wave is fully reflected on the wall. Therefore the normalized free surface is equal to 2. When the heave damping is added (Fig. 9-8) it is obvious that a great part of the reflected wave on the wall is absorbed and consequently the normalized free surface approaches the value level of 1. To sum up, Figure 9-8 illustrates that when the heave response is significant, viscous phenomena arising from the heave response are also significant. Thus, when a heave dissipation term is added, in other words when the dissipation caused by viscous phenomena due to heave resonance is accounted for, the reflected wave on the wall seems to reduce.

At this point, the free surface elevation when the negative drift force is maximum is plotted.

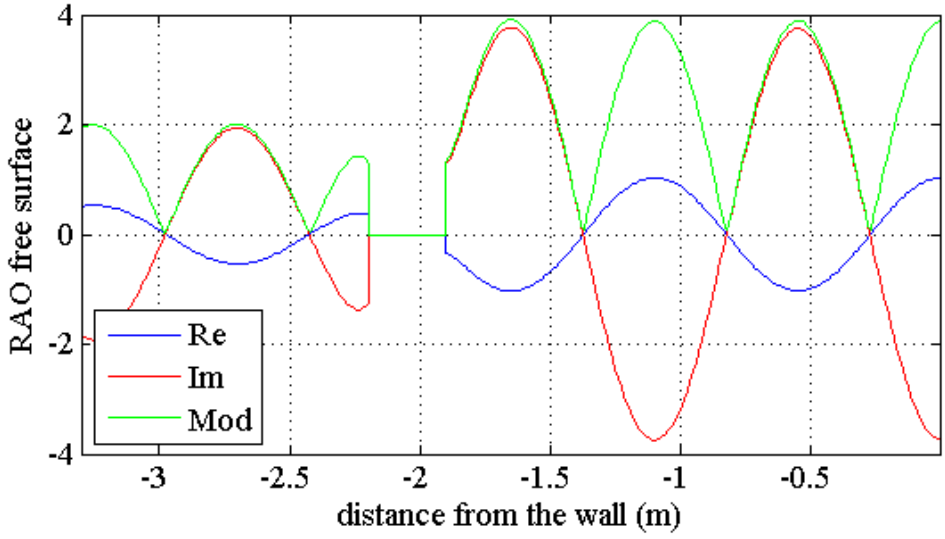

Figure 9-9: Free surface profile for *T*= 0.842 sec (maximum negative drift force) with viscous damping in roll.

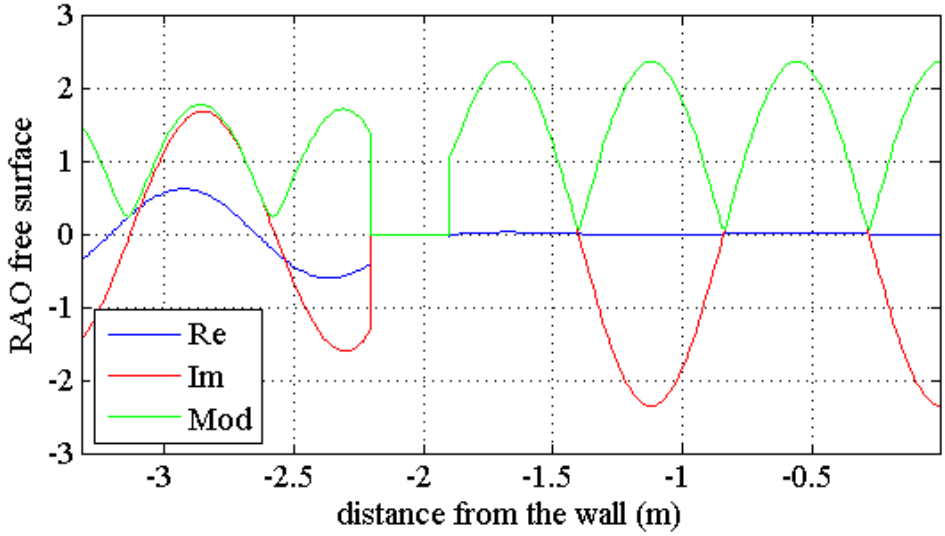

Figure 9-10: Free surface profile for *T*= 0.850 sec (maximum negative drift force) with roll and heave dissipation terms.

In both Figures 9-9, 9-10 it is obvious that the maximum negative drift force coincides with a maximum free surface elevation in the gap between the barge and the wall. It is mentioned that this maximum depicts a resonance of the free surface linked with the phenomenon of high sloshing modes. It is not surprising that when heave damping is added in the equations (Fig. 9-10), this phenomenon is reduced in magnitude. However, the phenomenon even if reduced in magnitude is not nullified. The viscous effects do not cause the total damping of the high sloshing modes.

The following graphs concern the case where the distance between the wall and the barge is equal to 0.9 m.

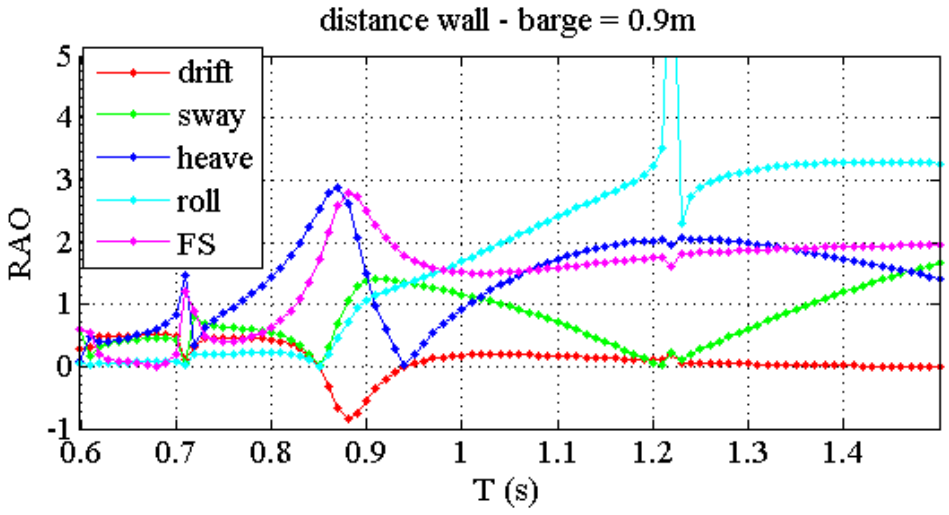

Figure 9-11: Barge 1.9 m from the wall with no dissipation terms in the equations.

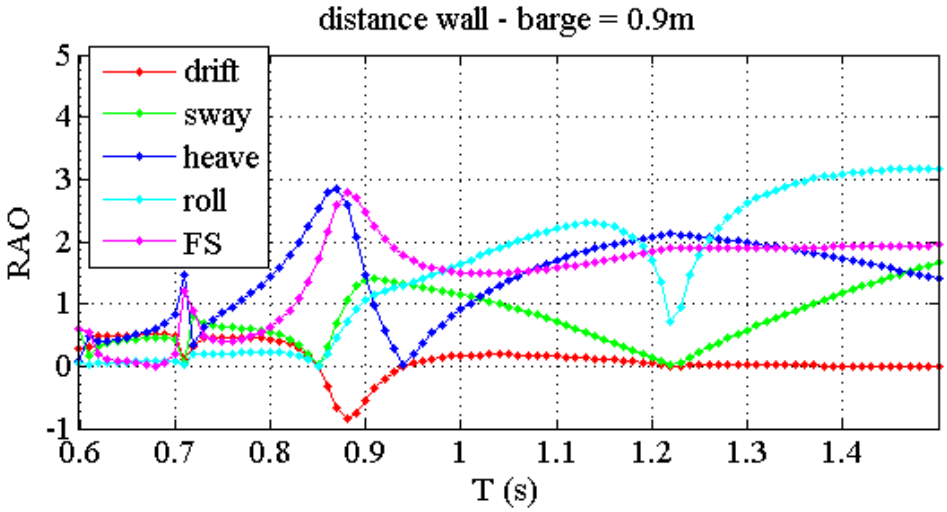

Figure 9-12: Barge 0.9 m from the wall with viscous damping in roll.

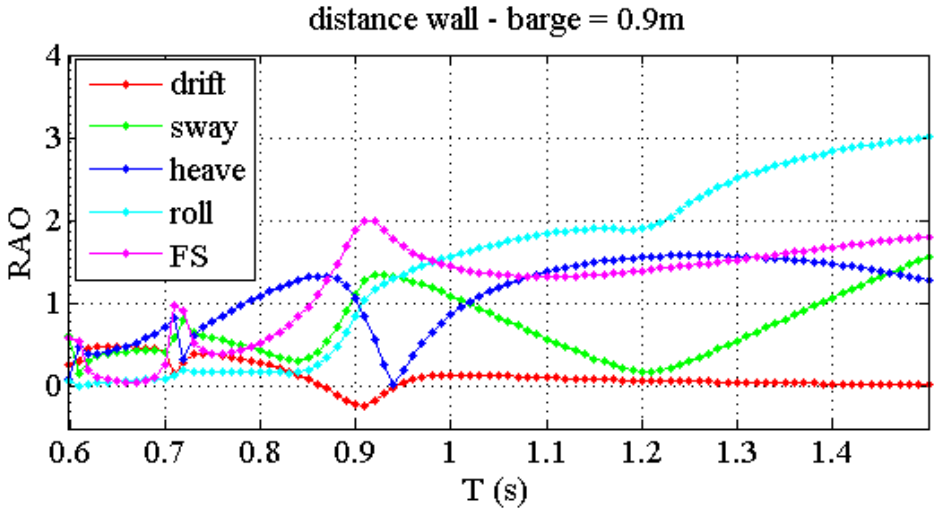

Figure 9-13: Barge 0.9 m from the wall with viscous damping in roll and heave.

By comparing Figures 9-11, 9-12, 9-13 corresponding to distance wall-barge equal to 0.9 m, we come to the same conclusion about the impact of the viscous roll and heave damping on the total results: the viscous roll damping mainly diminishes the roll response whereas under the influence of both roll and heave damping the heave, the free surface elevation and the negative drift force are also reduced in magnitude. In Figure 9-13 similarly to Figure 9-4 the normalized free surface elevation never exceeds the value level of 2.

Moreover, it is observed that in total the RAOs plotted for the smaller distance exhibit less pronounced maxima (especially for the case with no viscous dissipation terms or with only a roll dissipation term) and show a smoother oscillation with a smaller number of peaks than the RAOs corresponding to a greater distance.

To continue with, the free surface elevation as a function of the distance from the wall is plotted for two periods where in the first case (T = 0.86 sec) neither sway nor roll are observed and in the second case (T = 0.95 sec) heave is equal to zero. In both cases a roll and a heave dissipation terms are added in the equations.

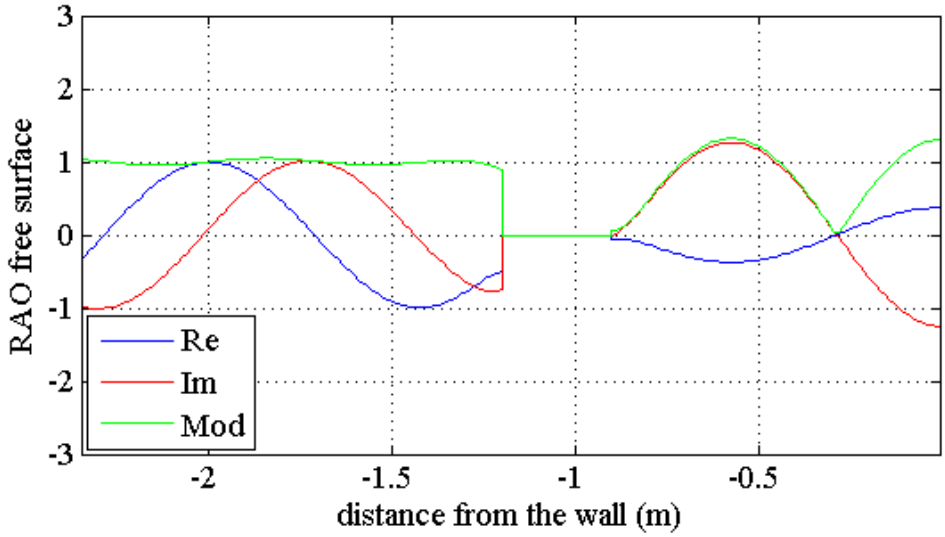

Figure 9-14: Free surface profile for *T*= 0.86 sec (neither sway nor roll) with viscous damping in roll and heave.

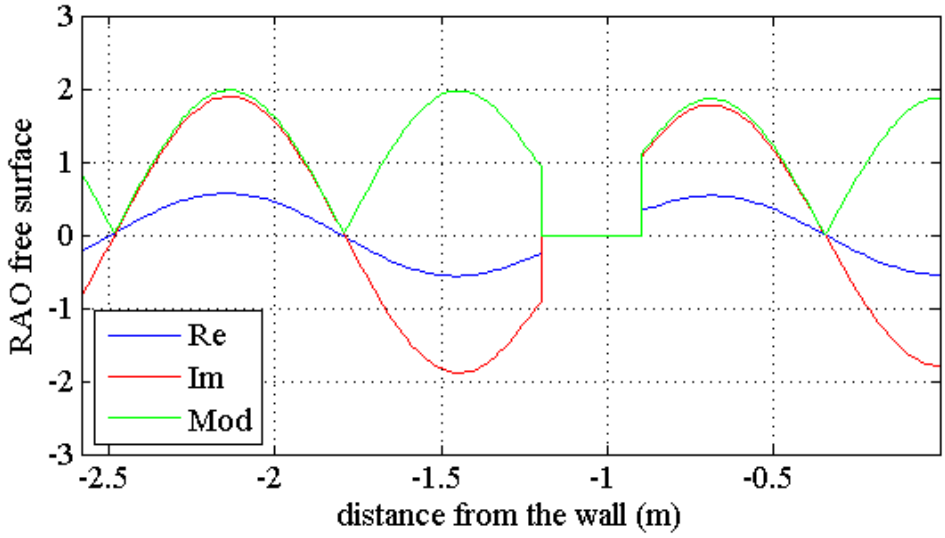

Figure 9-15: Free surface profile for *T*= 0.95 sec (no heave) with viscous damping in roll and heave.

Similarly to Figure 9-8, in period $T = 0.86$ sec where the heave is maximum and there are both roll and heave viscous damping terms added in the theoretical model the reflected wave on the wall is fully absorbed mainly due to the viscous effects caused by the heave resonance (Fig. 9-14). Concerning Figure 9-15, this graph is in line with Figure 9-6.

In the following graphs the case *distance wall-barge* = 0.2 m is presented:

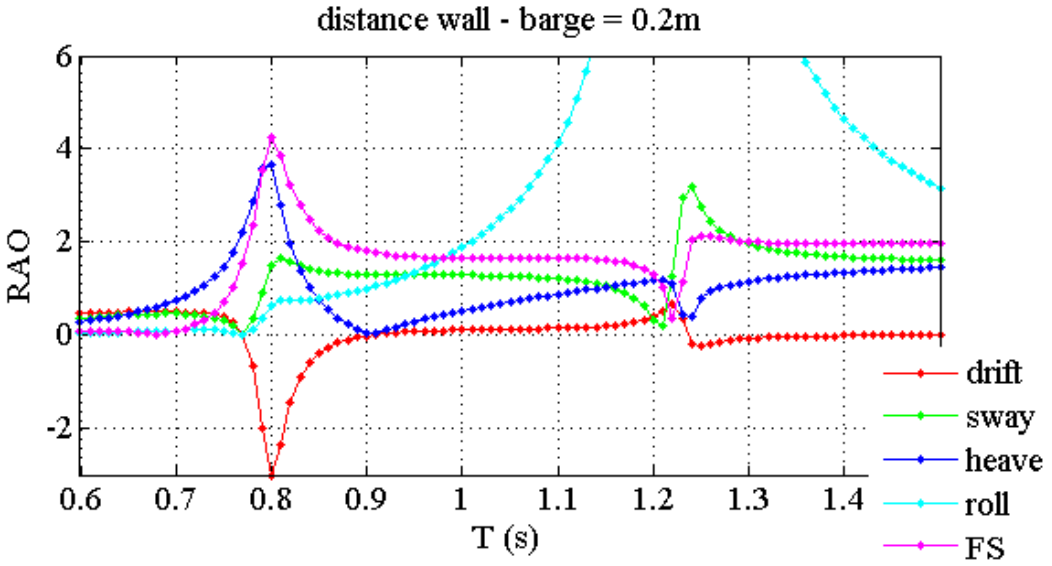

Figure 9-16: Barge 0.2 m from the wall with no viscous dissipation terms

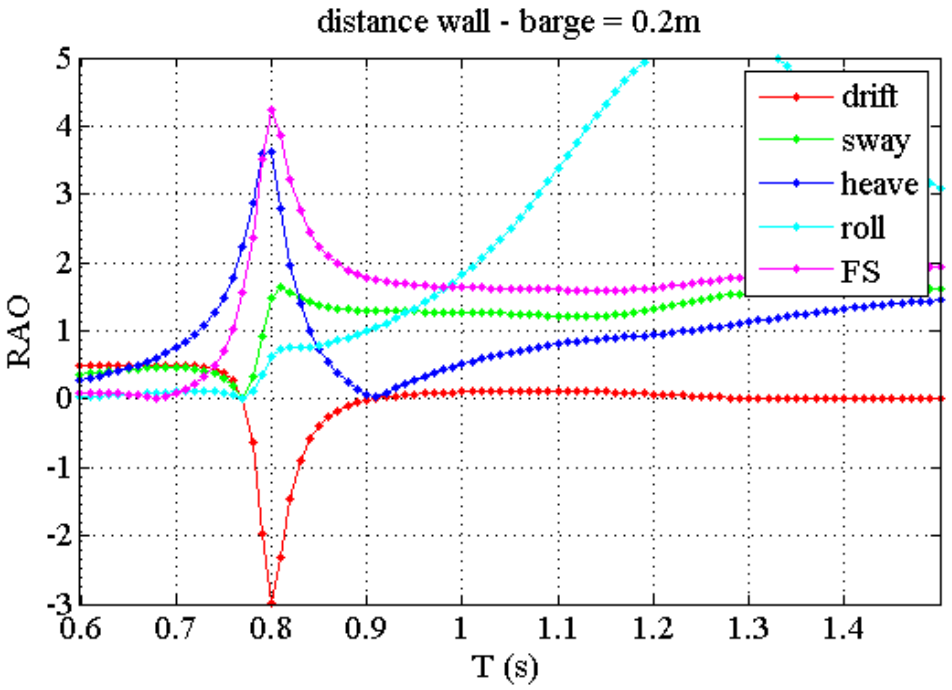

Figure 9-17: Barge 0.2 m from the wall with viscous damping in roll.

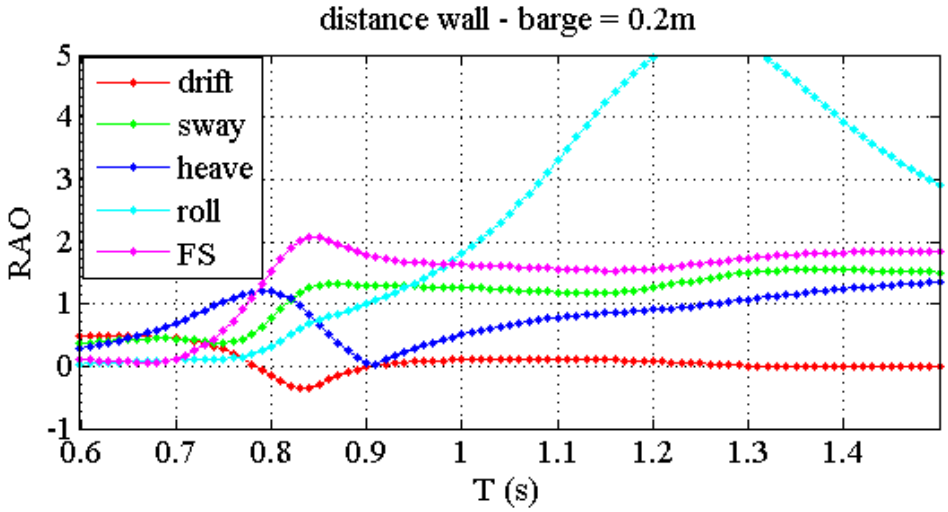

Figure 9-18: Barge 0.2 m from the wall with viscous damping in roll and heave.

In this case, it is depicted that the responses develop more pronounced maxima (especially for the case with no heave dissipation term) in comparison with the responses of a distance wall-barge equal to 0.9 m. However, these maxima are less pronounced compared to the maxima of the case where the distance is equal to 1.9 m. Therefore a general conclusion cannot be drawn concerning the impact of the distance on the considered degrees of freedom. However, the RAO of heave and the normalized free surface elevation at periods close to the period of maximization of the negative drift force can be considered as indicators of the magnitude of the negative drift force.

Concerning the oscillatory behavior, this case confirms the aforementioned remark that while the barge approaches the wall the oscillations of all degrees of freedom become smoother.

As a consequence of the short distance from the barge to the wall, the evanescent modes which are significant at close distance from the model become very important. They mainly influence the normalized free surface, at a point situated between the barge and the wall, and the normalized drift force. In Figure 9-17 with viscous damping in roll, the free surface elevation is strongly amplified when the peak of the negative drift force is observed ($RAO \approx 4$ at $T = 0.8$ s). This effect disappears when the heave damping is added. Furthermore, in Figure 9-18 it is shown that the value of the maximum negative drift force is lower when the heave damping is present.

To continue with, the experimental results are presented and compared with the theoretical results when possible. The first experimental series with no obstacle downwave the flow is now presented.

The diagrams corresponding to different parameters of the problem are plotted. A direct comparison between experiments and model is presented. Viscous damping coefficients in roll and heave have been taken into consideration in all the numerical results. The waterdepth is equal to 0.565 m for all the experiments of this series. The steepness is fixed at various values.

Experiments 1-20

Variable	Value
number of springs	4
period range [sec]	[0.5:1.45]
waterdepth [m]	0.565
roll viscous damping	0.2
heave viscous damping	3

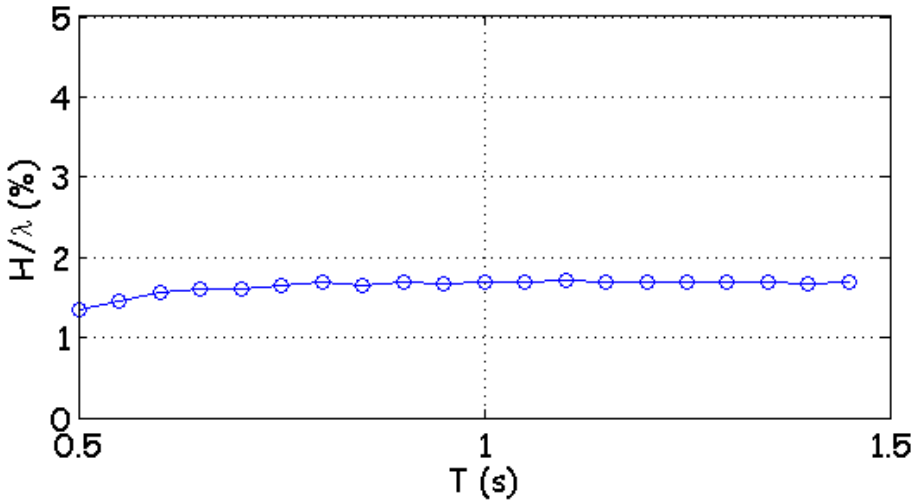

Figure 9-19: Steepness for experiments 1-20.

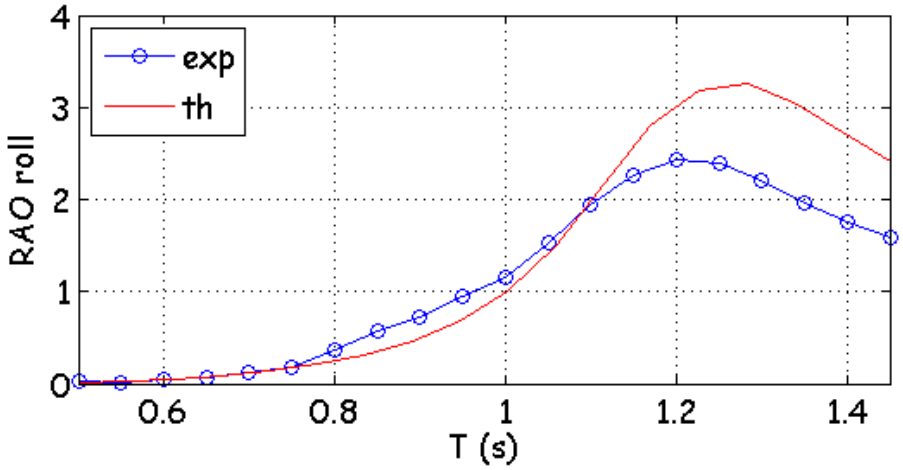

Figure 9-20: RAO of roll for experiments 1-20.

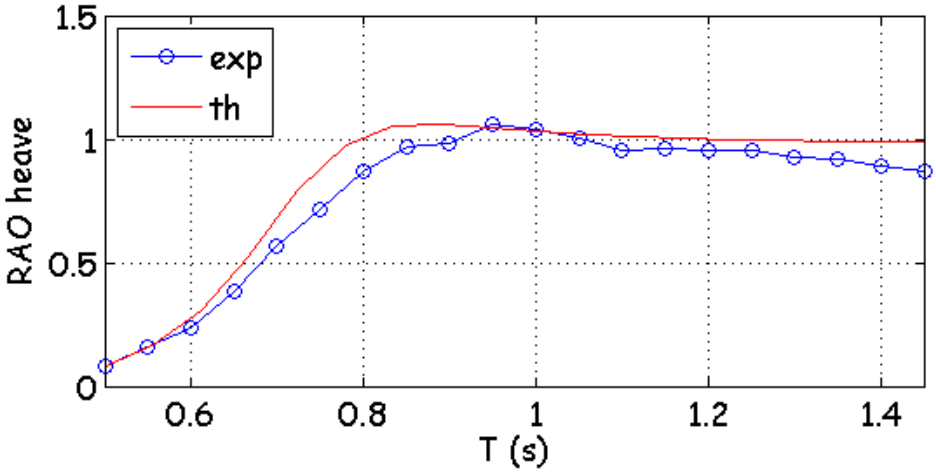

Figure 9-21: RAO of heave for experiments 1-20.

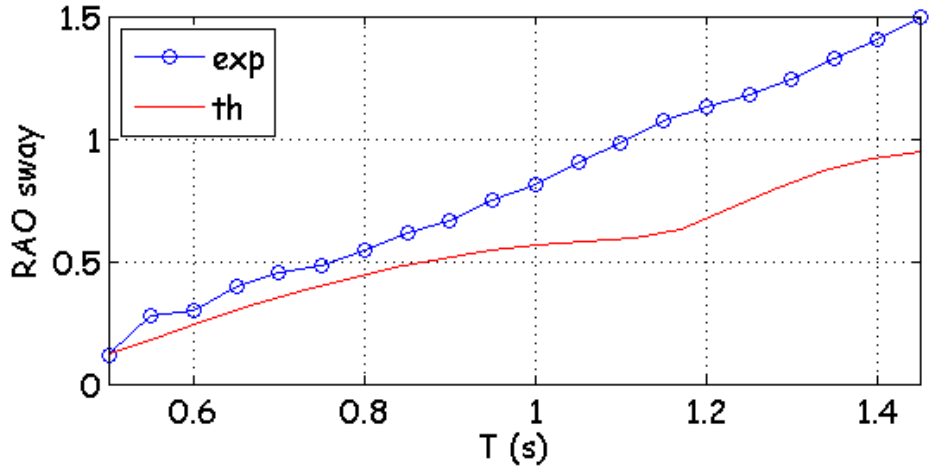

Figure 9-22: RAO of sway for experiments 1-20.

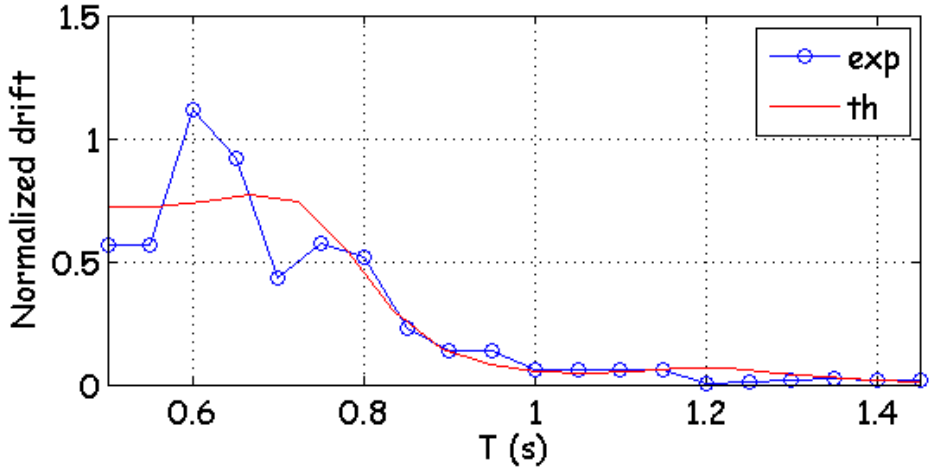

Figure 9-23: Normalized drift force for experiments 1-20.

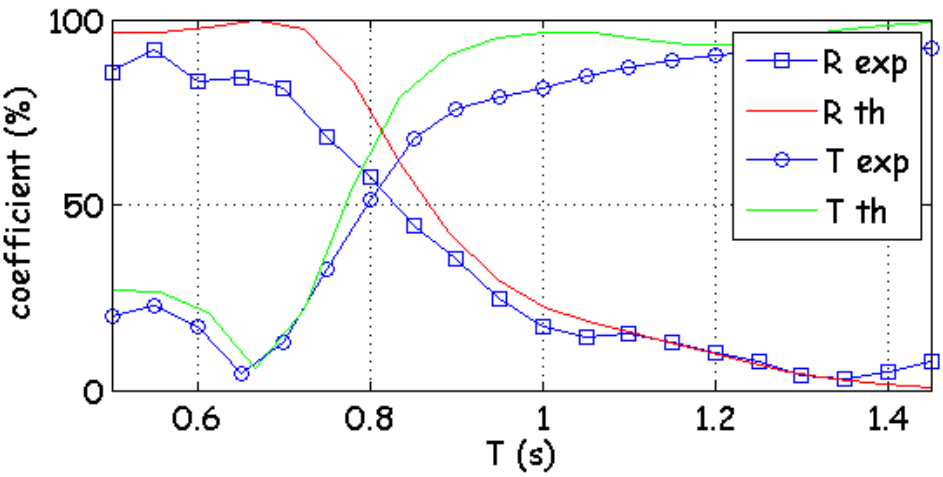

Figure 9-24: Coefficients of reflection and transmission for experiments 1-20.

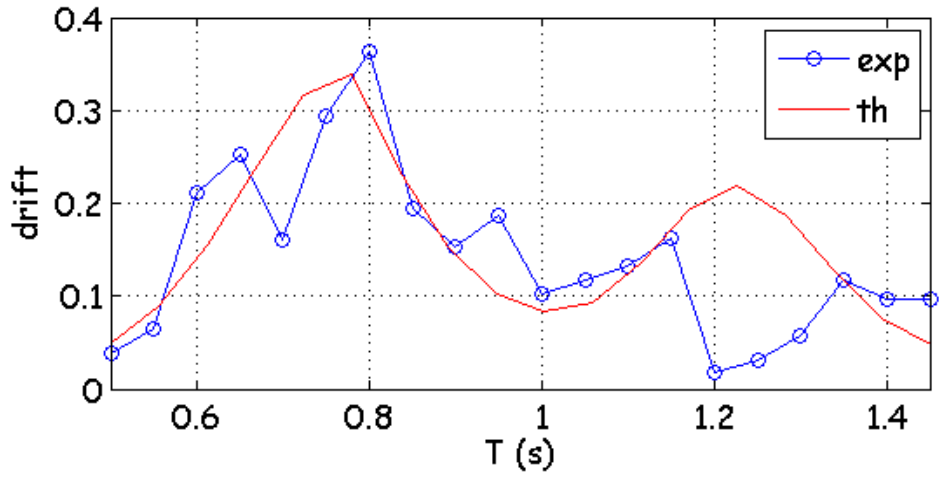

Figure 9-25: Drift force [N] for experiments 1-20.

Experiments 21-40

Variable	Value
number of springs	6
period range [sec]	[0.5:1.45]
waterdepth [m]	0.565
roll viscous damping	0.13
heave viscous damping	3

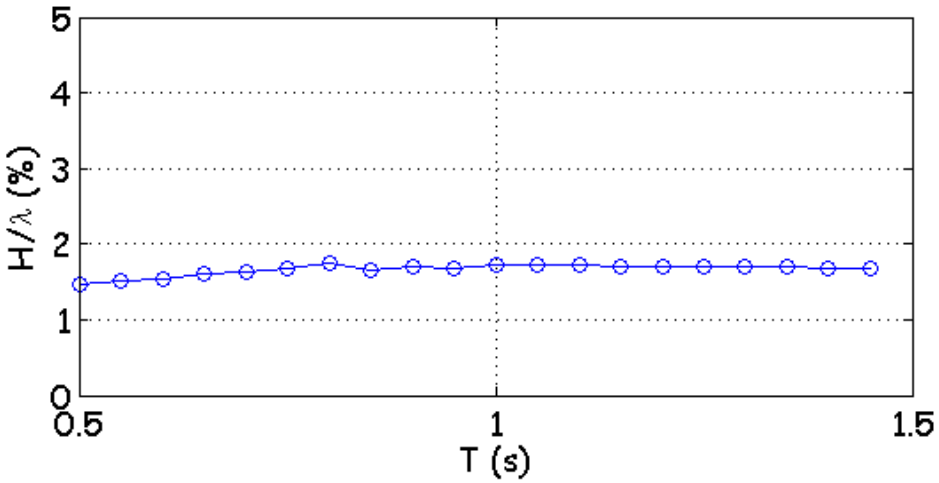

Figure 9-26: Steepness for experiments 21-40.

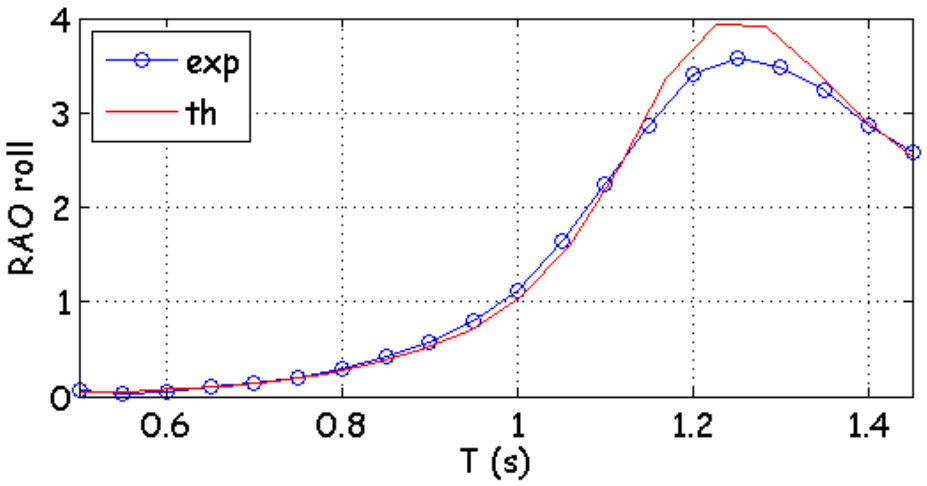

Figure 9-27: RAO of roll for experiments 21-40.

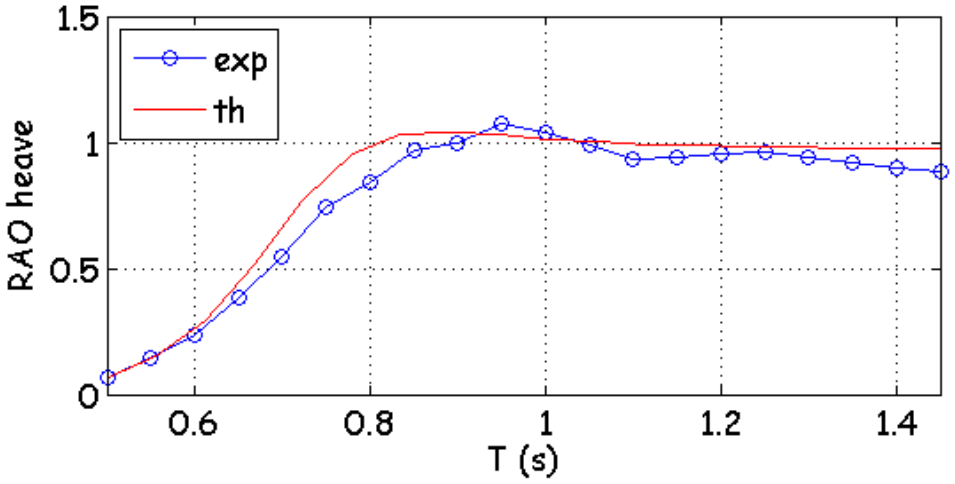

Figure 9-28: RAO of heave for experiments 21-40.

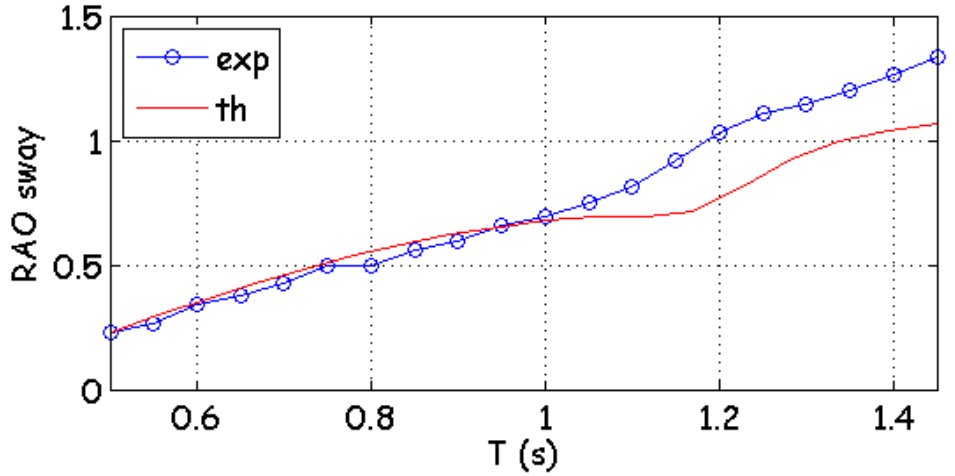

Figure 9-29: RAO of sway for experiments 21-40.

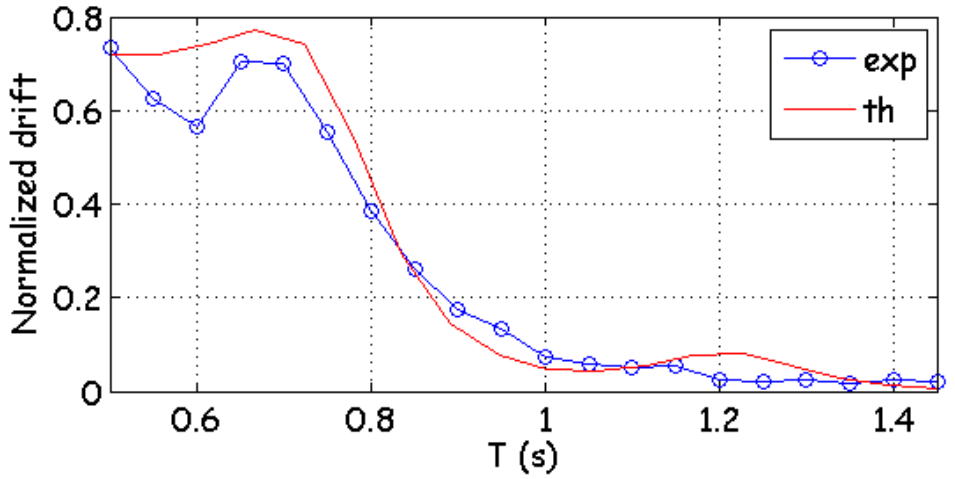

Figure 9-30: Normalized drift force for experiments 21-40.

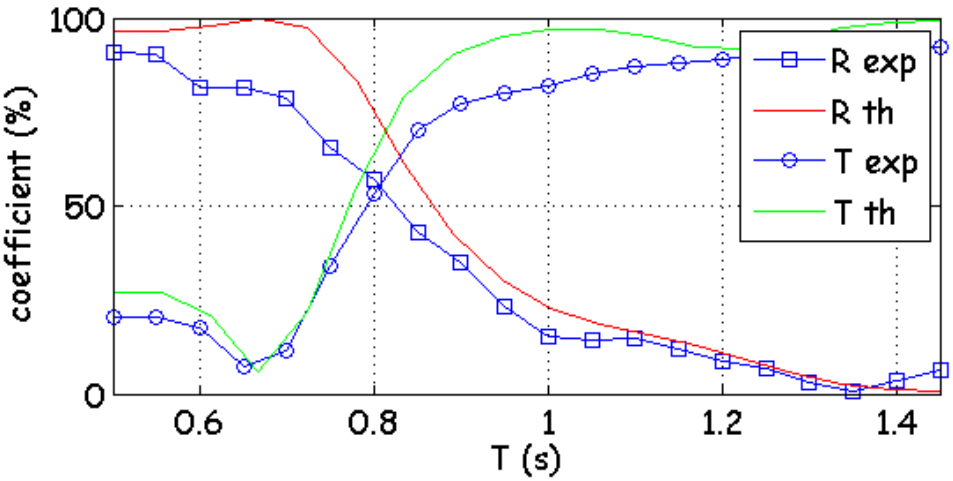

Figure 9-31: Coefficients of reflection and transmission for experiments 21-40.

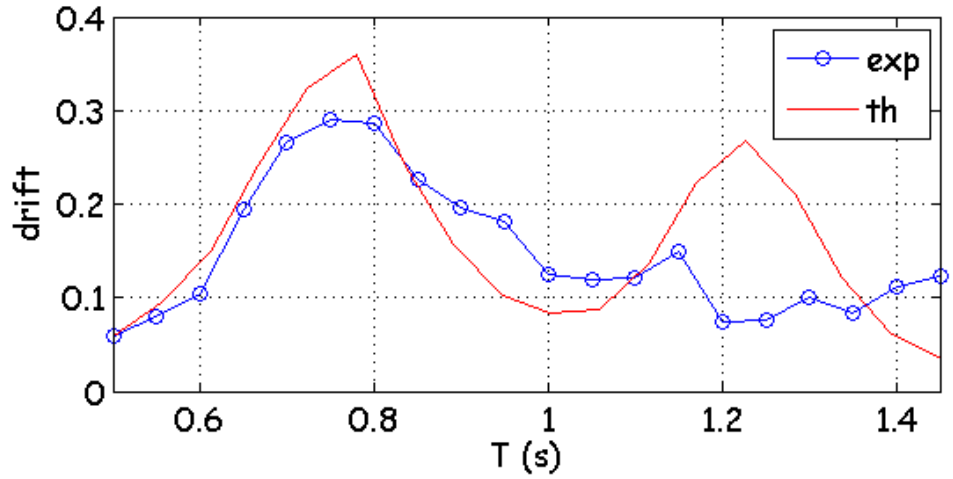

Figure 9-32: Drift force [N] for experiments 21-40.

Experiments 41-60

Variable	Value
number of springs	6
period range [sec]	[0.5:1.45]
waterdepth [m]	0.565
roll viscous damping	0.13
heave viscous damping	3

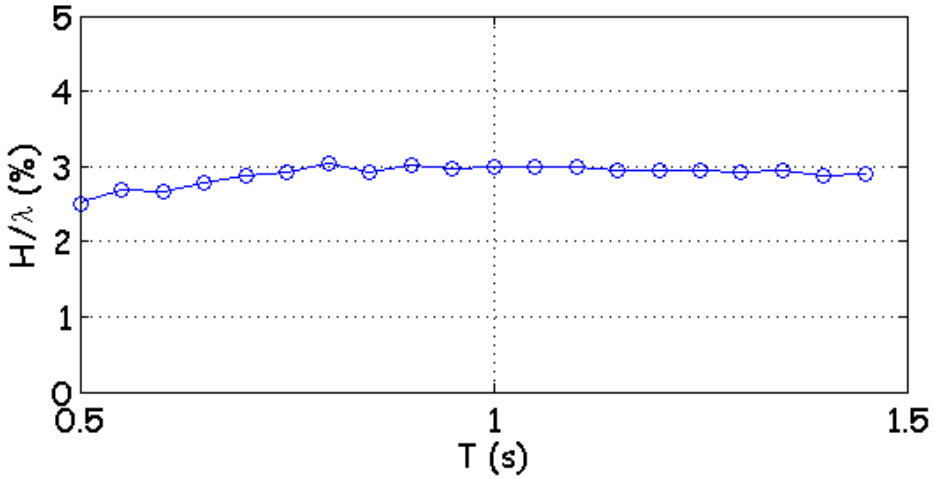

Figure 9-33: Steepness for experiments 41-60.

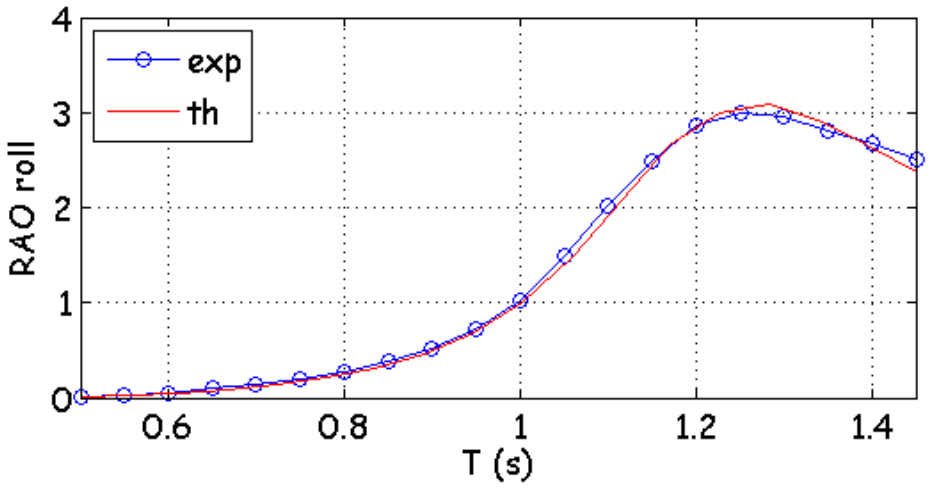

Figure 9-34: RAO of roll for experiments 41-60.

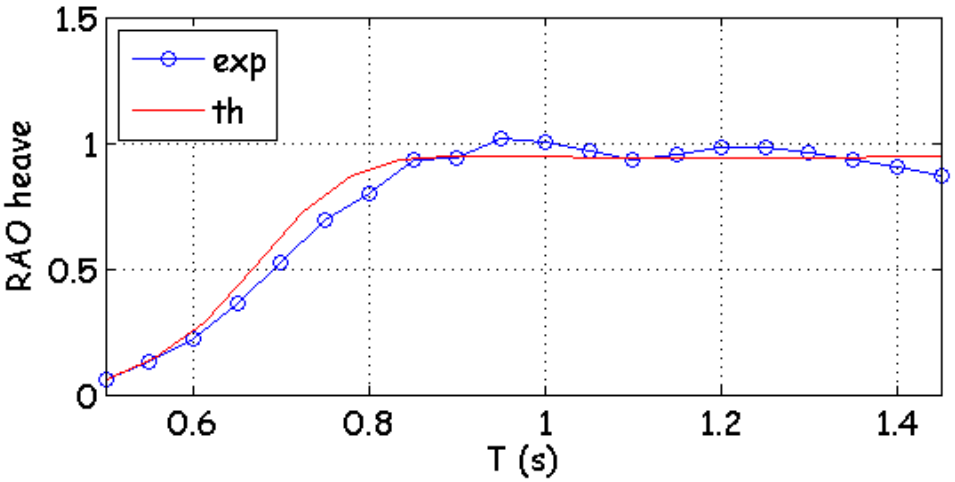

Figure 9-35: RAO of heave for experiments 41-60.

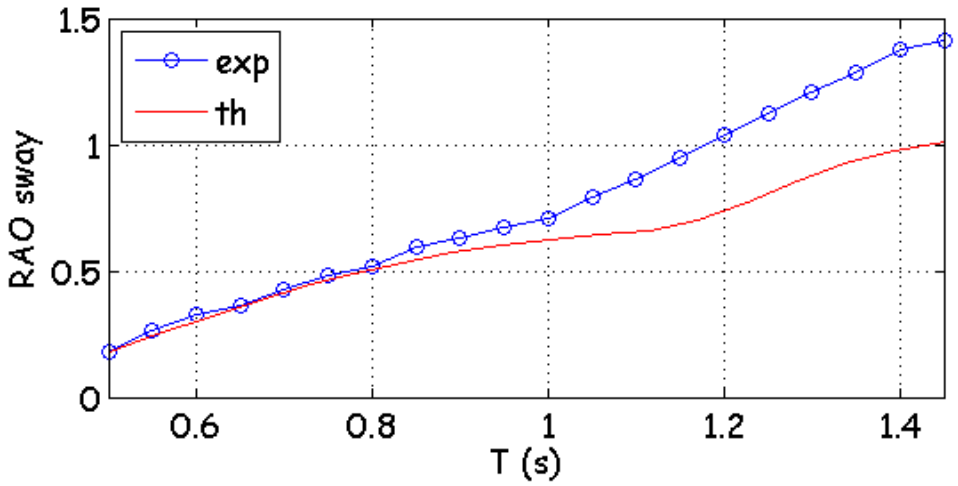

Figure 9-36: RAO of sway for experiments 41-60.

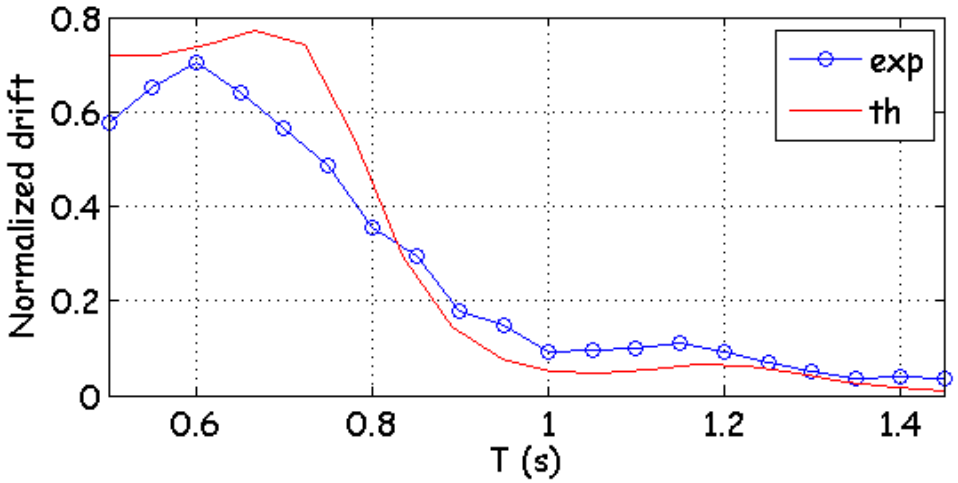

Figure 9-37: Normalized drift force for experiments 41-60.

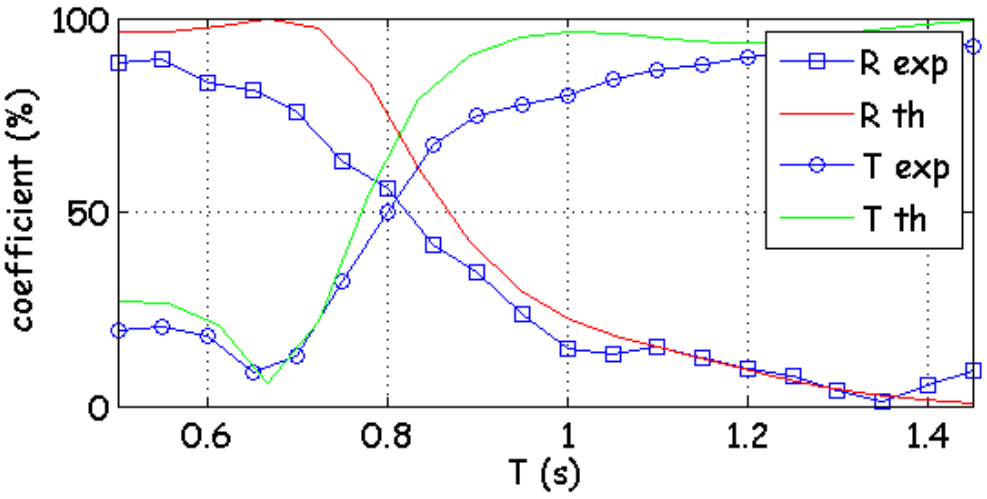

Figure 9-38: Coefficients of reflection and transmission for experiments 41-60.

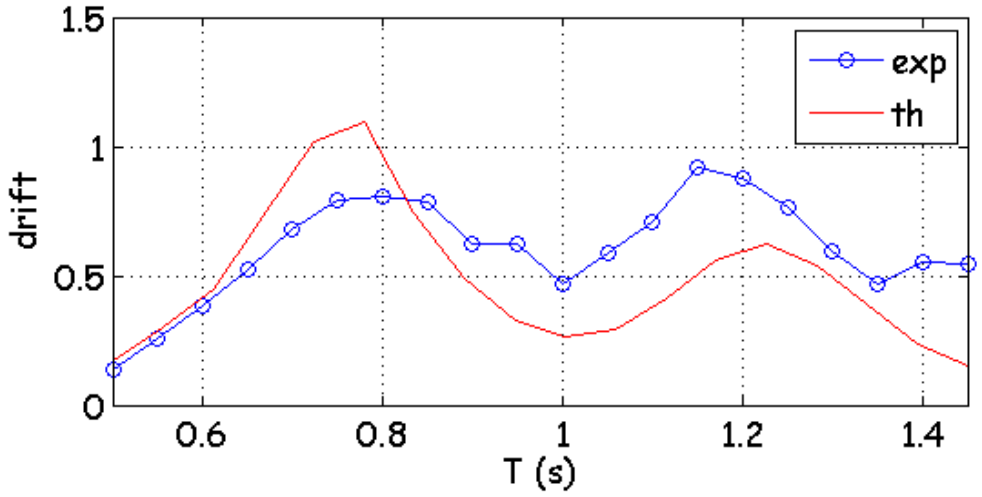

Figure 9-39: Drift force [N] for experiments 41-60.

Experiments 71-90

Variable	Value
number of springs	8
period range [sec]	[0.5:1.45]
waterdepth [m]	0.565
roll viscous damping	0.1
heave viscous damping	5

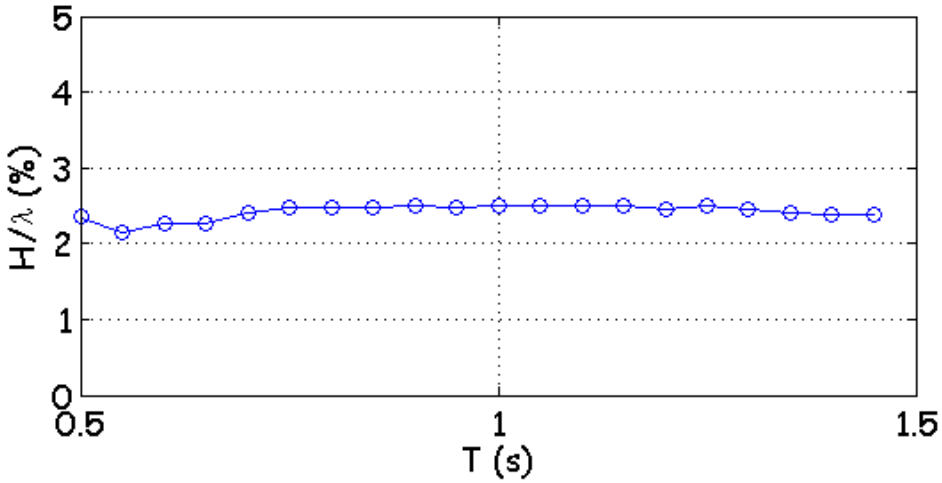

Figure 9-40: Steepness for experiments 71-90.

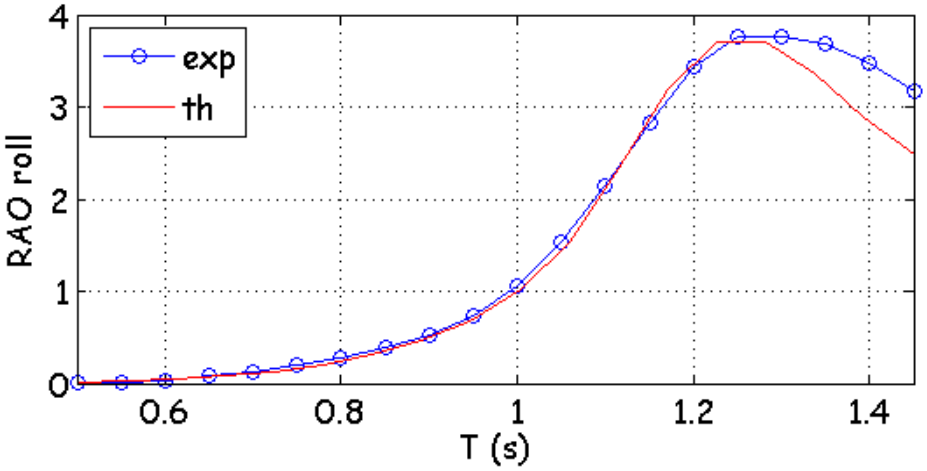

Figure 9-41: RAO of roll for experiments 71-90.

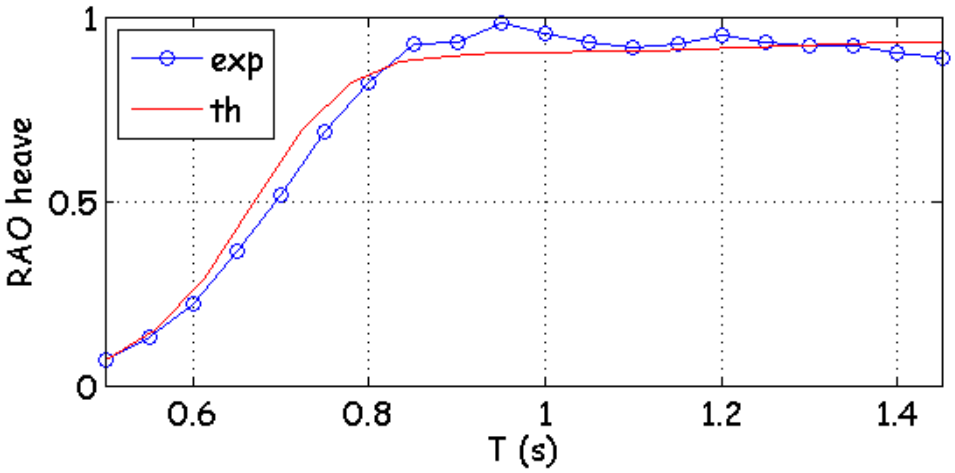

Figure 42: RAO of heave for experiments 71-90.

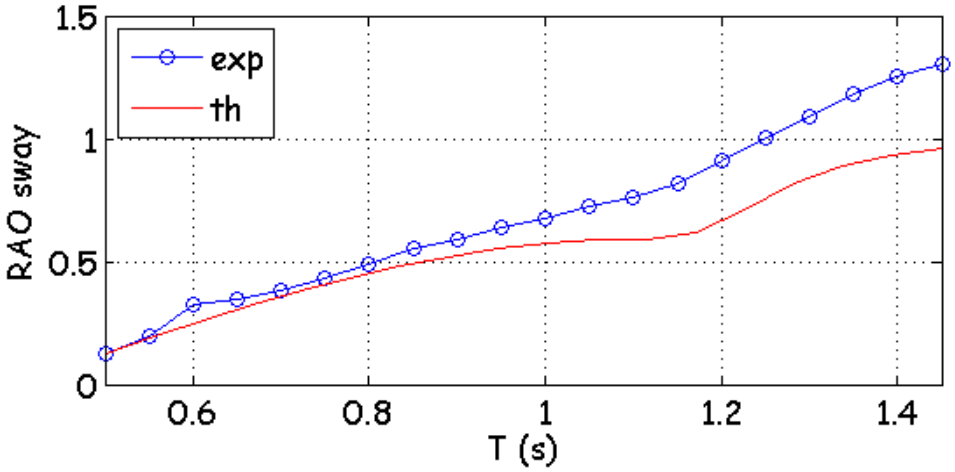

Figure 9-43: RAO of sway for experiments 71-90.

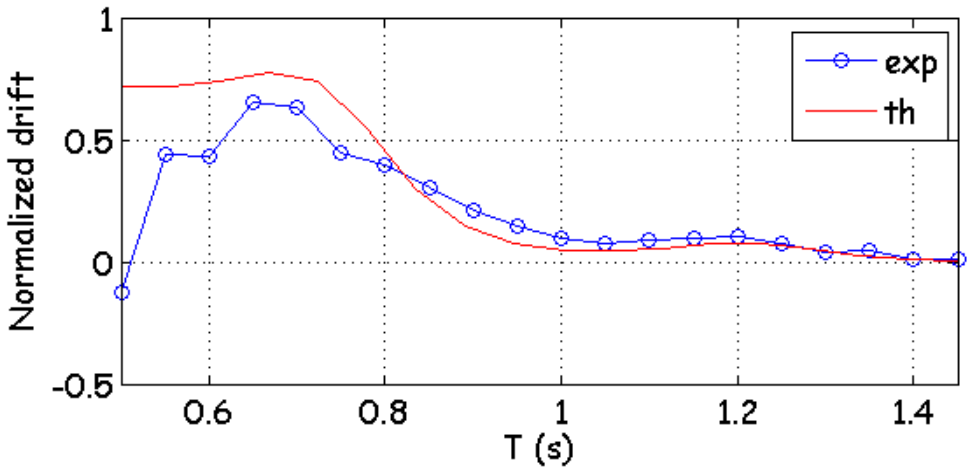

Figure 9-44: Normalized drift force for experiments 71-90.

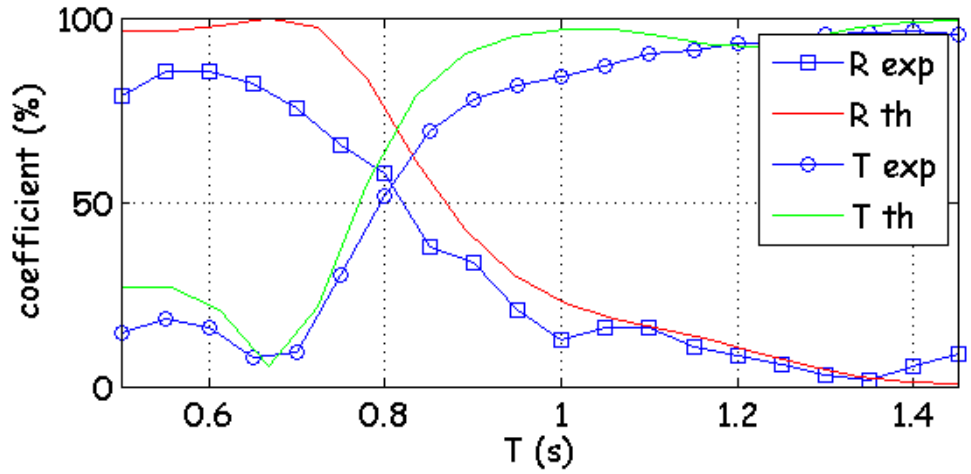

Figure 9-45: Coefficients of reflection and transmission for experiments 71-90.

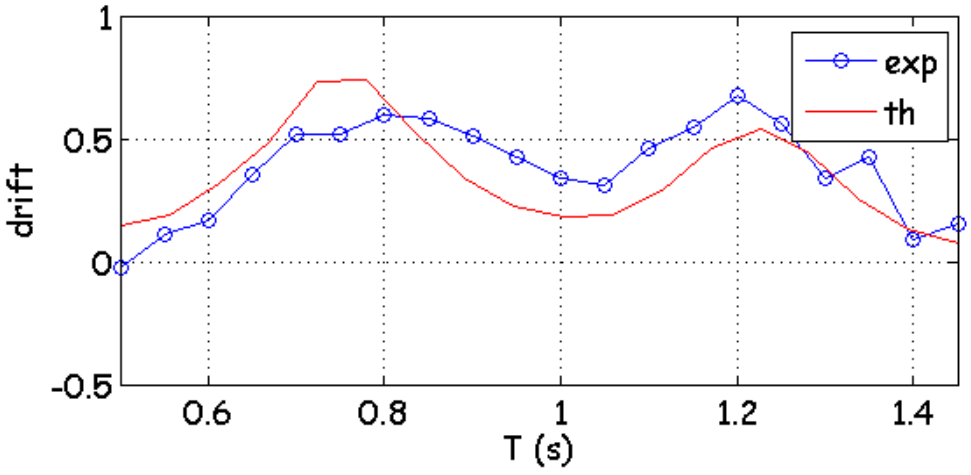

Figure 9-46: Drift force [N] for experiments 71-90.

It is shown that generally there is good agreement between experimental and theoretical results. For the drift force and for the normalized drift force there are greater discrepancies between theory and experiments and this is due to the difficulty of drift to reach a stable state. However, there is better agreement between theory and experiments for the drift force when the number of springs is equal to 8 (Fig. 9-44 and Fig. 9-46). When the number of springs is greater, the body exhibits a greater initial displacement but it more easily oscillates around a mean position, compared with a case with a smaller number of springs. If the drift movement attains a state of equilibrium, the average used for the experimental calculation of the drift force yields more realistic results. We must also not leave behind the fact that the numerical model cannot precisely follow a non-stable state where the mean position of the barge is not constant.

We come to the conclusion that the number of springs is a critical parameter in the measurement of the drift forces. However, the mooring system must be neither too loose nor too stiff. Before studying the drift forces it is important to formerly ensure that the first-order wave induced motions will not be influenced by the mooring system. In theory this requirement is satisfied if the only force induced by the mooring system is a constant force equal and opposite to the mean second-order wave drift force. For example, in our case of a spring system consisted of lines incorporating springs the spring system gives rise to a force which includes two parts: a constant and an oscillating part. The constant part is equal to the mean second-order drift force while the oscillating part is linked with the first-order motions and the spring characteristics of the mooring system. If the spring is too stiff, the oscillating part is more intense and may modify the first-order responses. If this is the case, the drift force may be also affected. [Pinkster (1980)]

Moreover, the stiffness is also connected with the natural frequency of the horizontal-plane motions (surge, sway, yaw). As the stiffness increases, the natural frequency also increases. Hence, there is the danger that the resultant higher natural frequency of the system coincides with the frequency range of the waves and resonance takes place. In a case of resonance both first-order motions and mean drift forces are affected.

At this point, the drift movement connected with the experiments 71-90 is plotted. The difficulty of drift to attain a stable position, even in a case with a greater number of springs, is depicted.

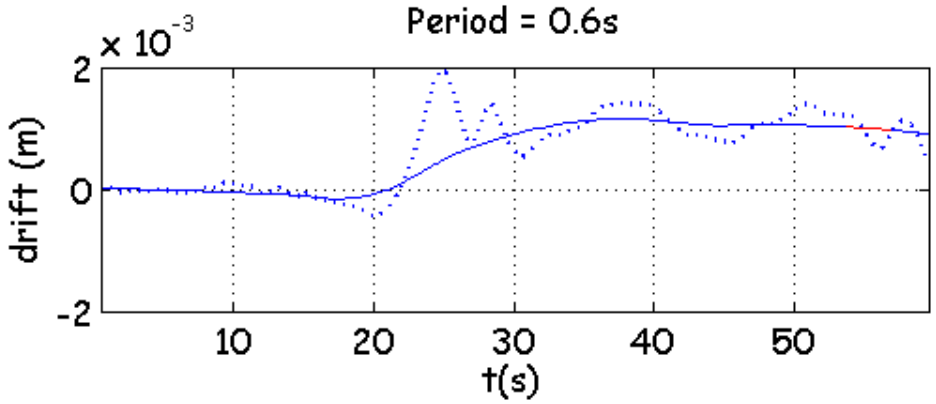

Figure 9-47: Drift movement for experiments 71-90 at T = 0.6 sec.

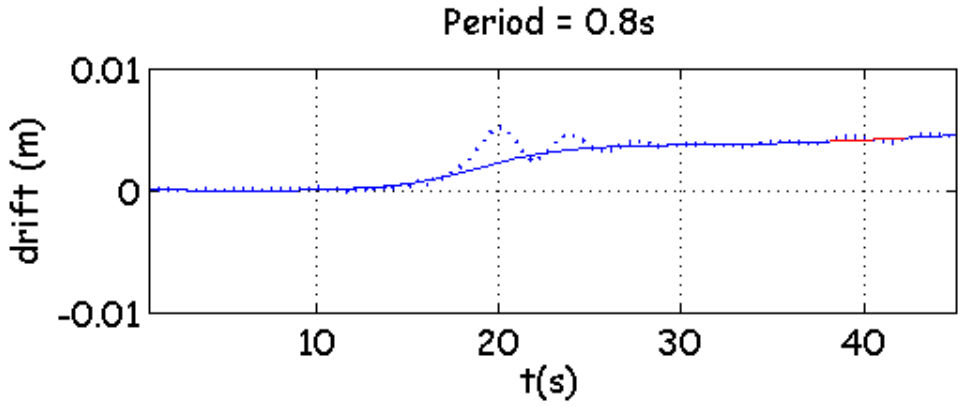

Figure 9-48: Drift movement for experiments 71-90 at T = 0.8 sec.

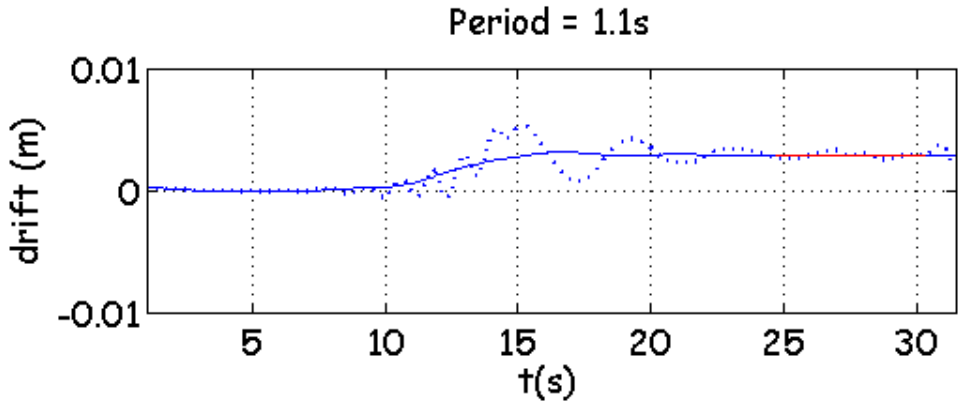

Figure 9-49: Drift movement for experiments 71-90 at T = 1.1 sec.

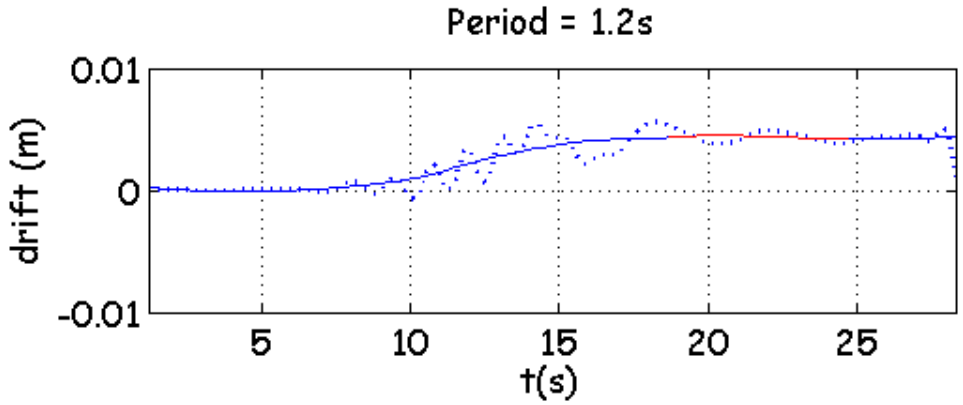

Figure 9-50: Drift movement for experiments 71-90 at T = 1.2 sec.

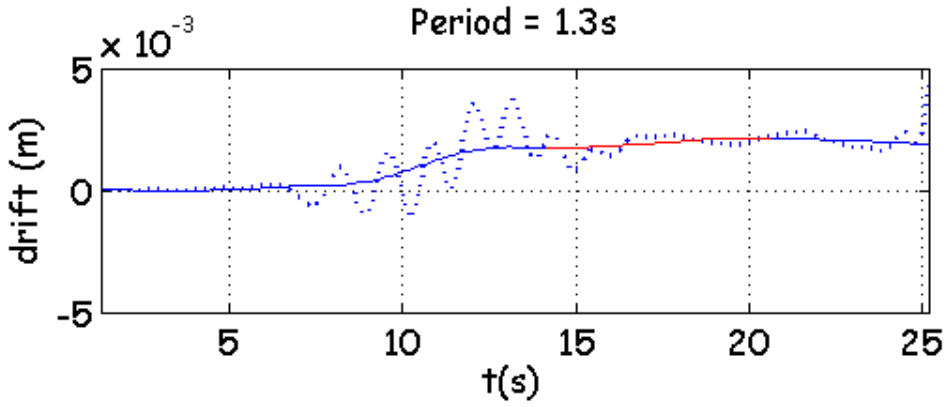

Figure 9-51: Drift movement for experiments 71-90 at T = 1.3 sec.

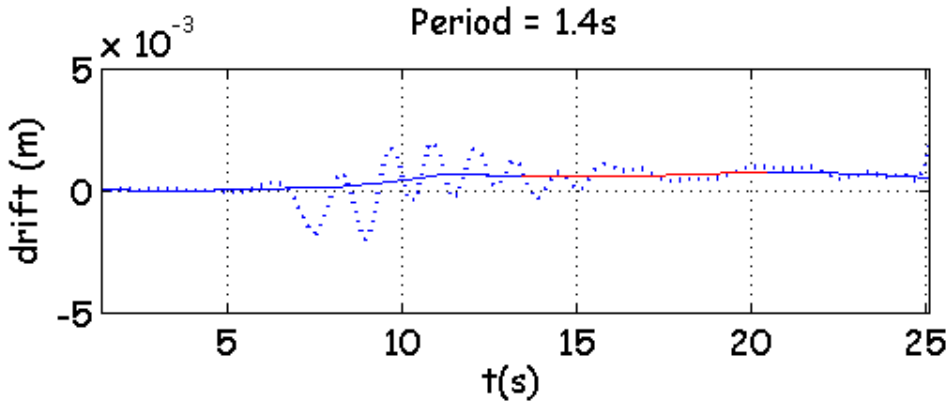

Figure 9-52: Drift movement for experiments 71-90 at T = 1.4 sec.

In the following, the case of the barge moored in front of a wall is studied. The distance between wall and barge is equal to 1.9 m, as measured from the right corner of the barge. The parameters of this experimental series are the following:

Experiments 241-258

Variable	Value
number of springs	6
period range [sec]	[0.6:1.45]
waterdepth [m[	0.506
roll viscous damping	0.1
heave viscous damping	5

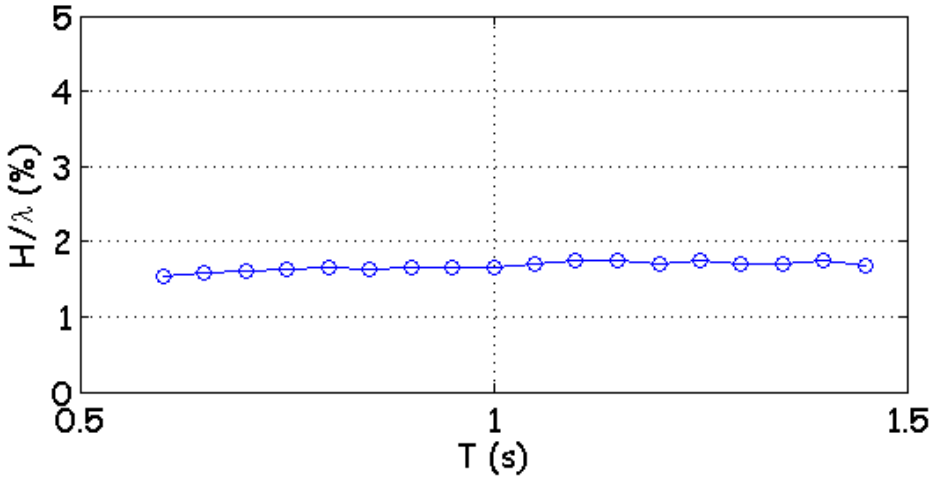

Figure 9-53: Steepness for experiments 241-258.

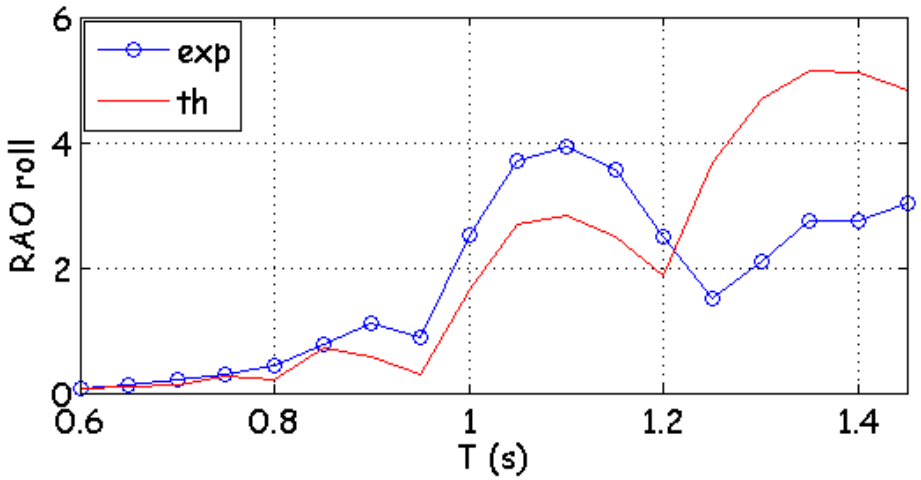

Figure 9-54: RAO of roll for experiments 241-258.

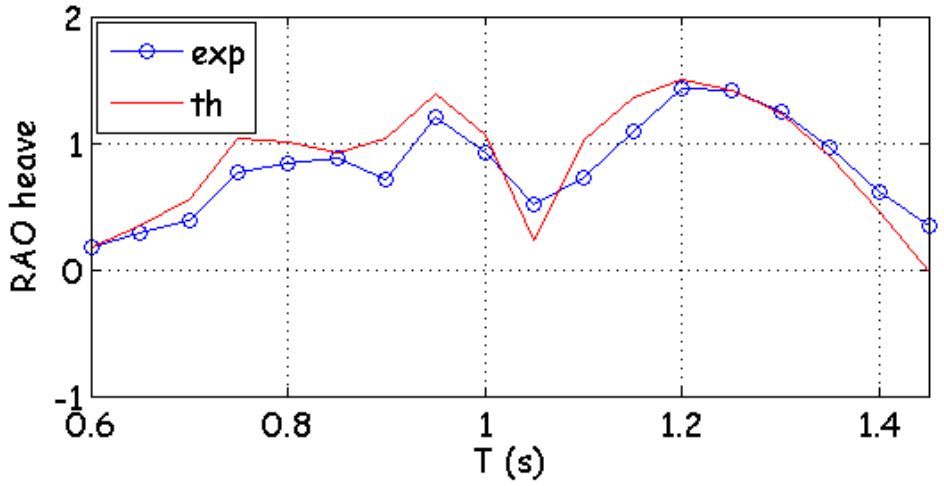

Figure 9-55: RAO of heave for experiments 241-258.

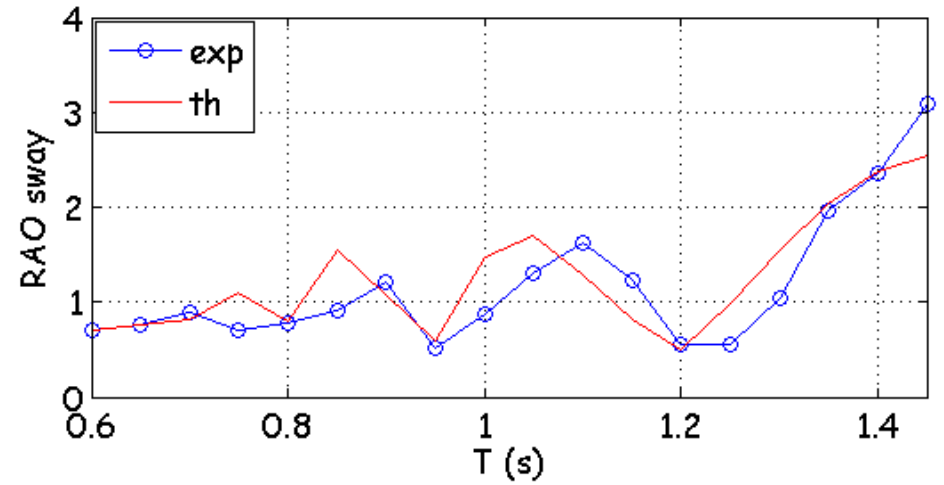

Figure 9-56: RAO of sway for experiments 241-258.

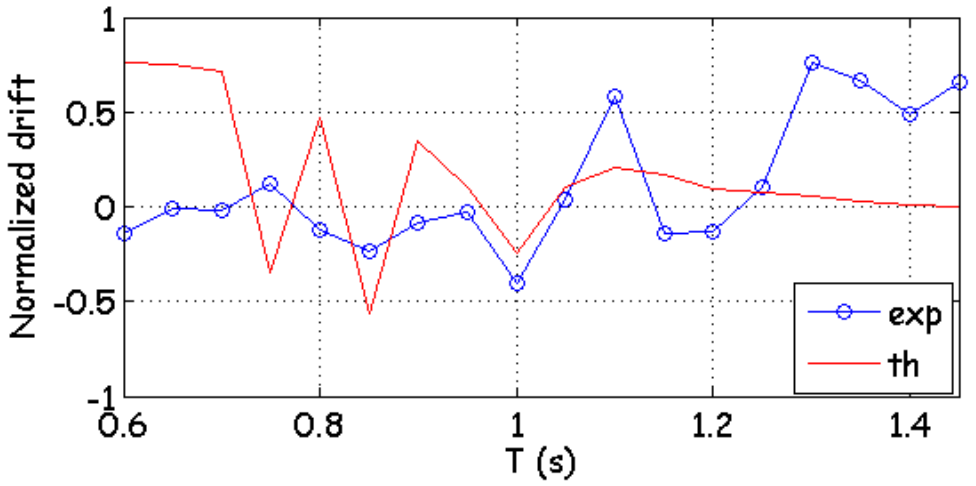

Figure 9-57: Normalized drift force for experiments 241-258.

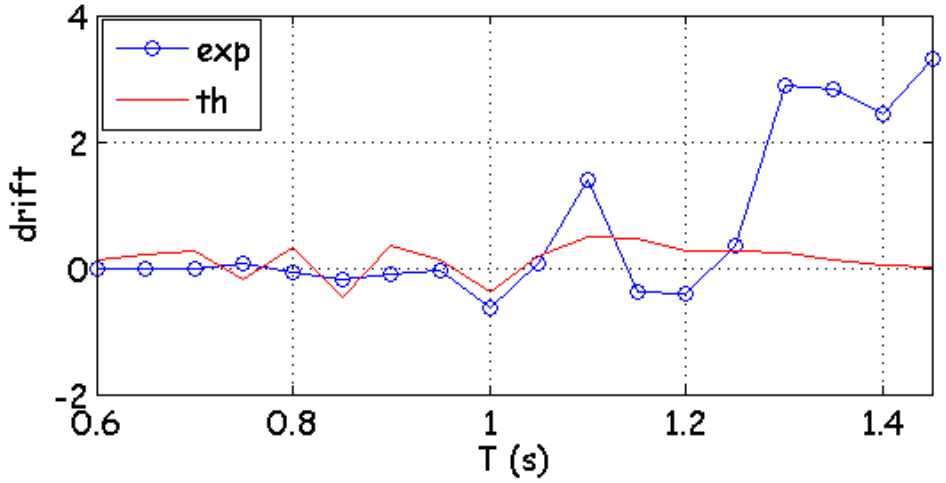

Figure 9-58: Drift force [N] for experiments 241-258.

It is shown that the results for roll and heave between experiments and theoretical model are in good agreement. The discrepancies observed for the RAO of sway and for the drift can be attributed to the mooring system because the experimental results present a lot of peaks in the drift graphs (for $T > 1$ sec) which are not predicted by the numerical model.

The reflection coefficient is plotted in Figure 9-59. By considering Figure 9-58 and Figure 9-59, it is observed that the minima of the reflection coefficient coincide with a zero or almost zero drift force. In particular, this is obvious for $T = 0.75$ sec, $T = 0.85$ sec, $T = 1.05$ sec. Therefore, the experimental results confirm the statement that when the drift force is equal to zero or approaches zero, the structure of the body is considered to be transparent and the wave reflected from the body tends to zero.

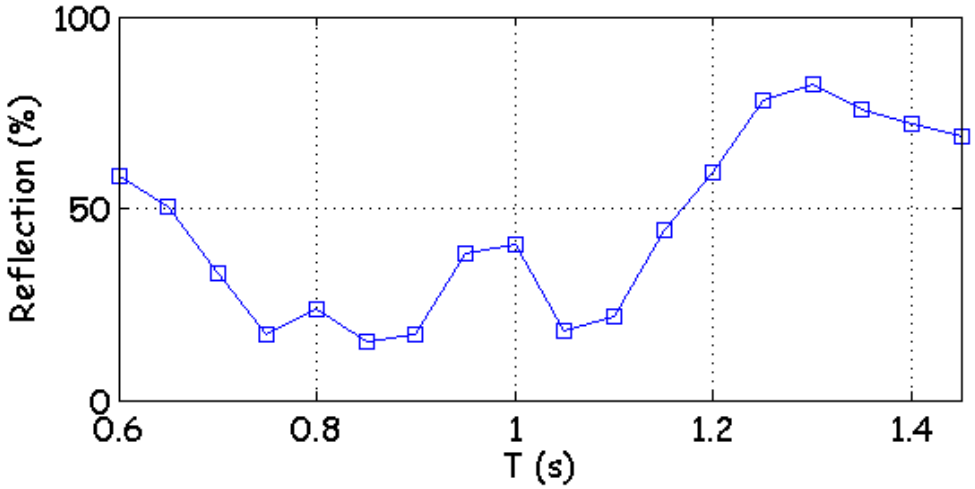

Figure 9-59: Coefficient of reflection for experiments 241-258.

The experimental results for $T = 0.95$ sec and $T = 1.45$ sec are now studied. As already mentioned, these are two characteristic cases of the theoretical model where while the drift force is equal to zero, we observe respectively either cancellation of sway and roll motion or cancellation of heave motion. The calculations of the numerical model for *distance wall-barge* = 1.9 m and *waterdepth* = 0.506 m are plotted (Fig. 9-60).

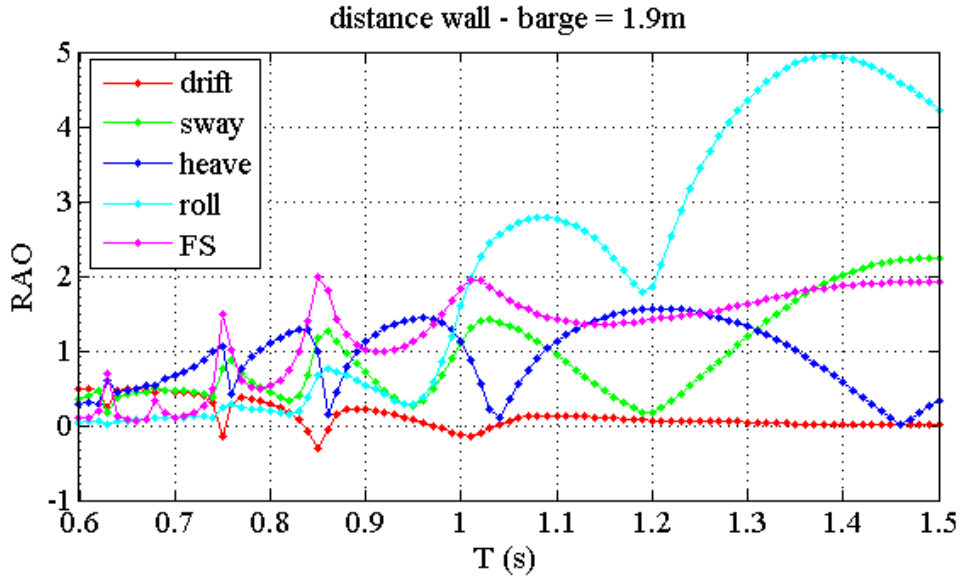

Figure 9-60: Barge 1.9 m from the wall with viscous damping in roll and heave.

At T = 0.95 sec the experimental results confirm the cancellation of sway and roll (Fig. 9-61). In the same period, a local maximum of heave is observed in Figure 9-55.

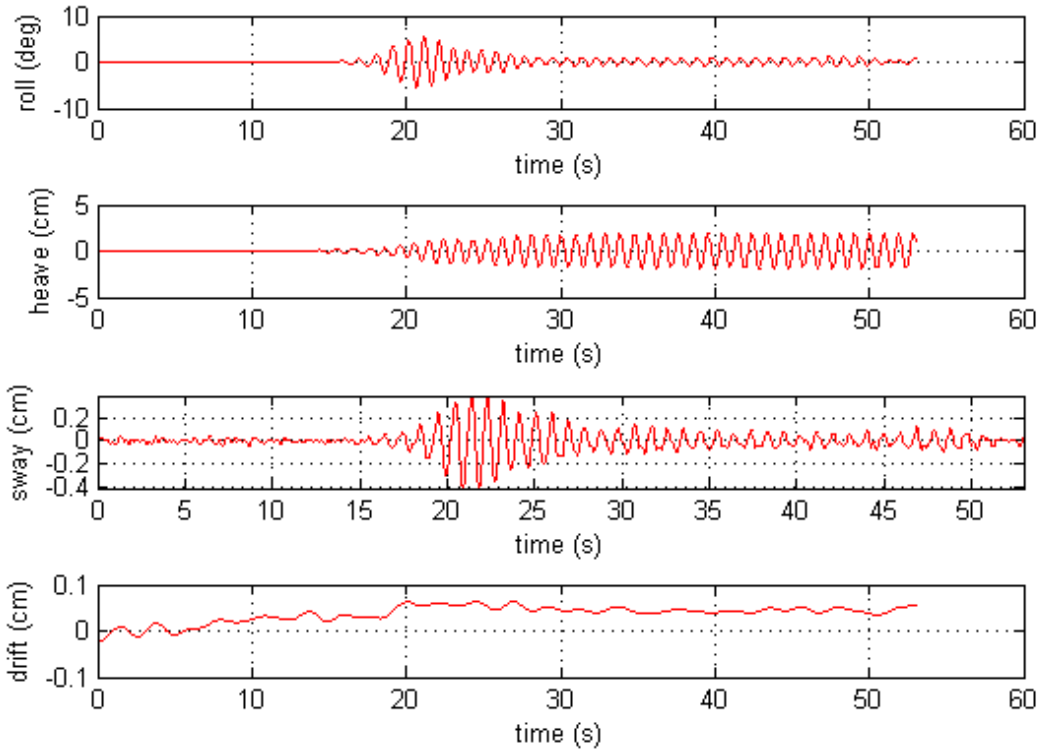

Figure 9-61: Responses for experiments 241-258 at T = 0.95 sec.

At T = 1.45 sec the extinction of heave is also observed for the experimental results (Fig. 9-62). In addition, at this period the roll and the sway responses are situated in area of increasing value (Fig. 9-54 and Fig. 9-56).

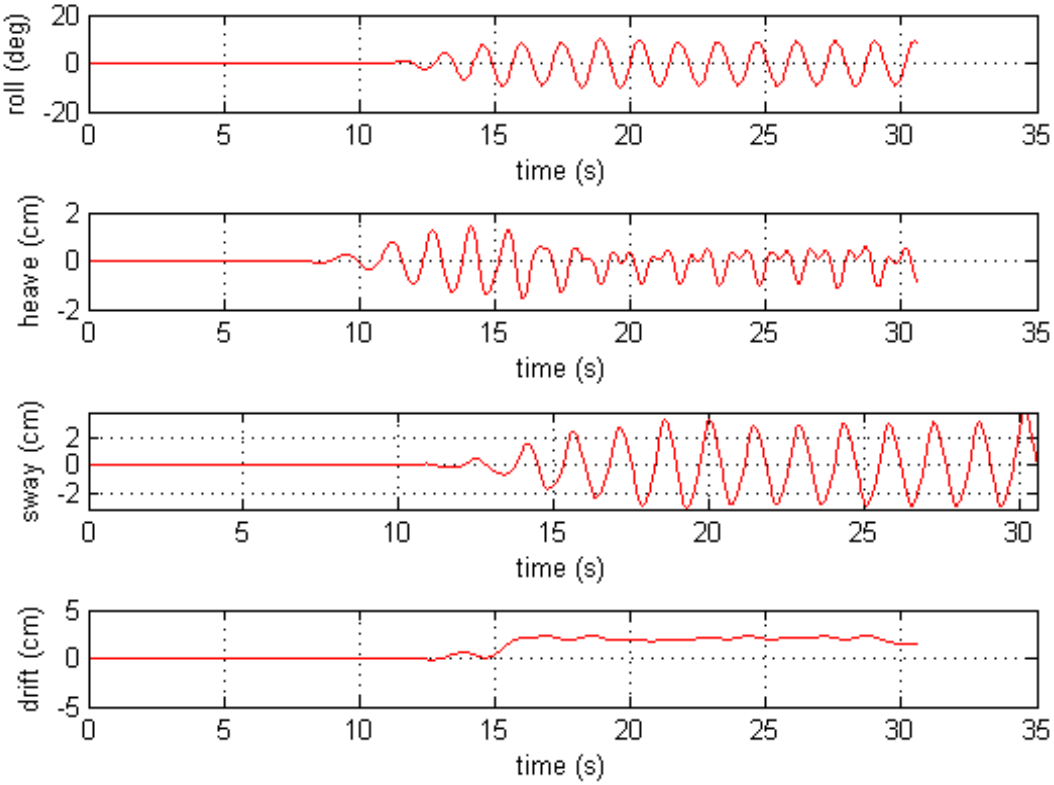

Figure 9-62: Responses for experiments 241-258 at T =1.45 sec.

The case of the freely drifting rectangular barge in front of a wall is now considered. The distance between wall and barge is equal to 0.2 m, as measured from the right corner of the barge. The parameters of this experimental series are the following:

Experiments 151-162

Variable	Value
period range [sec]	[0.5:1.05]
waterdepth [m]	0.513
roll viscous damping	0.1

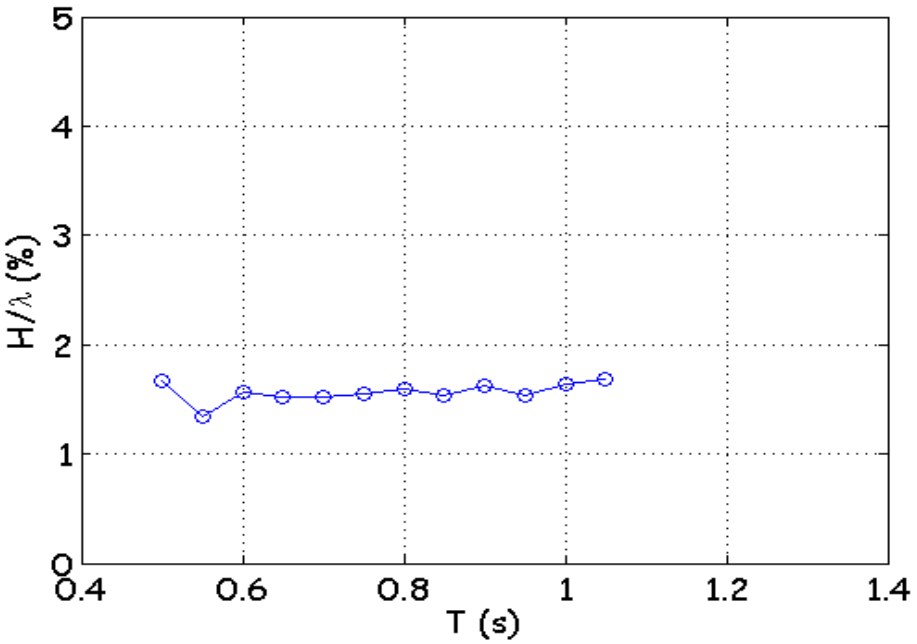

Figure 9-63: Steepness for experiments 151-162.

As already mentioned in *Chapters 7 and 8*, the drift force can neither be calculated nor measured when the barge is not moored. The numerical model is practical only when the model is oscillating around a mean position. Furthermore, the drift force is a function of the distance between wall and barge and it changes continuously depending on the exact position of the barge with reference to the wall. As it will be shown, in the solution of the free barge problem the drift force must be calculated for the instantaneous position of the barge.

To this end, the experimental results for the case of $T = 0.8$ sec are presented (Fig. 9-65, 9-66). The RAO of heave is maximum for this period (Fig. 9-64).

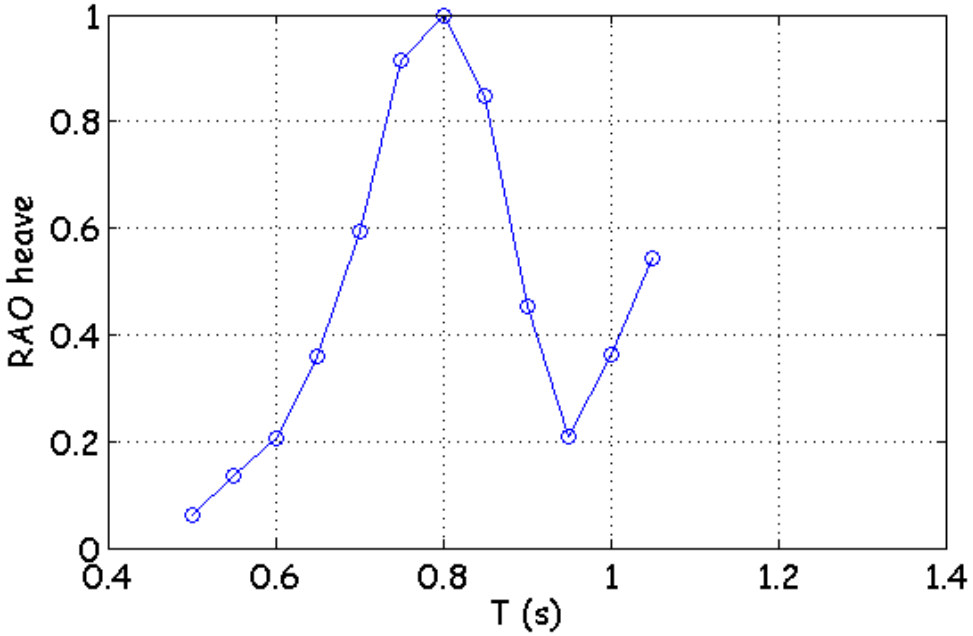

Figure 9-64: RAO of heave for experiments 151-162.

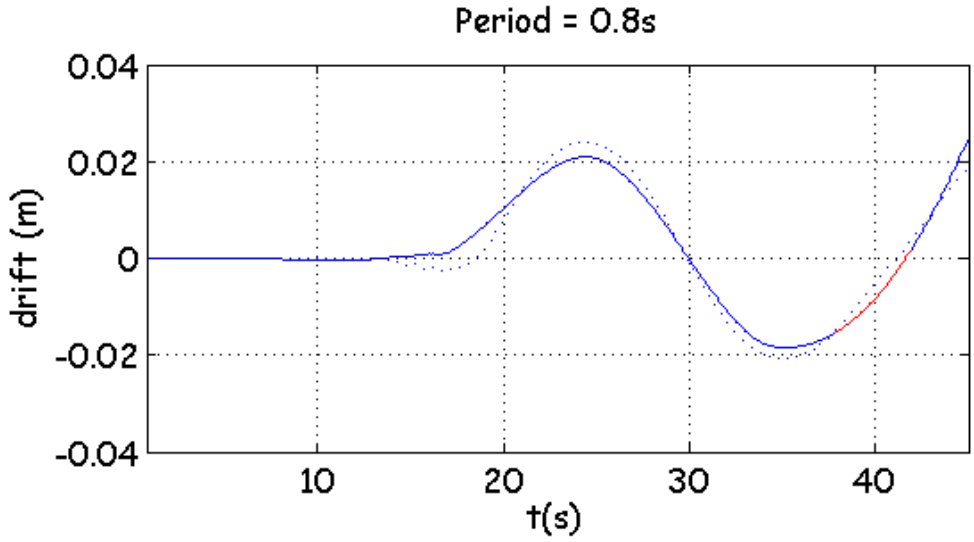

Figure 9-65: Drift movement for experiments 151-162 at T = 0.8 sec.

It is observed that in this case where the barge is set free the drift movement, before applying the matlab function `smooth()`, is smoother comparing it with a case where the barge is moored (Figure 9-65).

In the following graph (Fig. 9-66), at T = 0.8 sec the extinction of roll and sway motion in the time interval $t = 30 - 40$ sec is shown. The heave response has a constant value and as it is apparent from Figure 9-64 this is also the maximum value as far as this experimental series is concerned. In addition, we become aware of the fact that at $t = 35$ sec the drift movement attains its maximum negative value.

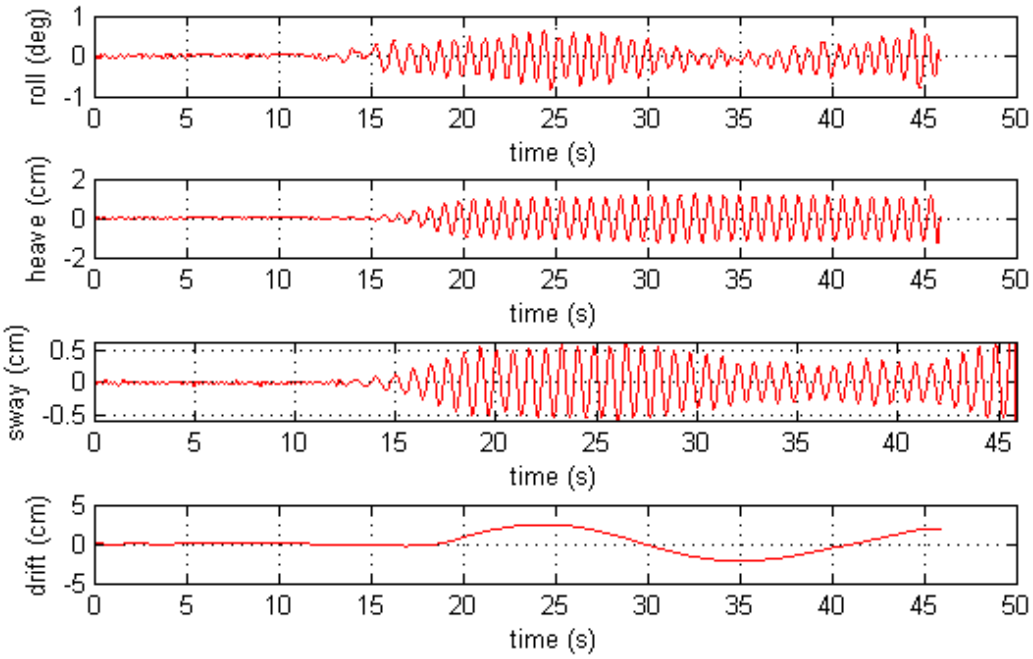

Figure 9-66: Responses for experiments 151-162 at $T = 0.8$ sec.

In the theoretical results for $T = 0.8$ sec, plotted for the corresponding position of the barge when the negative drift is maximum and assuming the barge fixed, the responses of roll and sway are also attenuating at $T = 0.8$ sec (Fig. 9-67).

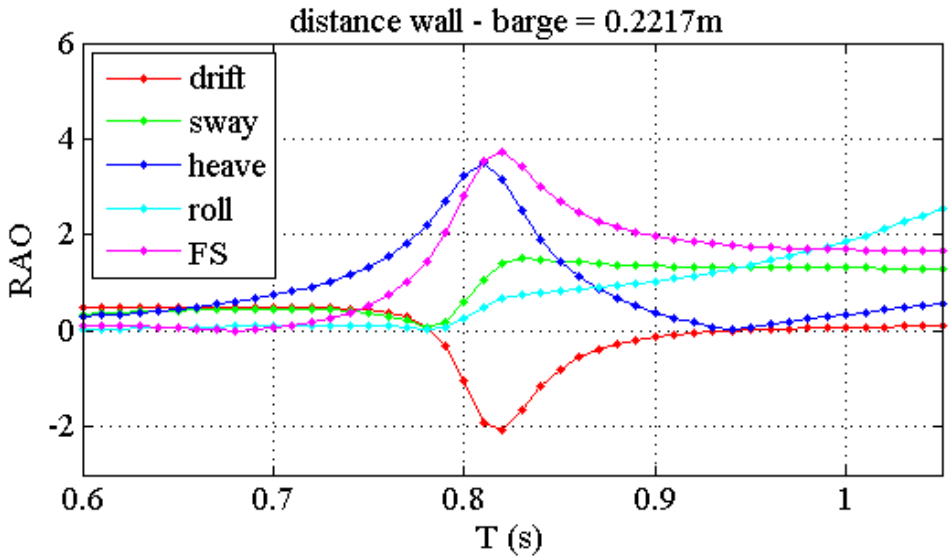

Figure 9-67: Barge 0.2217 m from the wall with viscous damping in roll.

The effect of the variable distance between wall and barge on the RAOs of the considered degrees of freedom is going to be illustrated. The theoretical RAOs and the normalized drift force corresponding to different positions of the barge, as experimentally measured for $T = 0.8$ sec, are plotted.

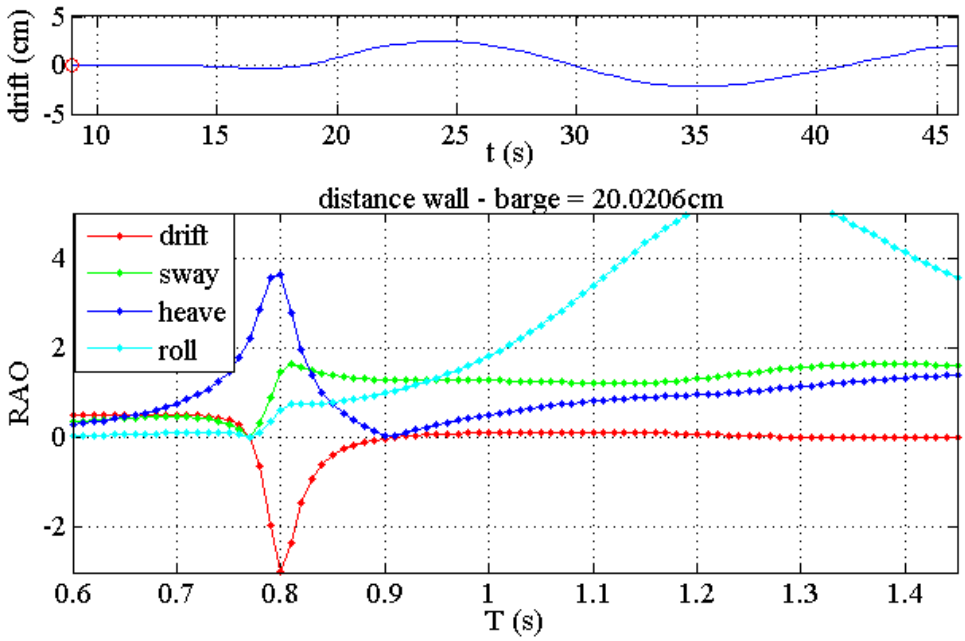

Figure 9-68: Barge 0.2002 m from the wall with viscous damping in roll.

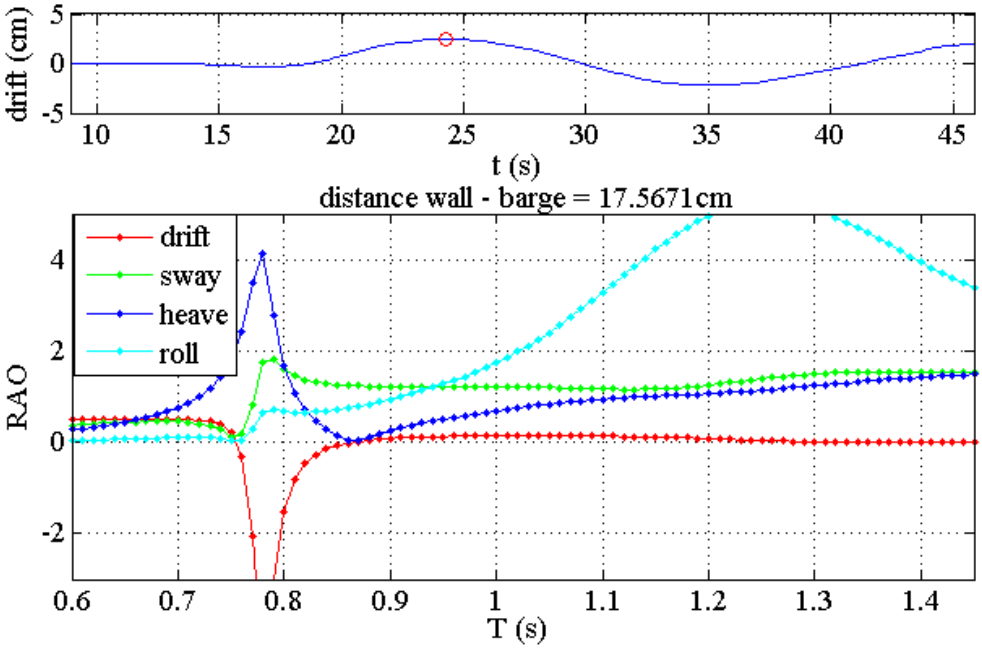

Figure 9-69: Barge 0.1757 m from the wall with viscous damping in roll.

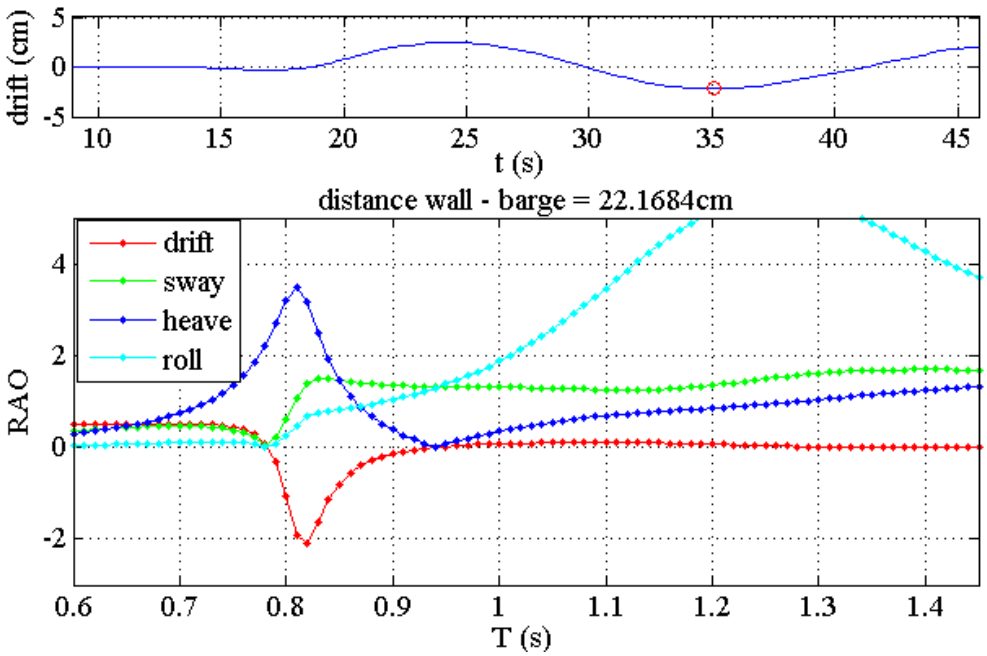

Figure 9-70: Barge 0.2217 m from the wall with viscous damping in roll.

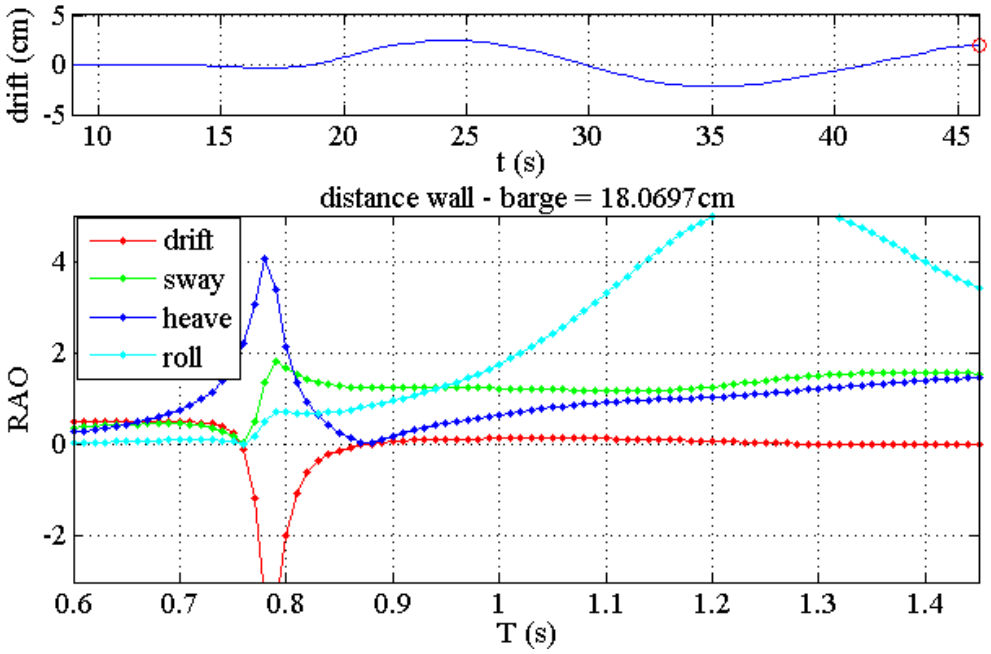

Figure 9-71: Barge 0.1807 m from the wall with viscous damping in roll.

In the global results, it is observed that while the distance wall-barge becomes smaller, the drift force becomes more negative and the negative drift force peak takes place in a smaller period.

Therefore for a same wave period it would be interesting to study the drift force as a function of the wall-barge distance. The RAOs as a function of the wall-barge distance are presented schematically for T = 0.8 sec in Figure 9-72. No viscous damping is added in the equations of the theoretical model.

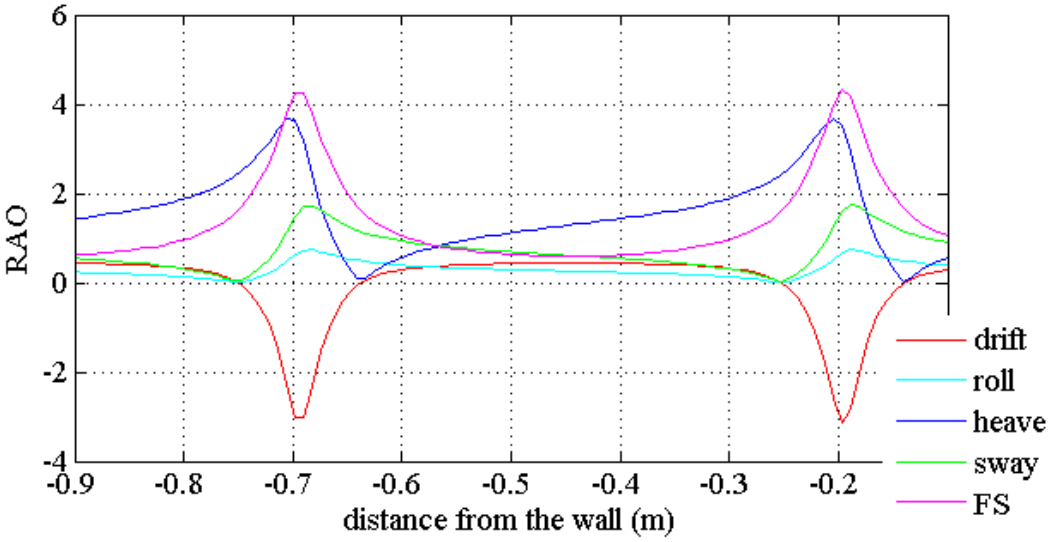

Figure 9-72: Barge at variable distance in front of the wall with no dissipation terms in the equations.

Intuitively, it could be claimed that the magnitude of the negative drift force would increase steadily while the body was approaching the wall. However this is not confirmed by the theoretical results as presented in the beginning of this *Chapter*, where a general conclusion for the effect of the distance wall-barge on the drift force could not be deduced. Furthermore, this is also depicted in Figure 9-72. In the same wave period, when the barge approaches the wall there is a negative drift force (-0.75 m up to -0.65 m approximately). Then, a balance when there is no more drift motion is observed and afterwards another negative drift force peak takes place (-0.2 m). During experiments this balance was not achieved and oscillations were observed. Noteworthy is also the fact that depending on the starting point, the drift force can attain two different positions of nullification. The first one, situated at -0.75 m from the wall, is characterized by a stable equilibrium, because if the barge drifts away from the equilibrium position the force tends to bring it back to its equilibrium position. The second one (–0.63 m) corresponds to an unstable equilibrium because if the barge departs from the equilibrium position the drift force has the tendency to move it further away. We show that the steady equilibrium occurs simultaneously with the extinction of roll and sway while the unsteady equilibrium coincides with the cancellation of heave motion. It is also observed that due to the unsteady equilibrium the heave response finds more difficulty in being cancelled completely contrary to sway's and roll's extinction which are complete.

To continue with, some results of a space-time representation of the free surface between the wall and the barge as depicted by the laser and the numerical model are presented. In this case, the freely drifting barge is placed at distance equal to 0.4 m in front of the wall. The waterdepth is equal to 0.513 m.

Experiments 131-150

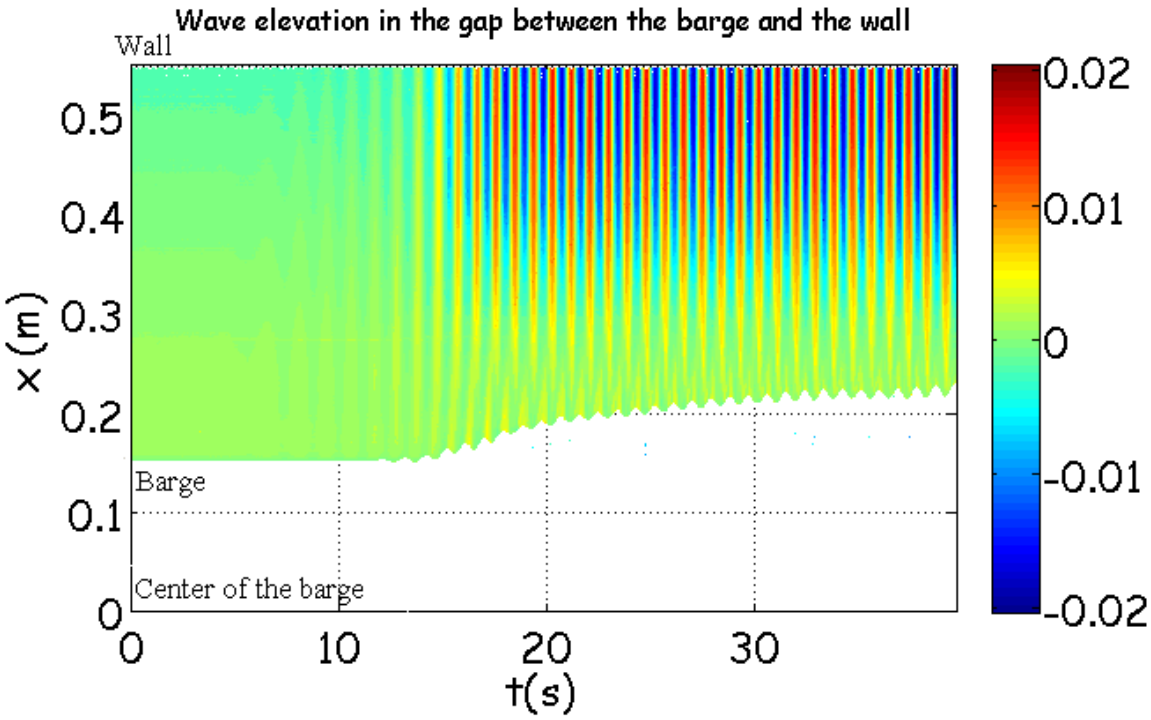

Figure 9-73: Space time representation of the free surface between the wall and the barge for T = 0.90 sec and $A_{incident}$ = 0.01 m.

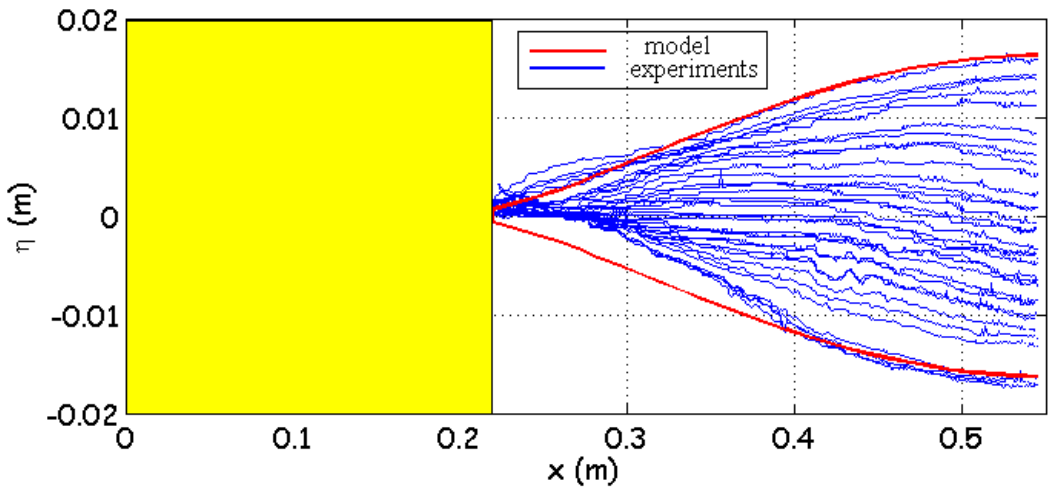

Figure 9-74: Free surface elevation between the wall and the barge for T = 0.90 sec and $A_{incident}$ = 0.01 m.

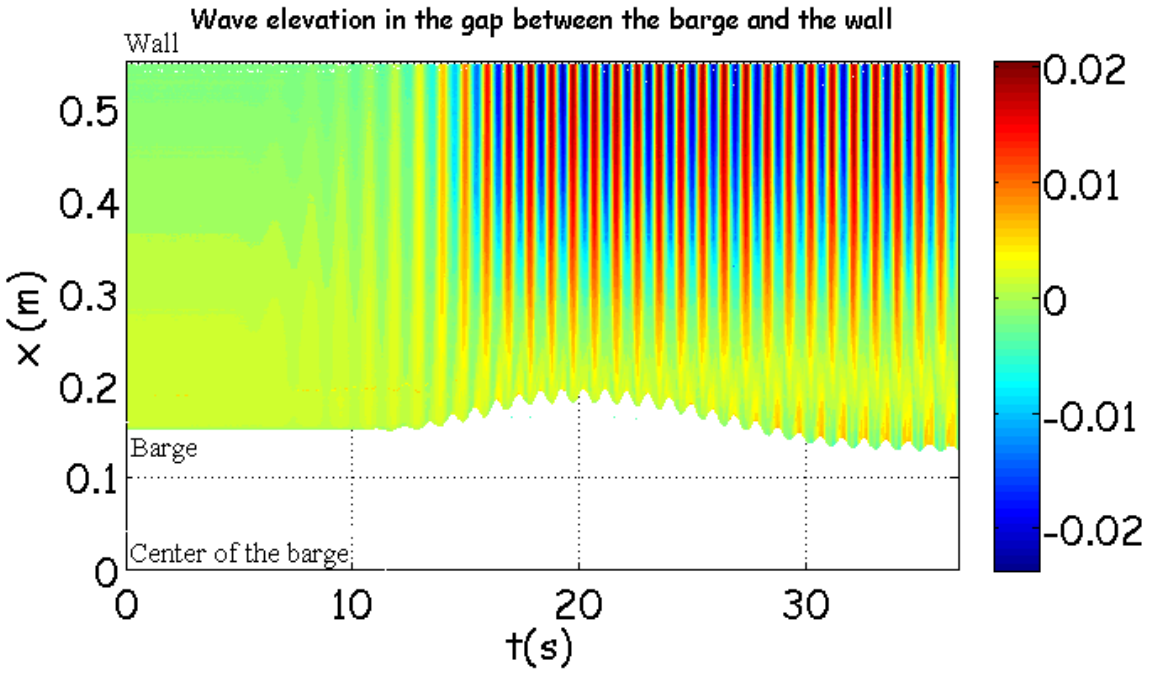

Figure 9-75: Space time representation of the free surface between the wall and the barge for T = 0.95 sec and $A_{incident}$ = 0.011 m.

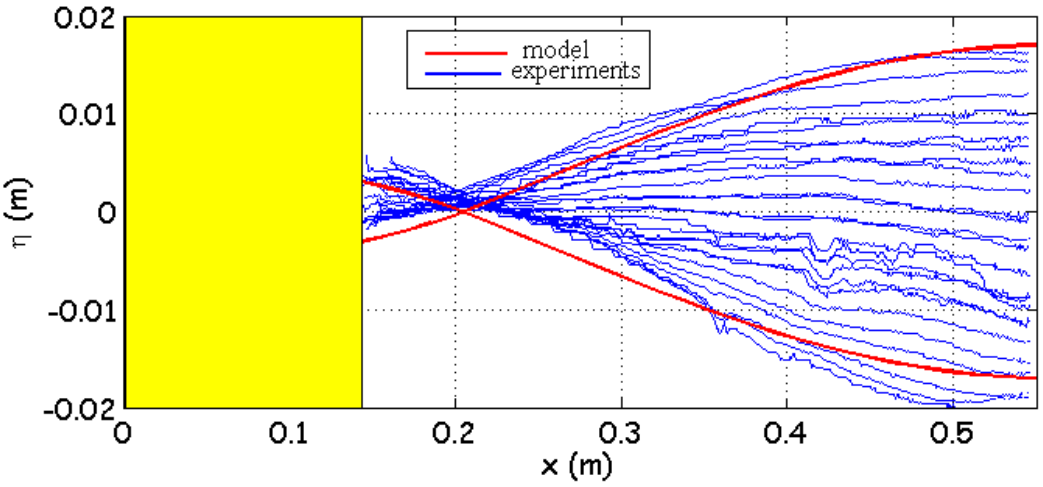

Figure 9-76: Free surface elevation between the wall and the barge for T = 0.95 sec and $A_{incident}$ = 0.011 m.

It is observed that experimental and theoretical results are in good agreement concerning the free surface elevation in the gap between the wall and the barge (Fig. 9-74 and Fig. 9-76). By comparing Figure 9-73 with Figure 9-75, it is deduced that the free surface elevation corresponding to T = 0.95 sec displays greater oscillation. Furthermore, in Figure 9-77, it is shown that this greater oscillation takes place simultaneously with a negative drift response which is not observed for T = 0.90 sec.

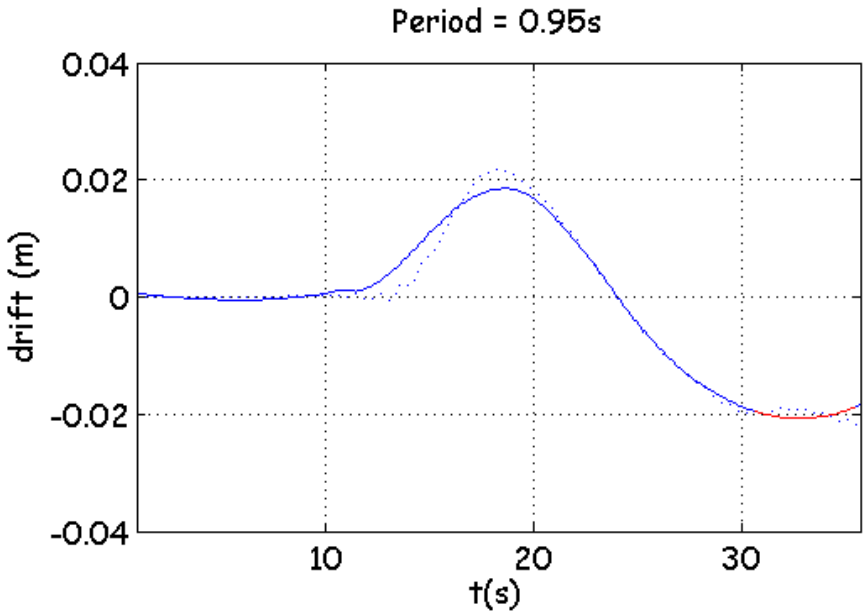

Figure 9-77: Drift movement for experiments 131-150 at T = 0.95 sec.

Last but not least, the case of the freely floating barge in front of a vertical transition is presented. The distance between the vertical transition and the barge is equal to 0.4 m, as measured from the right corner of the barge. The waterdepth h_1 of the weather side is equal to 0.561 m and in the lee side the waterdepth h_2 is equal to 0.515 m. Results of the drift movement as experimentally measured and calculations of the numerical model assuming the barge moored are shown. In the global results no negative drift values are observed.

Experiments 94-122

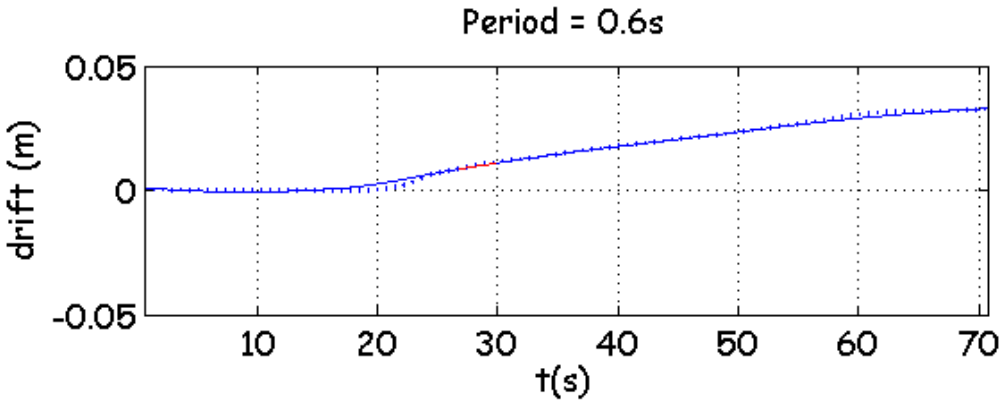

Figure 9-78: Drift movement for experiments 94-122 at T = 0.6 sec

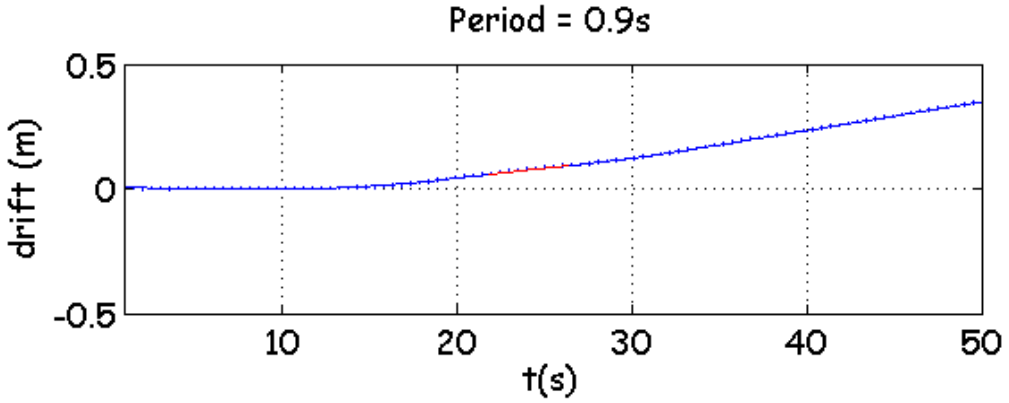

Figure 9-79: Drift movement for experiments 94-122 at T = 0.9 sec.

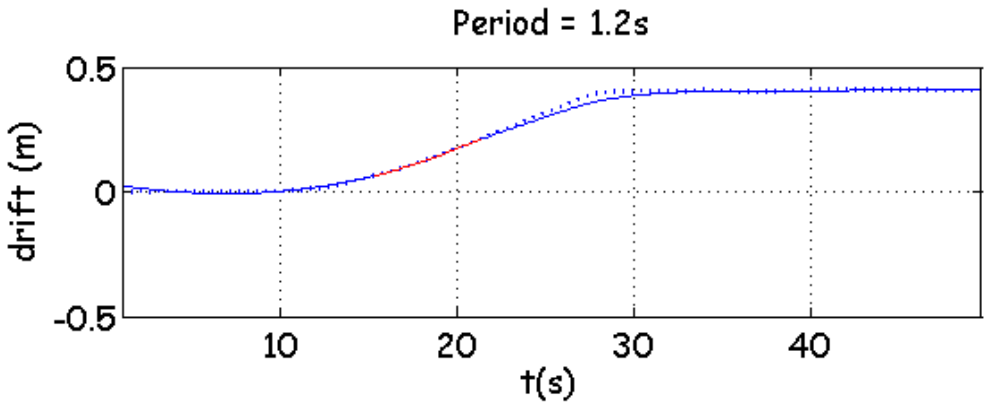

Figure 9-80: Drift movement for experiments 94-122 at T = 1.2 sec.

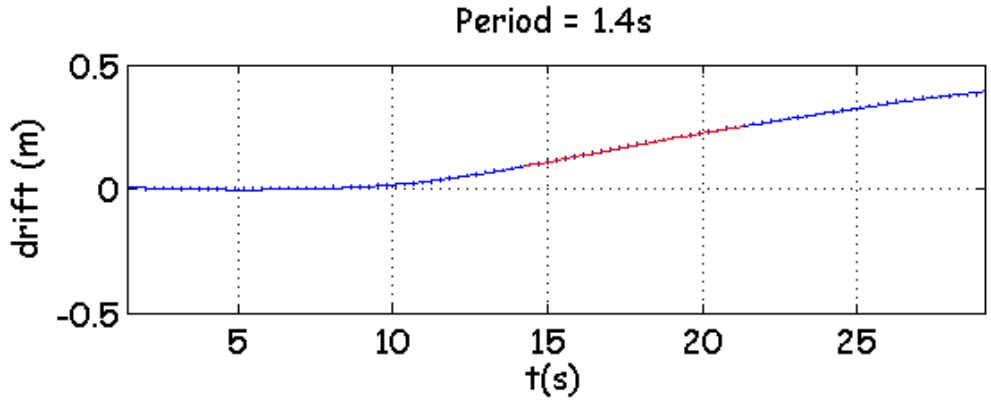

Figure 9-81: Drift movement for experiments 94-122 at T =1.4 sec.

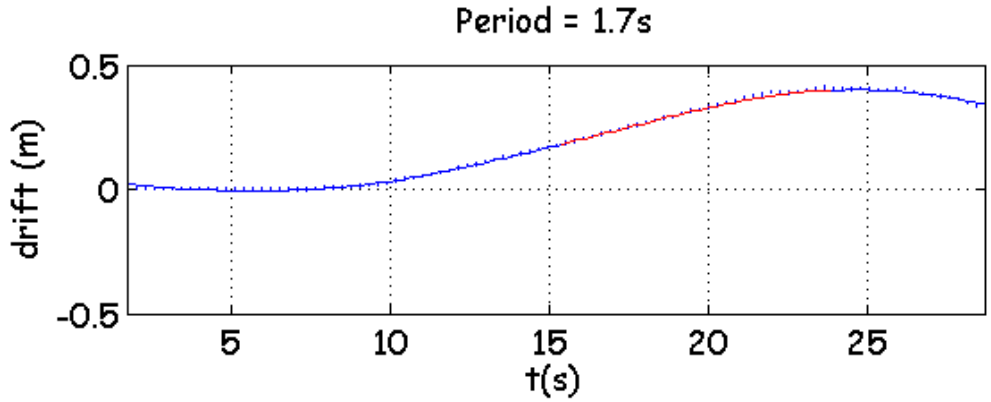

Figure 9-82: Drift movement for experiments 94-122 at T = 1.7 sec.

The preceding Figures 9-78 – 9-82 besides the positive drifting, confirm the statement that the drift movement is smoother compared with a moored barge case.

Figure 9-80 depicts that at t = 28 sec the barge reaches the step and there is no more drifting. In Figure 9-83 the responses of the considered degrees of freedom are plotted for T = 1.2 sec. After t = 28 sec some time is required until the oscillation of roll, heave and sway diminishes.

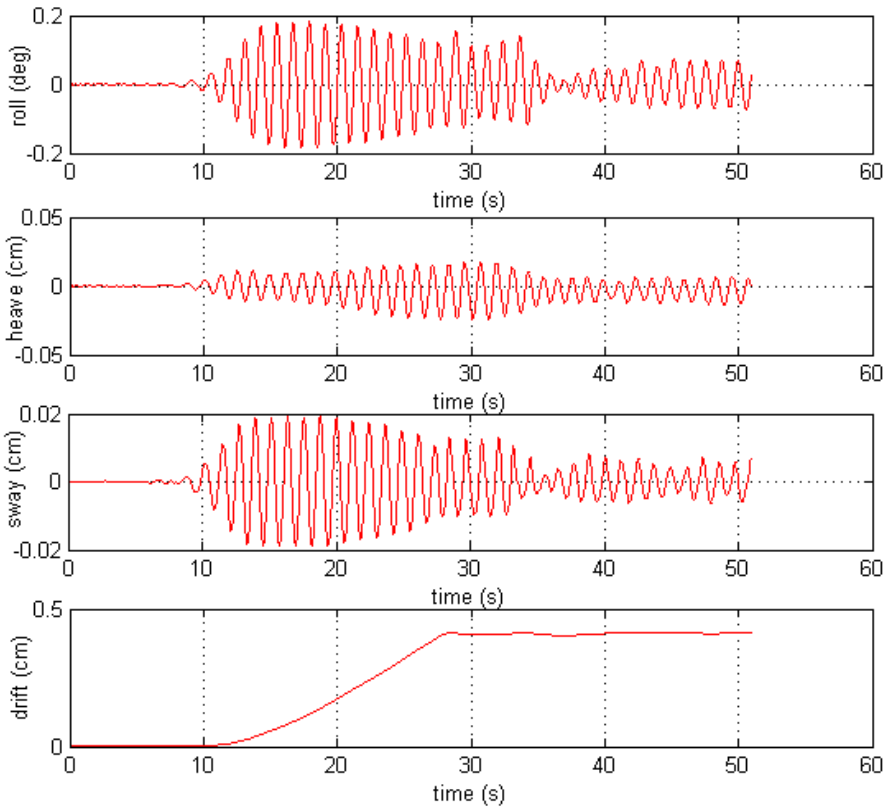

Figure 9-83: Responses for experiments 94-122 at $T = 1.2$ sec.

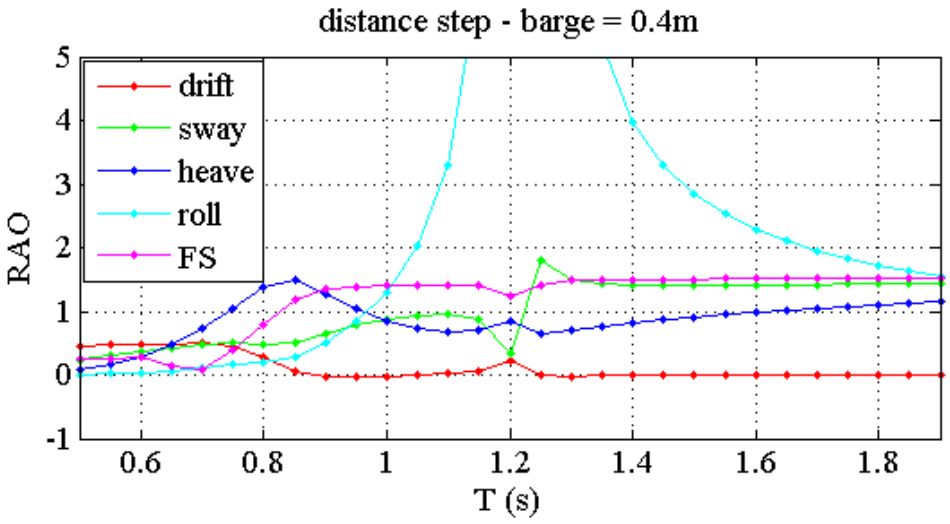

Figure 9-84: Barge 0.4 m from the step with no dissipation terms in the equations.

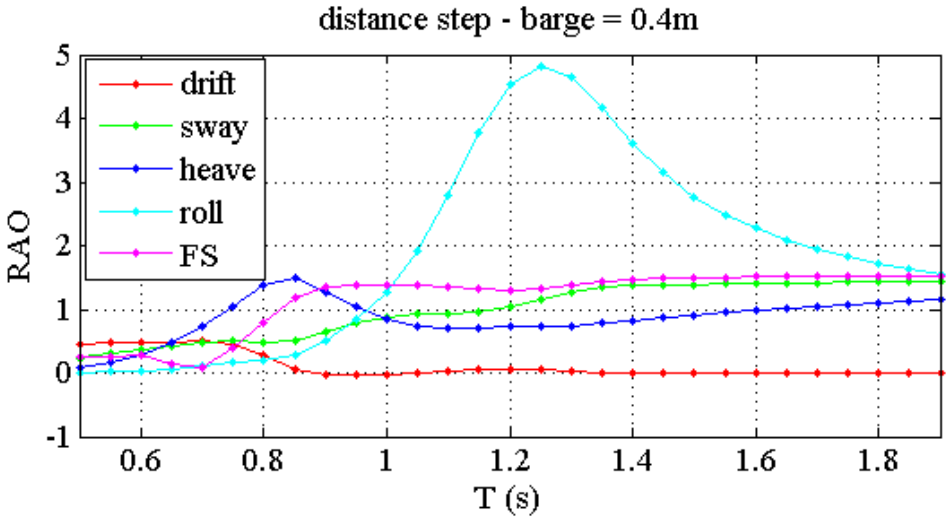

Figure 9-85: Barge 0.4 m from the step with viscous damping in roll.

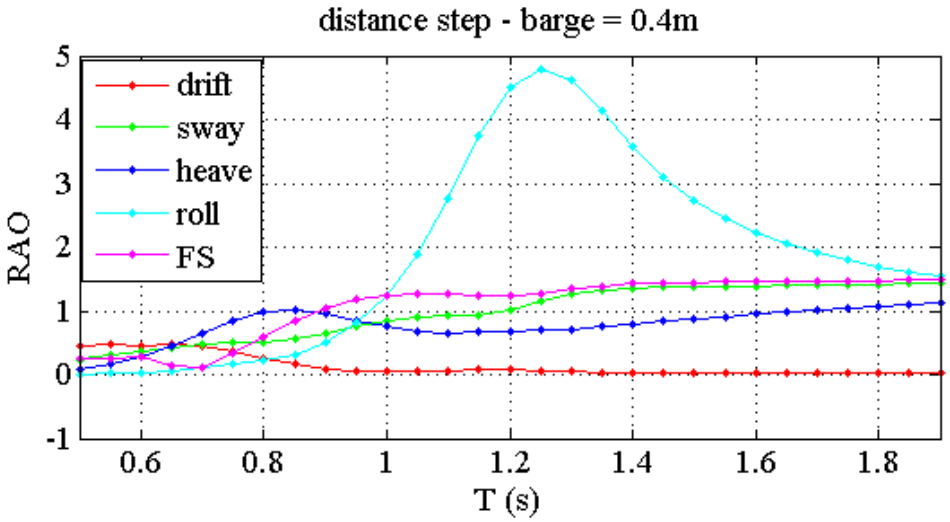

Figure 9-86: Barge 0.4 m from the step with viscous damping in roll and heave.

This case as also depicted by the numerical model does not present a remarkable interest. Merely between T = 0.9 sec and T = 1 sec, when a heave dissipation term is not added in the equations, the drift force reaches some negative value which is not noticeable. A possible reason no drifting opposite to the waves' direction is observed is that the height of the step is not adequate to cause this negative drift force ($h_2 \approx 0.92 \cdot h_1$). Our case is very close to the $h_1 = h_2$ case presented in Liu et al. (2010a) (Fig. 9-1), where no negative peaks are observed. The drift forces' calculation formula as already mentioned in *Chapter 8* is the following:

$$F_d = \frac{1}{2}\rho g \frac{C_G}{C} A^2 \left(1 + R_1 R_1^* - T_3 T_3^* - R_3 R_3^*\right) \tag{9.1}$$

The height of the step influences the magnitude of the lee side's reflected wave amplitude coefficient which determines the sign of the wave drift force.

In the following Figures 9-87, 9-88 the same problem, except that the step is replaced with a wall, is considered. The theoretical results are presented:

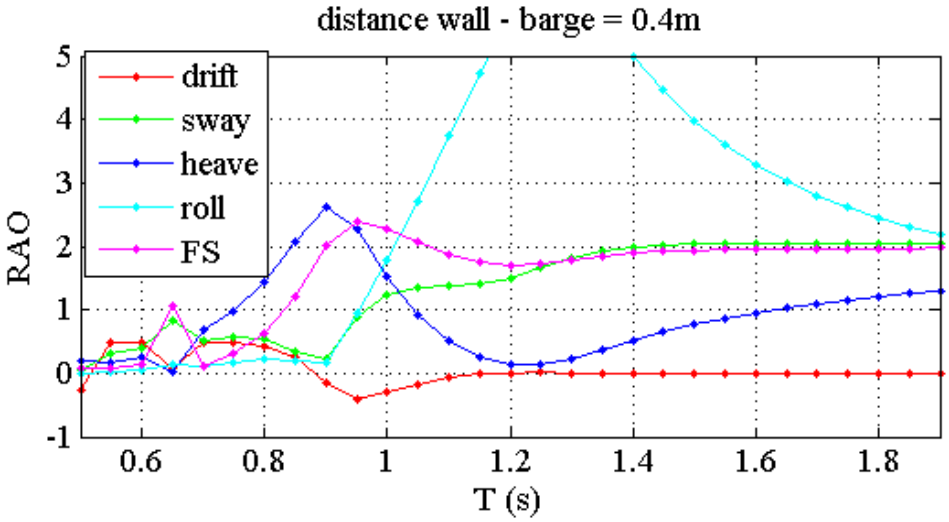

Figure 9-87: Barge 0.4 m from the wall with viscous damping in roll.

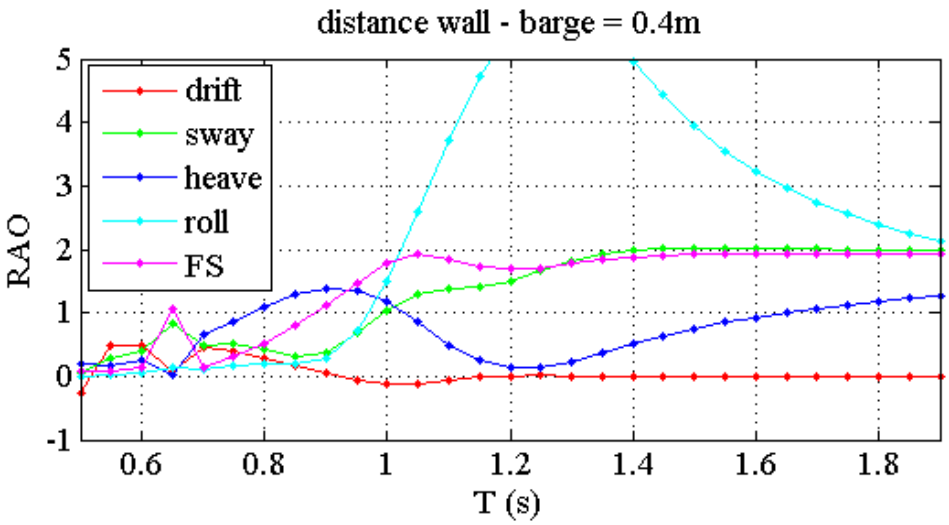

Figure 9-88: Barge 0.4 m from the wall with viscous damping in roll and heave.

In Figure 9-87 with no heave dissipation term, in the vicinity of $T = 0.9$ sec it is observed a more noticeable negative drift force compared with the case of the vertical step. The RAO of heave and the normalized free surface elevation also take greater values near $T = 0.9$ sec thus some negative drifting is connected also with this fact. The effects of piston mode resonance and sloshing are present in the case of the wall where the fluid is entrapped between the wall and the barge. When the viscous damping in heave is added the negative peak is almost eliminated. By comparing Figures 9-85, 9-86 with Figures 9-87, 9-88 it is deduced that the viscous effects arising from the heave resonance of the model and the piston mode resonance and sloshing modes of the fluid are more significant in the case of the wall.

From Figures 9-72, 9-87 and 9-88 it is concluded that in addition to the height of the step, the distance between step and barge in the current experiments is not the most characteristic distance for the illustration of the negative drift force.

10. CONCLUDING REMARKS AND PERSPECTIVES

In the present work the 2-D drift force exerted on a floating body has been both experimentally and numerically examined. Special attention has been paid to the occurrence of negative drift forces on the floating body. The work has been carried out in the framework of the ERASMUS Programme in collaboration with the Ecole Centrale Marseille (ECM).

The main findings of the present work can be summarized as follows:

We concluded, as it was traced back from the foregoing analysis that the source of the negative drift force is of potential origin. We are going to show this upon closer inspection. Actually, in the case of the wall the body-wave interaction can be considered as the superposition of two cases. In the first one, the wall is not taken into consideration. The system is excited by the incident wave and consequently a reflected (due to the diffraction and the radiation caused by the isolated body) and a transmitted wave component are produced. In the second case, the reflection on the wall is considered. The reflected wave on the wall corresponds to the incoming wave of this case. Both cases are regarded as identical except that they are acting in opposite directions. Concerning the sign of the drift force, the most dominant or in other words the case which will induce the greatest reflection on the body, determines the final sign of the drift force. Hence, even if a negative drift force is observed, this drift force can still be considered to have the propagation direction of the incoming wave, which in this case is the one of the reflected wave on the wall. The sign of the mean drift force is in accordance with the ideal-fluid theory and thus it is a potential effect. Nevertheless, the phenomenon is much more complicated if we take into consideration that multiple reflections on the model and on the wall take place and affect the drift force in magnitude and in sign.

The global experimental and theoretical results have shown that another factor that might be susceptive for the negative wave drift force can be the excessive oscillation of the barge and of the free surface in the heave direction; especially is the case where the reflecting wall is present and the fluid is entrapped in a small gap between the barge and the wall. This is also a potential effect. However, in the second case the potential effect gives rise to co-existing non-linear effects, as it is the flow separation, which may cause the damping of the negative drift force.

As far as the further perspectives of the present work are concerned, difficulties emanating from the experimental setup have to be solved. As already mentioned in *Chapter 10* the number of springs is a critical parameter in the calculation of the drift force. Therefore, the mooring lines must be properly sized in order to enable the drift force to attain a stable state without in the same time modifying the first-order responses. Concerning the theoretical model, a better formulation of the viscous damping should be implemented so that the flow separation at the barge bilges is properly accounted for. This is the case of the barge's resonance in roll or in heave as well as of the gap resonance in between the barge and the wall. For the latter case, we make reference to two techniques which are mentioned in Kimmoun et al. (2011). In Kristiansen and Faltinsen (2011) a numerical domain-decomposition method is proposed to take into consideration the damping induced by the flow separation at bilge keels. More specifically, a combination of the Bernoulli equation in the greatest part of the water and of the Navier-Stokes equations in the viscous domain near the ship bilges is used. Another technique consists in adding a massless lid at the inner free surface and attributing to it a quadratic damping force (Molin et al. 2009).

11. BIBLIOGRAPHY

Abul-Azm, A.G., Williams, A.N. (1988): "Second-Order diffraction loads on truncated cylinders". Journal of Waterway, Port Coastal and Ocean Engineering, Vol.114, No. 4.

Athanassoulis, G.A. (2008): "Ship Dynamics and Laboratory", Lecturing notes (in greek), Laboratory for Ship Hydrodynamics, School of Naval Architecture and Marine Engineering, National Technical University of Athens.

Bowers, E.C. (1976): "Long period oscillations of moored ships subject to short wave seas". Trans. Royal Institution of Naval Architects, 118 (181-191).

Chen, X.B. (2007): "Middle-field formulation for the computation of wave-drift loads". J. Engineering Mathematics, pp. 61-82.

Dev, A.K., Pinkster J.A. (1994): "Experimental evaluation of the viscous contribution to mean drift forces on vertical cylinders". Proceedings, 7th International Conference on the Behaviour of Offshore Structures. (BOSS'94), Massachusetts Institute of Technology, Editor C. Chyssostomidis, Elsevier, Vol. 2, pp. 855 - 875.

Eatock Taylor, R., Hung, S.M. (1987): "Second-order diffraction forces on a vertical Cylinder in Regular Waves". Appl. Ocean Research Vol. 9, pp.19-30.

Faltinsen, O. M. (1990): "Sea Loads On Ships and Offshore Structures". Trondheim: Cambridge University.

Faltinsen, O.M. (1972): "Wave forces on a restraiined ship in head-sea waves". Proc. 9th Symp. on Naval Hydrodynamics, Paris, Office of Naval Research ACR-203, pp. 1763-1840.

Faltinsen, O.M., Loken, A.E. (1978): "Drift forces and slowly varying horizontal forces on ships in waves". Timman Symposium on Applied Mathematics, Delft.

Faltinsen, O.M., Michelsen, F. (1974): "Motions of large structures in waves at zero Froude number". Symposium of the dynamics of marine vehicles and structures in waves.

Foss M.M. (2006): "Offshore LNG Receiving Terminals". CEE-BEG-UT Austin.

Gerritsma, J., Beukelman, W. (1971): "Analysis of the resistance increase in waves of a fast cargo ship". Report No. 334 Laboratorium voor Scheepsbouwkunde, Technical Univ. of Delft.

Havelock, T.H. (1942): "The drifting force on a ship among waves". Phil. Mag. 33, pp. 467-475.

Hermans, A.J (1999): “Low-frequency second-order wave-drift forces and damping”. Journal of Engineering Mathematics, 35, 181-198.

Hsu, F. H., Blenkarn, K.A. (1970): “Analysis of peak mooring forces caused by slow vessel drift oscillation in random waves”. Proc. 2nd Offshore Technology Conf., pp. I-135- I-146

Huse, E. (1976): “Wave induced mean force of platform in direction opposite to wave propagation”. Interocean.

Huse, E. (1977): “Wave induced mean force on platforms in direction opposite to wave propagation”. Norwegian Maritime Res., 5, 2-5.

Joseph, D.D. (1973): “Domain perturbations: the higher order theory of infinitesimal water waves”. Arch. Rational Mech. Anal. Vol. 51 (295-303).

Kaplan, P., Sargent, T.P. (1976): “Motions of offshore structures as influenced by mooring and positioning systems”. BOSS, Trondheim.

Kim, M.H., & Yue, D.K.P. (1990): “The complete second-order diffraction solution for an axisymmetric body. II. Bichromatic incident waves and body motions”. J. Fluid Mech., 211, 557-593

Kim, M-H, & Yue, D.K.P. (1989): “The complete second-order diffraction for an axisymmetric body. Part 1. Monochromatic incident wave”. J. Fluid Mech., 200, 235-264.

Kimmoun, O : “Etude experimentale du mouvement d'une barge rectangulaire travers la houle”. Ecole Centrale Marseille.

Kimmoun, O., Molin, B. (2007) : “Projet CHEEPP-Comportement sur Houle en Eau Peu Profonde”

Kimmoun, O., Molin, B., Oikonomidou, H. (2011): “Wave drift force on a rectangular barge by a vertical wall”. Proc. 26th Workshop Water Waves and Floating Bodies, Athens.

Kirby, J.T., & Dalrymple R.A. (1983): “Propagation of obliquely incident waves over a trench”. J. Fluid Mech., 133, 47-63.

Kristiansen, T., Faltinsen, O.M. (2011): “Gap resonance analyzed by a domain decomposition method”. Proc. 26th Workshop Water Waves and Floating Bodies, Athens.

Lee, C.M., Newman, J.N. (1971): “The vertical force and moment of submerged bodies under waves”. J. of Ship Research, Vol. 15, No. 3.

Liu, Y.N. (2010b): "Effect of variable bathymetry on the linear and slow-drift wave responses of floating bodies". PhD-thesis. Universite de Provence.

Liu, Y.N., Molin, B., Kimmoun, O. (2010a): "Wave drift forces on a rectangular barge in varying bathymetry". Proc. 25th Int. Workshop Water Waves and Floating Bodies, Harbin.

Loken, A. (1986): "Three dimensional second orer hydrodynamic effects on ocean structures in waves". PhD-thesis, Dept. Marine Technology, NTNU.

Longuet-Higgins, M.S. (1977): "The mean forces exerted by waves on floating or submerged bodies with applications to sand bars and wave power machines". Proc. Royal Soc. London Ser. A, 352, 463-480.

Maruo, H. (1960): "The drift of a body floating in waves". J.of Ship Research, Vol. 4, No. 3.

Maruo, H., Sasaki, N. (1974): "On the wave pressure acting on the surface of an elongated body in head seas". Jour. Soc. Naval Architects of Japan, 136, 34-42.

Mavrakos, S.A. (1988): "The vertical drift force and pitch moment on axisymmetric bodies in regular waves". Appl. Ocean Research Vol.10, pp. 207-218.

Mavrakos, S.A. (1995): "Mean drift loads on multiple vertical axisymmetric bodies in regular waves". Proc. 5th Int. Offshore and Polar Engineering Conf., The Hague, The Netherlands.

Mavrakos, S.A. (1999): "Design of Floating Structures", Lecturing Notes (in greek), Laboratory for Floating Structures and Mooring Systems, School of Naval Architecture and Marine Engineering, National Technical University of Athens.

Mavrakos, S.A., Peponis, V. (1992): "Second-order sum and difference frequency loads on axisymmetric bodies restrained in irregular waves". Proc. 2nd Int. Offshore and Polar Engineering Conf. San Francisco, USA.

Molin, B. (1979a): "Computations of drift forces". Paper No. 3627, O.T.C, Houston.

Molin, B. (1979b): "Second-order diffraction loads upon three-dimensional bodies". Appl. Ocean Research Vol.1, pp. 197-202.

Molin, B. (2002) : "Hydrodynamique des structures offshore". Editions Technip.

Molin, B., Kimmoun, O., Remy, F. (2011): "Slow-drift excitation in varying bathymetry". Proc. 26th Workshop Water Waves and Floating Bodies, Athens.

Molin, B., Remy, F., Camhi, A., Ledoux, A. (2009): "Experimental and numerical study of the gap resonance in-between two rectangular barges". Proc. 13th congress

of Intl. Maritime Assoc. of Mediterranean, IMAM2009.

Newman, J. N. (1974): "Second order, slowly varying forces on vessels in irregular waves". Int. Symp. on the Dynamics of Marine Vehicles and Structures in Waves, University College, London.

Newman, J.N. (1967): "The drift force and moment on ships in waves". J. of Ship Research, Vol. 11, No. 1.

Newman, J.N.and Lee, C.H. (1992): "Sensitivity of wave loads to the discretization of bodies". Proc. of the Int. Conference on the Behaviour of Offshore Structures. BOSS' 92, London, U.K.

Ogilvie, T.F. (1983): "Second-Order Hydrodynamic Effects on Ocean Platforms". Proc. Int. Workshop on Ship and Platform Motion. Berkeley, 205-265.

Ogilvie, T.F.(1963): "First- and second-order forces on a cylinder submerged under a free surface". J. Fluid Mech. 16 (451-472).

Pijfers, J.G.L, Brink, A.W. (1977): "Calculated drift forces of two semi-submersible platform types in regular and irregular waves". Paper No. OTC 2977, Offshore Technology Conference, Houston.

Pinkster, J.A. (1976): "Low frequency second-order wave forces on vessels moored at sea". Eleventh Symposium on Naval Hydrodynamics, University College, London.

Pinkster, J.A. (1979b): "Mean and low frequency wave drifting forces on floating structures". Ocean Engineering, Vol.6, pp. 593-615.

Pinkster, J.A. (1980): "Low frequency second-order wave exciting forces on floating structures". PhD-thesis, Technical University of Delft.

Pinkster, J.A.(1979a): "Wave drifting forces". Proceedings of WEGEMT, Aachen.

Pinkster, J.A., Hooft, J.P (1978): "Low frequency drifting forces on moored structures in waves". 5th International Ocean Development Conference Tokyo.

Pinkster, J.A., Huijsmans, R.H.M. (1982): "The low frequency motions of a semi-submersible in waves". Proc. 3rd internat. Conf. on Behaviour of Offshore Structures (BOSS), Mass. Inst. Of Tech., pp. 447-466.

Pinkster, J.A., Van Oortmerssen, G. (1977): "Computation of the first- and second-order wave forces on bodies oscillating in regular waves". Second International Conference on Numerical Ship Hydrodynamics, Berkeley.

Prins, H. (1995): "Time domain calculation of Wave drift forces and moments". PhD-

thesis, Technical University of Delft.

Remery, G.F.M., Hermans, A.J. (1972): "The slow drift oscillation of a moored object in random seas". Soc. of Petroleum Engineers Journal.

Salvesen, N. (1974): "Second order steady-state forces and moments on surface ships in oblique regular waves". Proc. Internat. Symp. On Dynamics of Marine Vehicles and Structures in Waves, Univ. Coll. London, pp. 212-226.

Suyehiro, K. (1924): "The drift of ships caused by rolling among waves". Tr. INA Vol. 66, pp. 60-76.

Triantafyllou, M.S. (1982): "A consistent hydrodynamic theory for moored and positioned vessels". Jour. Ship Res., 26 , 97-105.

Ursell, F. (1975): "The refraction of head seas by a long ship". Jour. Fluid Mechanics, 67, 689-703.

Wahab, R. (1974): "Waves induced motions and drift forces on a floating structure". Report No.186 S, Netherlands Ship Research Centre, TNO, Delft.

Watanabe, Y. (1938): "Some contributions to the theory of rolling". Tr. INA Vol.80, pp. 408-432.

Wehausen, J.V., Laitone, E.V. (1960): "Surface waves". Encyclopedia of physics. Vol. IX, Ed., S. Flugge, pp. 446-778.

Weiler, O., Cozijn, H., Wijdeven, B., Le Guennec, S., Fontaliran, F. (2009): "Motions and mooring loads of an LNG-Carrier moored at a jetty in a complex bathymetry". Proc. 28th Intl. Conf. Offshore Mech. & Arctic Engng, OMAE2009-79420.

Zaraphonitis,G., Papanicolaou, A. (1991): "Second-order calculations of motions and loads of arbitrarily shaped bodies in waves". 1st International Workshop on very large floating structures, Honoloulou, Hawai.

Zhao, R., Faltinsen, O.M. (1988): "Interaction between waves and current on a two-dimensional body in a free surface". Applied Ocean Research 1987 Vol.10, pp. 87-99.